IOWA STATE UNIVERSITY
Digital Repository

Retrospective Theses and Dissertations

Iowa State University Capstones, Theses and Dissertations

1968

The effect of a dispersed second phase on the mechanical properties of copper containing two weight percent cobalt

Barry George Koepke
Iowa State University

Follow this and additional works at: https://lib.dr.iastate.edu/rtd

 Part of the Metallurgy Commons

Recommended Citation

Koepke, Barry George, "The effect of a dispersed second phase on the mechanical properties of copper containing two weight percent cobalt " (1968). *Retrospective Theses and Dissertations*. 4605.
https://lib.dr.iastate.edu/rtd/4605

This Dissertation is brought to you for free and open access by the Iowa State University Capstones, Theses and Dissertations at Iowa State University Digital Repository. It has been accepted for inclusion in Retrospective Theses and Dissertations by an authorized administrator of Iowa State University Digital Repository. For more information, please contact digirep@iastate.edu.

This dissertation has been
microfilmed exactly as received

69-9868

KOEPKE, Barry George, 1937-

THE EFFECT OF A DISPERSED SECOND PHASE ON THE MECHANICAL PROPERTIES OF COPPER CONTAINING TWO WEIGHT PERCENT COBALT.

Iowa State University, Ph.D., 1968
Engineering, metallurgy

University Microfilms, Inc., Ann Arbor, Michigan

THE EFFECT OF A DISPERSED SECOND PHASE ON THE MECHANICAL PROPERTIES OF COPPER CONTAINING TWO WEIGHT PERCENT COBALT

by

Barry George Koepke

A Dissertation Submitted to the
Graduate Faculty in Partial Fulfillment of
The Requirements for the Degree of
DOCTOR OF PHILOSOPHY

Major Subject: Metallurgy

Approved:

Signature was redacted for privacy.

In Charge of Major Work

Signature was redacted for privacy.

Head of Major Department

Signature was redacted for privacy.

Dean of Graduate College

Iowa State University
Ames, Iowa

1968

TABLE OF CONTENTS

I. INTRODUCTION

The ability of a metallic matrix to be strengthened by the introduction of a dispersed second phase is an extremely useful property of metals and as a result, precipitation hardened alloys have always played a major part in the advancement of technology. Ever since it was discovered that metals deform by the generation and propagation of defects, notably dislocations, it has been realized that any description of the strengthening mechanisms in metals involves a consideration of the interactions between these dislocations and barriers tending to obstruct their motion (1). Since the major barriers restricting dislocation motion in precipitation hardened alloys are the precipitates themselves an attempt to describe in detail the origin of precipitation hardening naturally involves detailed considerations of the interactions of glide dislocations and precipitates. It will become evident that this is not a simple matter, even if the characteristics of the dispersion are well known, because of the large number of ways in which the above mentioned interactions can occur. As a result, although many theories exist, the problem is far from completion.

Most theoretical considerations of the origin of precipi-

tation hardening are restricted to the region of the yield point because the undeformed state in a precipitation hardened material is the only one that can be characterized with certainty (2). Detailed considerations of the work hardening behavior of these alloys are still mainly qualitative in nature. The mechanisms responsible for the thermally activated component of the flow stress in precipitation hardened alloys is another aspect of their deformation behavior that has not been extensively studied and is not fully understood. Thermally activated deformation is especially important when the low temperature mechanical behavior of metals is considered because the thermal component of the flow stress is, in many instances, a large fraction of the total flow stress (3).

This investigation was initiated to study the effect of a dispersed second phase on the thermally activated component of the flow stress in a precipitation hardened alloy. The rate controlling dislocation mechanisms leading to the thermal component of the flow stress in pure metals have been extensively studied (3) and it was of interest to determine whether the presence of a second phase altered the mechanisms entirely or just changed their magnitude. Precipitates may be completely coherent with the matrix, partially coherent, or

incoherent (2). In an alloy containing incoherent precipitates it was found that the dislocation mechanisms responsible for the thermal component of the flow stress were the same as those for the matrix without any precipitates (4). It will become clear that this is not possibly the case for alloys containing coherent precipitates. For this reason it was decided to study a precipitation hardenable alloy containing completely coherent precipitates. Copper containing nominally 2 wt % cobalt is an ideal material for this type of study since the precipitates are homogeneously nucleated, coherent spheres (5). The aging characteristics and morphology of the alloy have been well studied[1] and the characteristics of the obstacles to dislocation motion are well known. Although the effect of a coherent second phase on the rate controlling dislocation mechanisms is the primary interest in this study, the relation between the current theories of precipitation hardening and the results contained herein will also be considered.

The following section will include a brief review of the current theories of precipitation hardening in alloys containing coherent precipitates as well as a discussion of thermally activated deformation. The research to date on Cu-Co alloys

---

[1] These will be covered in detail later.

will be reviewed. It should be emphasized at this point that discussion will be limited to those alloys known to precipitate coherent, spherical precipitates, namely Al-Ag, Al-Zn, and Cu-Co (2).

Since the flow stress of a metal is determined by the size and strength of the barriers restricting dislocation motion, it can be considered to arise from barriers of two types, long range and short range. Long range barriers (e.g. dislocation pile ups in the glide plane and precipitates with large stress fields) are those that interact with the glide dislocation over large distances in the lattice. Short range barriers are those that only interact with the glide dislocation over very short distances < 10 b. b is the Burgers vector. Examples of short range barriers are intersecting forest dislocations and the increase in energy associated with new interface produced when a coherent precipitate is cut by a dislocation. The retarding force a dislocation experiences from a long range barrier extends over large distances and is associated with a high activation energy, commonly several hundred electron volts (6). The retarding force due to a long range barrier generally is proportional to the shear modulus μ and only varies with temperature as μ. A short range barrier,

on the other hand, is associated with a small activation energy on the order of an electron volt and can be thermally activated. The retarding force due to a short range barrier, therefore, is usually quite temperature dependent. Since a metal can be considered to be composed of long and short range obstacles, it is convenient to divide the flow stress into components representing each (7). In this context the flow stress is usually written as

$$\tau = \tau_\mu + \tau^*$$

where τ is the applied shear stress, τ_μ the component arising from the long range forces, and τ^* the thermally activated component of the flow stress associated with the short range barriers. Usually $\tau_\mu \propto \mu$ and $\partial\tau_\mu/\partial T = \partial\mu/\partial T$.

For the above reasons, it was thought appropriate to divide the following discussion on hardening mechanisms in alloys containing coherent precipitates into two sections, one dealing with long range strengthening sources and one dealing with short range sources. This approach is also followed in the excellent comprehensive review by Kelly and Nicholson (2) and in the recent review by Gleiter and Hornbogen (8).

II. LITERATURE SURVEY

A. Long Range Theories

Long range interactions between glide dislocations and coherent precipitates arise mainly from the following sources.

1) Coherency strains surrounding the precipitates.
2) Difference in elastic modulii of precipitate and matrix.
3) Difference in chemical composition of precipitate and matrix.
4) Hydrostatic interaction between dislocation and precipitate.

Coherency strains surrounding spherical G.P. zones can be quite large if the difference in atomic volume between the matrix and precipitate are significant. This is the case in Al-Zn and Cu-Co alloys where the atomic mismatches of the precipitates with respect to the base metals are -1.2% (9) and -1.3% (10) respectively. In the case of Al-Ag alloys the mismatch (+0.7%) is much smaller (2).

The earliest theory of the yield stress in precipitation hardened alloys containing coherent precipitates was due to Mott and Nabarro (6,11,12,13). Their theory deals with the increase in strength resulting from the interaction of dis-

locations and the elastic coherency strains generated by a coherent precipitate having a different atomic volume than the matrix. The details of the theory are outlined by Kelly and Nicholson (2) and only the highlights will be presented here. If a spherical precipitate of atomic volume $(1+\delta)^3$ is inserted in a matrix of unit atomic volume the stress set up in the precipitate is a hydrostatic pressure P given by

$$P = 3\ K(\delta - \epsilon)$$

where $\epsilon = \dfrac{3\ K\ \delta}{3K + 2E/1+\nu}$

K = bulk modulus of precipitate

E = Young's modulus of matrix

ν = Poisson's ratio of matrix.

The strain in the matrix is a shear without dilation and is, at a distance r from the precipitate,

$$\frac{\epsilon r_o^{\ 3}}{r^3}$$

where r_o = radius of precipitate. Since the average distance from any point in the matrix to the nearest particle is $1/2N^{-1/3}$ (2) when N is the volume fraction of precipitate, the average shear strain is

$$\bar{\gamma} = 8\epsilon r_o^{\ 3} N.$$

The volume fraction, f, is $4/3\ \pi N r_o^{\ 3}$, so

$$\bar{\gamma} = 2\epsilon f.$$

The flow stress is then taken as the average of the internal stress or

$$\tau = 2\mu\epsilon f$$

where μ = shear modulus of matrix. The theory only applies when the dislocations can be bent to radii of curvature smaller than the interparticle separation since it is only when this condition holds that the average of the internal stresses can be taken. The theory then predicts that strengthening due to coherent spherical precipitates is independent of particle size and linearly dependent on volume fraction. This has not been found to be the case in Al-Zn alloys (14,15) and Cu-Co alloys (16). An application of the Mott-Nabarro theory to yield stress data of Al-Ag alloys (15,17) by Kelly and Nicholson (2) showed a predicted yield stress four times smaller than observed. Although this comparison indicates that the theory does not describe accurately the strengthening induced by coherent precipitates, its concepts are valuable in that they demonstrate the effectiveness of coherency stresses as dislocation obstacles.

Recent considerations of the effects of coherency strain fields on the strength of alloys containing coherent precipitates have predicted values much closer to the experimental data than did the theory of Mott and Nabarro. The newer

theories deal directly with the interaction of a dislocation and the strain field of a particle and consider this interaction to play the major role in strengthening. Gerold and Haberkorn (18) calculated the increase in strength $\Delta\tau_o$ at absolute zero due to precipitates over that of the matrix by starting with a relation given by Fleischer (19) for solid solution hardening. If K is the maximum repelling force on a dislocation due to the strain of a particle and L is the average distance between particles, then

$$\Delta\tau_o = \frac{K}{bL}$$

where b is the Burgers vector. By considering the stress fields of spherical particles determined from the strain fields given by Mott and Nabarro (11) they determined K for the cases of edge and screw glide dislocations. Noting that, when K is relatively small, the particles are cut by the dislocations they arrived at the following expressions for $\Delta\tau_o$:

$$\Delta\tau_o \simeq 3\mu|\delta|^{3/2}\left(\frac{Rf}{b}\right)^{1/2} \text{ for edge dislocations}$$

$$\Delta\tau_o \simeq \mu|\delta|^{3/2}\left(\frac{Rf}{b}\right)^{1/2} \text{ for screw dislocations}$$

where μ is the shear modulus of the matrix, δ the linear misfit parameter between precipitate and matrix, R the particle radius, and f is the volume fraction of precipitate. The

linear misfit parameter, δ, can be written in terms of the relative difference in Burgers vectors as:

$$\delta = \frac{b_p - b_m}{b_m}$$

where the subscripts p and m refer to the particle and matrix respectively. The increase in critical resolved shear stress (CRSS) and its particle size and volume fraction dependence found experimentally by Haberkorn for Al-Zn single crystals (20) was in good agreement with the formula for edge dislocations. They also found that Livingston's (16) results on polycrystalline Cu-Co alloys were in reasonable agreement for the edge dislocation case when a Schmid factor of 0.41 was used. It was concluded that edge dislocations determine the CRSS in both alloys. By considering the angle between the two branches of a dislocation as it bends around a particle it was found that the cutting process ceases when $R \approx 20b$. At this particle size the dislocations start to bow out between the particles according to the Orowan mechanism (21).

The above calculations on the increase in strength resulting from the elastic stress fields of coherent particles have been considerably extended and refined by Gleiter (8,22, 23). In the calculations of Gerold and Haberkorn (18), it was assumed that the dislocation was a straight line in the

vicinity of the particle. Gleiter considered the curvature of the dislocation resulting from its interaction with the stress field of the particles and solved the partial differential equation given by Peach and Koehler (24) for the form of a dislocation line under the influence of applied and internal stresses. The change in effective particle spacing with curvature was also accounted for. As with the results of Gerold and Haberkorn (18) the interaction of edge dislocations with particles was found to control the increase in shear stress at $0^{o}K$ over that of the particle depleted matrix. For an edge dislocation Gleiter (22) found[1]

$$\overline{\Delta\tau} = \left[\frac{27.4\ \varepsilon^3 E^3 b}{\pi T (1+\nu)^3}\right]^{\frac{1}{2}} f^{5/6} R^{\frac{1}{2}}$$

where $\varepsilon = \dfrac{3K\delta}{3K + \dfrac{2E}{1+\nu}}$

E = Young's modulus of matrix

K = bulk modulus of matrix

b = Burgers vector of matrix

f = volume fraction of precipitate

---

[1]The equation in Reference (22) has $(1-\nu)^3$ in the denominator and the one in Reference (23) has $(1+\nu)^3$. $(1+\nu)^3$ is used because the values it gives are much more reasonable than the other. In addition Gleiter's use of the equation as written gives good agreement with experiments.

R = precipitate radius

T = line tension of dislocation $\simeq \frac{1}{2}\mu b^2$

μ = shear modulus of matrix

ν = Poissons ratio of matrix

$\delta = \frac{b_p - b_m}{b_m}$ as before.

Gleiter's results show the strengthening to have an $R^{\frac{1}{2}}$ dependence on particle size as Gerold and Haberkorn found. The major difference is in the dependence on the 5/6 power of the volume fraction where Gerold and Haberkorn found a 1/2 power dependence on f. The two theories however do differ quite a bit in magnitude. If we assume isotropic elasticity holds with $\nu = 1/3$, then

$$\Delta\tau_o \simeq 3\mu|\delta|^{3/2}\left(\frac{Rf}{b}\right)^{\frac{1}{2}} \text{ for Gerold and Haberkorn (18)}$$

$$\overline{\Delta\tau} \simeq 8\mu|\delta|^{3/2}\left(\frac{R}{b}\right)^{\frac{1}{2}} f^{5/6} \text{ for Gleiter (22)}$$

i.e.: the two expressions differ by a factor of $\simeq 3f^{1/3}$ in their value of the strengthening.

The theories of Gleiter (22) and Gerold and Haberkorn (18) only consider the coherency stresses as contributing to the strengthening and obtain fairly good correlation with experiment. It appears then, that the coherency stresses play

the major (if not the entire) role in accounting for the large increases in flow stress observed when a coherent second phase is dispersed in the matrix.

Another source of long range stresses in a matrix containing coherent precipitates is the repulsion (or attraction) a dislocation feels when it is in the vicinity of a region having a shear modulus different than that of the matrix. Fleischer (25) has evaluated this contribution of the flow stress and found it to be approximately

$$\Delta\tau_\mu \cong \frac{\Delta\mu b}{8\pi(1-\nu)x}$$

where $\Delta\mu$ is the difference in shear modulus between particle and matrix.

$\Delta\mu = \mu_p - \mu_m$

ν = Poissons Ratio

x = distance from dislocation to particle.

This approximation is valid if $\Delta\mu \ll \mu_m$. Since the above equation is for a straight dislocation meeting a discontinuity in shear modulus along its entire length, Fleischer (19) has noted that, for the case of a solid containing precipitates, only a part of the dislocation will be interacting with particles. If f is the volume fraction of particles the increase in flow stress will then be approximately

$$\Delta\tau_{\mu} \cong \frac{f^{\frac{1}{2}}\ \Delta\mu b}{8\pi(1-\nu)x}$$

Since the dislocation line is assumed straight x can be considered as 1/2 the interparticle spacing as in the Mott-Nabarro theory, or $x = 1/2N^{-1/3}$, where N is the volume concentration of particles. Since $f = 4/3\ \pi NR^3$, where R is the mean particle radius, the strengthening due to modulus differences between particle and matrix is

$$\Delta\tau_{\mu} \cong \frac{0.050\ \Delta\mu b f^{5/6}}{R}$$

The known dependence of strengthening due to coherent precipitates on $R^{\frac{1}{2}}$ shows the above theory to be inapplicable. As Gerold and Haberkorn (18) have pointed out, however, Fleischer's theory (25) appears to explain much of the strengthening in solid solutions (9,19).

Strengthening due to the long range hydrostatic interactions of dislocations and coherent precipitates has been evaluated by Williams (26) but again, the relation derived shows the strengthening to be dependent only on volume fraction and not on particle size as is the case in Cu-Co and Al-Ag alloys.

B. Short Range Interactions

There are a number of ways a dislocation could interact with a spherical, disordered, coherent precipitate when it is close to the particle (<10b). These interactions are quite important for they may strongly influence both the temperature independent and temperature dependent components of the flow stress. These interactions arise mainly because of the following:

1) Differences in stacking fault energy between matrix and precipitate.

2) Differences in Burgers vector of precipitate and matrix.

3) Increased particle matrix interfacial area produced when particle is cut by dislocation.

4) Non-parallel slip planes in particle and matrix.

5) Different Peierls-force in particle and matrix.

The above mechanisms and their effect on the flow stress will be discussed in turn.

1) Differences in stacking fault energy between particle and matrix.

Hirsch and Kelly (27) have recently considered the strengthening resulting when differences exist in the

stacking-fault energies of the matrix and the precipitates. This is easy to imagine when precipitates having lower stacking-fault energy (SFE) are dispersed in a matrix of higher SFE. The width of extended dislocations in the matrix should be increased when the dislocations enter the particles. Various situations, depending on the relation of particle radius to dislocation width, are possible and only those pertinent to Cu-Co will be presented here.

The theory describes quite well the strengthening observed in Al-Ag alloys where coherency strains are small. It does not, however, adequately describe the strengthening observed in Al-Zn and Cu-Co alloys where coherency strains are large. Some aspects of the theory will be presented at this time, however, because the short range interactions involved will be considered in the discussion of the experimental results pertaining to the temperature and strain rate dependent component of the flow stress in Cu-1.9 wt % Co.

If the SFE of the particles is lower than the SFE of the matrix, dislocations will be attracted to the particles and will experience a friction stress when they pass through them. If the width w_m of an extended dislocation in the matrix is less than the mean particle diameter 2R and 2R is much less

than the width w_p of the dislocation in the particle, it is conceivable that the extended dislocation will fill the area of intersection of the slip plane with the particle. For the above case Hirsch and Kelly gave, for the increase in stress necessary to free the dislocation from the particle, $\Delta\tau_{SFE}$ -

$$\Delta\tau_{SFE} = 2\,\frac{(\gamma_m-\gamma_p)}{b\ l}\,R$$

where γ_m = SFE of matrix

γ_p = SFE of particle

b = Burgers vector of matrix

l = average separation of particles along dislocation.

This case was chosen because, as will be seen, it most closely fits the relation between R, w_m and w_p for Cu-Co.

The interaction energy U_o between the particle and dislocation is, to a first approximation

$$U_o \sim 2R\ w_m\ (\gamma_m-\gamma_p)$$

It is pointed out that this is a lower limit. In order to evaluate l, the interaction energy U_o and the increase in energy due to the increase in length of a dislocation when it passes through a particle are minimized. When this is done and the average spacing l is inserted into the relation for $\Delta\tau_{SFE}$ it is found that

$$\Delta\tau_{SFE} \simeq \frac{(\gamma_m-\gamma_p)^{4/3}\ f^{2/3}}{b_m{}^{5/3}} \left(\frac{w_m}{\mu}\right)^{1/3} \qquad w_m < 2R < w_p$$

If the following values are inserted into the above for a Cu-2% Co alloy,

$$\gamma_m = 40 \text{ erg/cm}^2 \text{ (27)}$$

$$\gamma_p = 10 \text{ erg/cm}^2 \text{ (27)}$$

$$b_m = 2.55 \text{ Å (28)}$$

$$w_m = 23 \text{ Å (27)}$$

$$\mu = 0.40\text{x}10^{12}\text{dyne/cm}^2 \text{ (18)}$$

$$f = 0.02$$

the influence of SFE differences is

$$\Delta\tau_{SFE} \simeq 0.3 \text{ kg/mm}^2$$

This value is much too low to account for the observed strengthening in Cu-Co and Al-Zn alloys. It is, however, the same order of magnitude as the change in flow stress accompanying a change in strain rate in an aged Cu-1.9 wt % Co alloy. This will become apparent when the experimental results are presented. One could speculate that stacking fault strengthening could be the rate controlling dislocation mechanism accounting for the thermal component of the flow stress in these alloys. To be sure, of course, both the strain rate and temperature dependence of $\Delta\tau_{SFE}$ would have to be studied

in detail. One fact that tends to discount the above observation is that when the interaction energy U_o is examined the value obtained is somewhat large to be associated with a thermally activated process. If we take

$$U_o \sim 2R\ w_m(\gamma_m-\gamma_p)$$

and let 2R = 100A as a typical value in aged Cu-2% Co we get

$$U_o \sim 4.3 \text{ ev}$$

which is a lower estimate and is much larger than kT at all but very high temperatures.

2) Differences in Burgers vector of precipitates and matrix.

Fleischer (25) has noted that when the Burgers vector of a matrix dislocation cutting a precipitate differs from that of the precipitate a misfit dislocation having a Burgers vector of magnitude (b_m-b_p) must be left at the interface. However, as Bonar (29) has pointed out, if a discontinuous change in lattice parameter existed at the particle matrix interface, the particles would probably be incoherent and could not be penetrated by glide dislocations. The maximum stress, according to Fleischer (25) due to a gradual change in lattice parameter along the slip plane after n dislocations have passed is

$$\Delta\tau = \frac{n\mu}{2\pi(1-\nu)} \frac{db}{dx} \ln\left(\frac{r_\infty}{b}\right)$$

where μ is the shear modulus

ν is Poisson's ratio

db/dx is the gradient of the lattice parameter at the particle-matrix interface

r_∞ is the extent of the gradient and is >> nb.

Bonar (29) has observed that, when reasonable values for the above parameters are inserted $\Delta\tau \sim n\,\mu/1000$ which could be appreciable. If a particle is completely sheared a loop of interface dislocation will be left around the particle. The stress required to create the loop could contribute strongly to the flow stress. Bonar (29), Kelly and Nicholson (2), and Fleischer (30) have considered this case and have found the stress to be on the order of $\mu/1000$ which is low but appreciable.

3) Increased particle matrix interfacial area produced when a precipitate is cut by a dislocation.

When a coherent, spherical precipitate is cut by a dislocation the portion of the precipitate on top of the glide plane is displaced relative to the bottom portion by an amount equal to the Burgers vector of the glide dislocation. New

particle-matrix interface is produced which requires energy and could thus be a source of strengthening. In addition a loop of misfit dislocation must be left around the precipitate which requires additional energy. Kelly and Nicholson (2) have considered this contribution by equating the work done to move a glide dislocation forward an amount b through the precipitate. If $\bar{d}$ is the average distance between precipitates along the dislocation, their derivation gives

$$\tau b^2 \bar{d} = A_i \gamma_s$$

where τ is the applied stress,

A_i is the interfacial area produced when the dislocation moves forward a distance b,

γ_s is the interfacial energy.

γ_s contains the chemical energy of misfit due to the difference in chemical composition of precipitate and matrix and the energy of the misfit dislocation produced. Kelly and Fine (31) estimated the chemical energy of misfit in Al-Cu and Al-Ag alloys from the heats of reversion of these alloys. Kelly (32) used the following expression for the chemical energy of misfit produced when a dislocation advances a distance b through a spherical precipitate

$$\gamma_s(\text{chem}) \approx \frac{\Delta E}{3b^2}$$

where ΔE is the heat of reversion per solute atom

b is the nearest neighbor separation.

In the case of Al-Ag, γ_s(chem) was found to be $\sim$ 150 erg/cm^2. γ_s(chem) has not been determined for Cu-Co alloys but is probably of the same order of magnitude as that found for Al-Ag.

The component of γ_s due to the creation of misfit dislocation was considered by Kelly and Nicholson (2). They observed the energy per unit length of the dislocation was approximately

$$E_\perp = \frac{\mu |b_p - b_m|^2}{4\pi(1-\nu)} \ln \frac{R}{r_o} .$$

R is the precipitate radius and r_o the radius of the dislocation core which is typically about 5b (33). It is assumed a length b of interface dislocation is produced when the glide dislocation moves forward by the distance b. For Cu-2% Co this energy is $\sim$ 5 erg/cm^2 which is quite low and at least an order of magnitude less than the most conservative estimates of incoherent boundary energies.

It is of interest to examine the total change in energy due to the formation of new interface and misfit-dislocations in order to determine whether the process could be thermally activated.

If R_i is the average particle radius when one particle is

cut, the area of particle-matrix interface produced is about $2R_i b$. The energy of the misfit dislocation loop left behind is approximately $3\mu' |b_m - b_p|^2 R_i$ (2) where μ' is an average shear modulus of the matrix and particle. The total energy change when one particle is cut is

$$E \approx 2R_i b_m \gamma_s(\text{chem}) + 3\mu' |b_m - b_p|^2 R_i$$

If we assume $\gamma_s(\text{chem}) \sim 150$ erg/cm^2

$$R_i \approx 50\text{Å}$$

$$b_m = 2.55\text{Å}$$

$$|b_m - b_p| = 0.033\text{Å}$$

$$\mu' \sim \frac{\mu_m + \mu_p}{2} \approx 6 \times 10^{11} \text{ dyne/cm}^2$$

we find $E \approx 2$ ev. This value is somewhat higher than that expected for a thermally activated process. Of course the value of $\gamma_s(\text{chem})$ is not known but it is expected that it would be at least of the order of magnitude of 100 erg/cm^2. The above mechanism may be important, however, at smaller particle sizes.

4) Non-parallel slip planes in particle and matrix.

Koda, Matsura, and Takahashi (34) have considered the case where the slip planes of the particle and matrix are not parallel. In this case the glide dislocation must jog as it passes through the precipitate. The jog will be sessile and

a length of dislocation must be created at the particle-matrix interface. This has been discussed in detail by Kelly and Nicholson (2) in terms of the trailing dipole left behind the moving dislocation. It is not expected that this mechanism will contribute to the deformation of Cu-Co alloys since both the coherent cobalt-rich precipitates and the Cu matrix have the same crystal structure.

5) Different Peierls-force in particle and matrix.

Gleiter (35) has suggested that the difference in Peierls stress between the particles and matrix could lead to a positive flow stress increment. He has derived the following expression

$$\Delta\tau = \frac{2.6\,\Delta\tau_p^{3/2} f^{1/3} R^{1/2}}{\mu^{1/2} b^{1/2}}$$

where $\Delta\tau_p$ is the difference in Peierls stress between precipitate and matrix

f is the volume fraction of precipitate

R is the mean particle radius

μ is the shear modulus

b is the Burgers vector.

The Peierls stresses of Cu and Co are not known with certainty. Conrad (36) has estimated τ_p for Cu and found it to be about

$1.8 \times 10^{-4}\mu$. τ_p has not been estimated for Co to the author's knowledge.

When reasonable values are inserted into the above equation for Cu-2% Co it becomes:

$$\Delta\tau \simeq 0.05\, \Delta\tau_p^{3/2}$$

Since the yield strength of aged Cu-2% Co is on the order of 5 kg/mm^2, τ_p for Cu is $\sim$ 1 kg/mm^2, and τ_p for Co is probably close to that of Cu, the Peierls stress difference accounts for a negligible contribution of the yield stress. It could, however, account for a significant part of the thermally activated component of the flow stress but the uncertainties in the magnitude and nature of $\Delta\tau_p$ prevent further discussion of this point at this time.

The above long and short range interactions were briefly presented in order to give an idea of the many ways in which glide dislocations can interact with coherent, spherical precipitate particles. Not all the ramifications of the mechanisms presented were discussed, but, where necessary, will be covered in detail in the discussion. Kelly and Nicholson (2), Bonar (29), and Gleiter and Hornbogen (8) discussed other interactions not presented here, especially those dealing with semi-coherent and incoherent precipitates as well as internally

ordered precipitates. To the author's knowledge no evidence of internal order has ever been demonstrated in aged Cu-Co alloys although Bonar (29) considered its presence a possibility.

Since the temperature and strain rate sensitivity of the flow stress in aged Cu-Co alloys is of major concern in this dissertation, some aspects of the thermally activated deformation of metals will now be presented.

C. Thermally Activated Deformation

Since it was observed (7) that the flow stress of metals and alloys could be considered to be composed of an athermal term and a thermal term, considerable effort has been focused on determinations of the dislocation mechanisms responsible for the thermal component (3,37,38). The athermal component of the flow stress reflects the long range interactions between glide dislocations and obstacles and is generally considered to have the same temperature dependence as the shear modulus. The thermal component is both strain rate and temperature dependent and results from short range obstacles whose activation energy is small enough to allow their being overcome by thermal activation. Basically, any study of the thermally

activated component of the flow stress involves the experimental determination of the stress, strain rate, and temperature dependence of the activation energy and activation volume of the rate controlling dislocation mechanism responsible for the thermal component of the flow stress. These parameters are then compared with those derived from theoretical models to determine which model most closely describes the observed mechanical behavior.

Many treatments of the thermodynamics of thermally activated deformation have been given in the literature and are the subject of several reviews (see for instance Conrad (3)). The most rigorous treatments are those due to Gibbs (39,40, 41) and Schoeck (42). An outline of these is given below.

The problem is always treated as a rate process wherein dislocations must overcome barriers dispersed in their glide planes which are characterized by a Gibbs free energy of magnitude ΔG. The strain rate is then

$$\dot{\epsilon} = NAb\nu\, e^{-\Delta G/kT} = \dot{\epsilon}_o e^{-\Delta G/kT}$$

where N is the number of points per unit volume at which dislocations are held up by local (short range) obstacles.

A is the area swept out by a dislocation when an obstacle is overcome

b is the Burgers vector

ν is the frequency at which the dislocation attempts to overcome the barrier.

One may experimentally determine the "activation energy" Q of the process from creep tests in which the temperature dependence of the creep rate is determined by the following,

$$Q = kT^2 \left(\frac{\partial \ln \dot{\varepsilon}}{\partial T}\right)_\tau = \Delta H - T\left(\frac{\partial \Delta H}{\partial T}\right)_\tau + T^2\left(\frac{\partial \Delta S}{\partial T}\right)_\tau$$

where ΔH is the enthalpy change

ΔS is the entropy change

τ is the applied stress.

If the dislocation is considered to surmount a rate controlling free energy "hill", the states at both the bottom of the hill and the top of the hill (i.e., the "excited" state) are states of lowest free energy within the constraints imposed by the crystal. At both states, then, we can say, providing recovery does not occur, that $(d\Delta G)_{\tau,T} = 0$ for all τ,T. It follows that

$$\left(\frac{\partial \Delta H}{\partial T}\right)_\tau = T\left(\frac{\partial \Delta S}{\partial T}\right)_\tau$$

The experimentally determined "activation energy" then is in

reality the activation enthalpy ΔH.

The Gibbs free energy of activation is a function of T and the applied stress τ and is,

$$\Delta G = \Delta U - \tau \Delta V - T\Delta S$$

where ΔU is the internal energy and ΔV is the activation volume. If l is the effective distance between obstacles and d the distance the dislocation must move under the influence of the obstacle before it can glide freely, the activation volume is,

$$\Delta V = l\ b\ d.$$

One way to look at the product $\tau \Delta \bar{V}$, then, is that it is the "total work done by external forces during the activation event" (41).

Since the Second Law holds at both the ground state and the saddle point, for each state we can write -

$$TdS = dU - \tau dV.$$

Hence, by difference -

$$Td\Delta S = d\Delta U - \tau d\Delta V.$$

At constant temperature then -

$$T\left(\frac{\partial \Delta S}{\partial \tau}\right)_T = \left(\frac{\partial \Delta U}{\partial \tau}\right)_T - \tau\left(\frac{\partial \Delta V}{\partial \tau}\right)_T \qquad (1)$$

The above expression can be used to obtain an experimental expression for ΔV.

From

$$\dot{\epsilon} = \dot{\epsilon}_o e^{-\Delta G/kT}$$

we see

$$kT \left(\frac{\partial \ln \dot{\epsilon}/\dot{\epsilon}_o}{\partial \tau}\right)_T = -\left(\frac{\partial \Delta G}{\partial \tau}\right)_T$$

Since $\Delta G = \Delta U - \tau \Delta V - T\Delta S$

$$\left(\frac{\partial \Delta G}{\partial \tau}\right)_T = \left(\frac{\partial \Delta U}{\partial \tau}\right)_T - \Delta V - \tau\left(\frac{\partial \Delta V}{\partial \tau}\right)_T - T\left(\frac{\partial \Delta S}{\partial \tau}\right)_T$$

or

$$kT \left(\frac{\partial \ln \dot{\epsilon}/\dot{\epsilon}_o}{\partial \tau}\right)_T = -\left(\frac{\partial \Delta U}{\partial \tau}\right)_T + \Delta V + \tau\left(\frac{\partial \Delta V}{\partial \tau}\right)_T + T\left(\frac{\partial \Delta S}{\partial \tau}\right)_T$$

Using Equation 1 we have

$$\Delta V = kT\left(\frac{\partial \ln \dot{\epsilon}/\dot{\epsilon}_o}{\partial \tau}\right)_T = 1\ b\ d$$

Hence, the activation volume can be obtained from tensile test data by determining the strain rate sensitivity of the flow stress at constant temperature.

It was shown that the activation enthalpy can be determined from creep tests using

$$Q = kT^2\left(\frac{\partial \ln \dot{\epsilon}/\dot{\epsilon}_o}{\partial T}\right)_\tau = \Delta H$$

where τ is the applied stress. The following indicates how ΔG also may be obtained from differential tensile tests. Writing the above equation in the form -

$$Q = \Delta G - T \left(\frac{\partial \Delta G}{\partial T} \right)_\tau$$

The Helmholz free energy is

$$\Delta F = \Delta G + \tau \Delta V$$

so

$$\Delta G = Q + T \left[\left(\frac{\partial \Delta F}{\partial T} \right)_\tau - \tau \left(\frac{\partial \Delta V}{\partial T} \right)_\tau \right]$$

Since ΔU only varies with temperature as the coefficient of thermal expansion the last term may be neglected. In addition, Helmholz free energy change is the free energy change in the absence of an applied stress and is primarily elastic in nature. To a good approximation, then, ΔF may be considered to be proportional to the shear modulus μ. In light of the above approximations we may write,

$$\Delta G = Q + T \frac{\Delta F}{\mu} \frac{d\mu}{dT}$$

$$= Q + T \left(\frac{\Delta G + \tau \Delta V}{\mu} \frac{d\mu}{dT} \right)$$

Rearranging and collecting terms ΔG is seen to be

$$\Delta G = \frac{Q + \frac{T}{\mu} \frac{d\mu}{dT} \tau \Delta V}{1 - \frac{T}{\mu} \frac{d\mu}{dT}}$$

Since

$$Q = kT^2 \left(\frac{\partial \ln \dot{\epsilon}/\dot{\epsilon}_o}{\partial T} \right)_\tau$$

and is measured by the change in strain rate accompanying a change in temperature in a creep test, the term must be transformed into quantities readily measurable in tensile tests, namely

$$\left(\frac{\partial \ln \dot{\epsilon}/\dot{\epsilon}_o}{\partial \tau}\right)_T \text{ and } \left(\frac{\partial \tau}{\partial T}\right)_{\dot{\epsilon}}$$

Since $\dot{\epsilon} = f(\tau,T)$, if no structural changes occur when $\left(\frac{\partial \ln \dot{\epsilon}/\dot{\epsilon}_o}{\partial T}\right)_\tau$, $\left(\frac{\partial \ln \dot{\epsilon}/\dot{\epsilon}_o}{\partial \tau}\right)_T$, and $\left(\frac{\partial \tau}{\partial T}\right)_{\dot{\epsilon}}$ are measured, only two of the three above quantities are independent and we may write

$$\left(\frac{\partial \ln \dot{\epsilon}/\dot{\epsilon}_o}{\partial T}\right)_\tau = -\left(\frac{\partial \tau}{\partial T}\right)_{\dot{\epsilon}} \left(\frac{\partial \ln \dot{\epsilon}/\dot{\epsilon}_o}{\partial \tau}\right)_T$$

In addition,

$$\Delta V = kT \left(\frac{\partial \ln \dot{\epsilon}/\dot{\epsilon}_o}{\partial \tau}\right)_T$$

Hence, in terms of quantities determined by differential tensile tests ΔG is as follows:

$$\Delta G = \frac{-kT^2 \left(\frac{\partial \ln \dot{\epsilon}/\dot{\epsilon}_o}{\partial \tau}\right)_T \left[\left(\frac{\partial \tau}{\partial T}\right)_{\dot{\epsilon}} - \frac{\tau}{\mu}\frac{d\mu}{dT}\right]}{1 - \frac{T}{\mu}\frac{d\mu}{dT}}$$

Since τ is the applied shear stress, the above equation must be multiplied by a geometrical factor in order to write it in terms of applied tensile stresses. In addition, the constant structure restriction naturally implies the constancy of $\dot{\epsilon}_o$

during all strain rate and temperature changes.

The force-distance curve of a dislocation overcoming a rate controlling obstacle can be approximately determined experimentally by considering the variation in activation volume ΔV with effective stress $\tau - \tau_\mu$ (41,43,44). It will become apparent in the experimental results section of this dissertation that the effective stress cannot be experimentally defined for Cu-Co by the experiments conducted in this investigation. For this reason, force-distance profiles will not be considered in detail. It could be mentioned, however, that once the force-distance profile of an obstacle is determined, either experimentally or theoretically, the temperature dependence of the flow stress can usually be predicted (41, 45). The temperature dependence of the flow stress is not a good indication of the nature of the rate controlling obstacle because, as Ono (45) pointed out, several force-distance relations yield similar flow stress-temperature relationships. This point is of value since many discussions of the nature of the rate controlling obstacles depend heavily on the flow stress temperature relation (45). It would appear that direct comparisons of the experimentally determined temperature and stress dependence of the activation volume and energy with

those predicted from models are the best ways to decide on the rate controlling obstacle.

Spherical, coherent precipitates present energy profiles that are relatively independent of stress. In other words, a coherent precipitate is a good example of a rigid barrier. In this case the Helmholz free energy at absolute zero ΔF_o can be considered to be independent of the effective stress (41). Mott and Nabarro (6) have determined the stress dependence of the activation energy for a solid containing rigid obstacles and arrived at the following equation, modified slightly by Gibbs (41).

$$\Delta G(\tau) = \Delta F_o^* \left[1 - \frac{\tau - \tau_\mu}{\tau_o - \tau_\mu} \right]^{3/2}$$

where ΔF_o^* is the Helmholz free energy change at 0^oK associated with a rigid barrier in which the term due to the long range internal stresses i.e.: $\tau_\mu \Delta V$ is absent.

τ is the applied stress

τ_μ is the long range internal stress

τ_o is the flow stress extrapolated to 0^oK

A derivation of the above relation is given in detail by Kelly and Nicholson (2) and will not be given here. It is the purpose of this discussion to illustrate how the activation volume and temperature dependence of the flow stress may be

found if ΔG is known as a function of stress. At $0^{o}K$ when no thermal activation can take place

$$\Delta G_{\tau=0,\tau=\tau_o} = \Delta F_o^* - \alpha(\tau_o - \tau_\mu)\Delta V_o$$

and

$$\Delta F_o^* = \alpha(\tau_o - \tau_\mu)\Delta V_o$$

where α is a parameter describing the shape of the energy profile.

Since $\Delta V = -\left(\frac{\partial \Delta G}{\partial \tau}\right)_T$

$$\Delta V = \frac{3}{2}\frac{\Delta F_o^*}{\tau - \tau_\mu}\left[1 - \frac{\tau - \tau_\mu}{\tau_o - \tau_\mu}\right]^{\frac{1}{2}}$$

or

$$\Delta V = \frac{3}{2}\alpha \Delta V_o\left[1 - \frac{\tau - \tau_\mu}{\tau_o - \tau_\mu}\right]^{\frac{1}{2}}$$

which shows the stress dependence of ΔV when ΔG is known. ΔV is predicted to depend on the 1/2 power of τ when the obstacle is rigid.

Since $\dot{\epsilon} = \dot{\epsilon}_o e^{-\frac{\Delta G}{kT}}$ it can be shown that

$$\tau - \tau_\mu = (\tau_o - \tau_\mu)\left[1 - \left(\frac{kT \ln \dot{\epsilon}_o/\dot{\epsilon}}{\Delta F_o^*}\right)^{2/3}\right]$$

or

$$\tau = \tau_\mu + \alpha\frac{\Delta F_o^*}{\Delta V_o}\left[1 - \left(\frac{kT \ln \dot{\epsilon}_o/\dot{\epsilon}}{\Delta F_o^*}\right)^{2/3}\right]$$

We see then that the flow stress should vary with the 2/3

power of T in a solid containing rigid barriers. This has been found to be the case in the Al-Cu system (46), the Al-Ag system (15), and the Al-Zn system (15) all aged to contain coherent precipitates. The exact form of the barrier (i.e., the parameter α) is not implicit when $\tau - T^{2/3}$ relation is found, however, and Mott (47) pointed out that this behavior is expected as long as the energy profile of the barrier is a smoothly varying function of distance. This is also apparent from the fact that Seeger (48) picked a different barrier profile and arrived at the same $\tau - T^{2/3}$ law. In fact the Mott-Nabarro energy profile was sinusoidal and the Seeger profile was exponential. Gibbs (41) noted, however, that $\tau - T^{2/3}$ behavior is not universal and will only hold when the activation distance is proportional to the term under the square root sign in the above expression for ΔV, i.e. when

$$d \propto 1 - \frac{\tau - \tau_\mu}{\tau_o - \tau_\mu}$$

It can be concluded, in light of the existing theories (2,6,41,45,47,48) of thermally activated deformation of metals containing spherical, coherent precipitates that, although the exact form of the energy barrier is still unknown (it was assumed in all cases), if it is a smooth function of distance,

the flow stress-temperature curve will obey a $T^{2/3}$ law. It should be noted here that the theories all assume τ_μ varies with temperature as the shear modulus μ does. In the next section it will become evident that this is not the case for an aged Cu-2% Co alloy and, in fact, the variation of τ_μ with temperature has not been determined. This prevents a complete study of the nature of the rate controlling obstacles in Cu-Co and forces attention to be focused on the activation volume only.

D. The Mechanical Properties of Cu-Co Alloys

The Cu-Co phase diagram is shown in Fig. 1 (49). Cu-rich Co alloys have been known to exhibit precipitation hardening for some time (50) but have only been studied in detail recently. An early metallographic study (51) did not reveal the hardening phase which is now known to be coherent with the matrix. The precipitates are paramagnetic (52) and the precipitate size, spacing, volume fraction, and morphology can be studied by magnetic methods. Magnetic studies of the Cu base alloys containing 1-3 wt % Co have shown that the precipitate is f.c.c., initially spherical, coherent with the matrix and contains about 10% Cu in solution (53-58). The spherical precipitate becomes octahedral in shape and incoherent only after

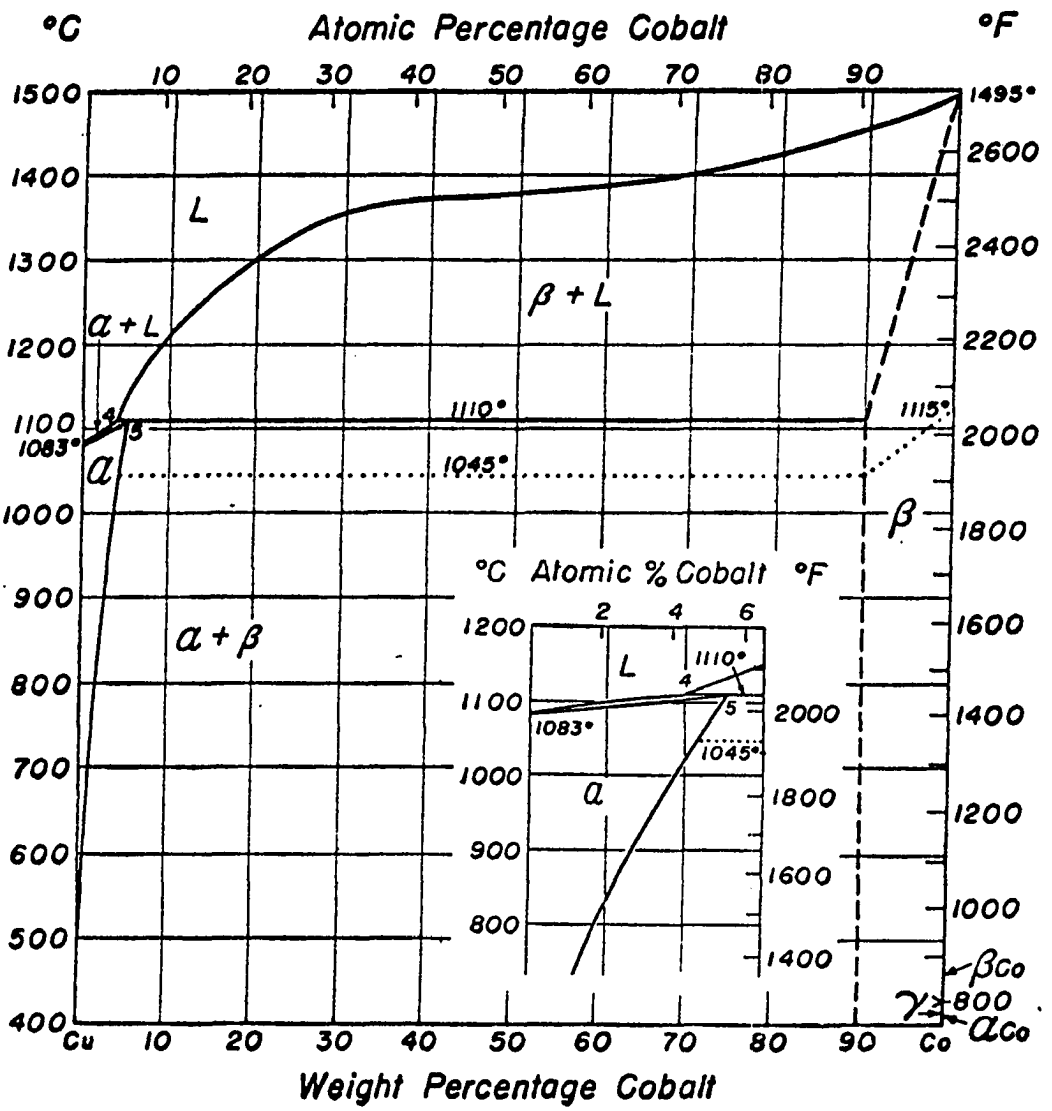

Figure 1. Copper-cobalt phase diagram taken from the 1948 edition of the ASM Metals Handbook

long aging times (5,29). The details of the magnetic methods to measure precipitate size and spacing will be covered in the section on experimental procedures. The magnetic studies also demonstrated that the volume fraction of precipitate remains essentially constant after short aging times and Livingston (16) has shown that the aging kinetics are in accord with Greenwood's (59) expression for the coarsening of a constant fraction of nucleated particles.

Some discontinuous precipitation occurs during aging of quenched polycrystals (5,51) but the amount is, in general, small.

The metallography of aged Cu-Co alloys has been studied in detail recently by electron microscopy and many of the results arrived at by magnetic studies have been confirmed by direct observation. Phillips (5) has extensively studied particle growth in a Cu-3.1 wt % Co alloy solution treated at 965° and 990°C and aged at 600° to 750°C. It was found that the nucleated phase was the stable phase and remained coherent to aging times much exceeding that for peak strength. In addition it was found that, as long as the particles were coherent they remained spheres. The coherent precipitates can be resolved at diameters of about 15 to 30 Å by transmission

electron microscopy. Resolution of the coherent particles is possibly due to the diffraction effects associated with the strain fields of the particles (10,60,61). Bonar and Kelly (2,29) have studied a Cu-2 wt % Co alloy aged at 600°C and also found the particles to remain spherical and coherent to aging times past peak hardness. Both Bonar and Kelly (2) and Phillips et al. (62) have noted that the agreement between magnetically measured particle sizes and those obtained from transmission electron microscopy is good. Tanner and Servi (63) noted, from observations by transmission electron microscopy, along with Phillips (5) that particles as large as 500Å in diameter remain coherent in aged Cu-1 to 3 wt % Co alloys. This is five times the size at peak hardening.

Servi and Turnbull (64) studied the aging kinetics of Cu-1 to 2.69 wt % Co alloys by quenching from the solution temperature to the aging temperature and, by the arguments of classical nucleation theory, deduced that the interfacial energy of the coherent precipitates is 190 erg/cm^2. In addition Ashby and Brown (10) analyzed the diffraction contrast around coherent precipitates in an aged Cu-2 wt % Co alloy in terms of the dynamical theory of electron diffraction and determined that the misfit between the precipitates and matrix

is -0.013 ± 0.002. In light of the above, it is apparent that Cu-Co alloys are ideal for studying the relation of mechanical properties to structure because the characteristics of the aged state have been studied extensively and are well defined.

Both Livingston (16) and Phillips (5) have studied the mechanical properties of aged Cu-Co alloys. A Cu-2% Co alloy aged at 600°C was found to reach peak strength, measured at room temperature, after about 1000 min. aging time (16). Livingston found that alloys containing varying amounts of Co aged at different temperatures all reached peak strength at a particle radius of about 70Å which was then interpreted as indicating that coherency stresses were the major causes of strengthening in the alloys. In addition, the critical particle size was taken to be indicative of the size corresponding to maximum internal stresses. Loss of coherency is initiated at this critical size. Phillips (5) conducted similar experiments and found no correlation between peak hardness and particle size and suggested that a critical particle spacing might be the criterion for peak hardness. It has already been mentioned in conjunction with Gleiter's (8,22,23) theory that both size and spacing must be taken into consideration if the strengthening is to be attributed to the coherency stresses around the particles. Bonar (29) explained

the strength of his aged crystals in terms of the sum of many contributions arising from long range forces, stacking fault strengthening, disordering of the particles, etc. Although the contributions qualitatively explained the increase in strength with aging time, quantitative correlation would be difficult.

The only study of the temperature dependence of the flow stress of an aged Cu-Co alloy known to the author is that due to Phillips (28). Phillips studied the temperature dependence of the flow stress of a Cu-3.12 wt % Co alloy by performing temperature change tests similar to those run by Cottrell and Stokes (65) and by expressing the results in terms of the reversible flow stress ratio at the two temperatures $\sigma_{T_2}/\sigma_{T_1}$ as a function of strain. His data showed quite an unexpected result. The flow stress ratios $\sigma_{T_1}/\sigma_{303^oK}$ for $T_1 < 303^oK$ extrapolated to zero strain were less than unity for aging times greater than a few minutes at 650°C indicating that the material became weaker at lower temperatures. This phenomenon was rationalized on the basis of the argument that the differences in thermal expansion of the precipitates and matrix permit the mismatch to decrease upon cooling. The resulting decrease in coherency strain fields then decreased the com-

ponent of flow stress attributed to these strain fields. It was shown that, if the flow stress could be considered to be composed of components due to solid solution hardening, dislocations, modulus differences, and coherency strains, the decrease in the coherency strain component accompanying cooling overshadowed the increases in the other components. The weakening was greatest in specimens aged to peak hardness. Furthermore, the Cottrell-Stokes ratio $\sigma_{T_2}/\sigma_{T_1}$ after a few percent strain was observed to approach that of pure copper. The constancy of volume fraction of precipitate indicated by magnetic methods was not corroberated by measurements made on transmission electron micrographs. Bonar (29) observed this discrepancy also. Because transmission electron microscopy can only resolve particles down to 15-30Å in diameter and the magnetic measurements can detect particles almost down to atomic dimensions the apparent discrepancy may simply reside in the lack of resolution of smaller particles by microscopy.

To the author's knowledge no investigation of the strain rate sensitivity of the flow stress of aged Cu-Co alloys has been attempted other than that contained in this dissertation.

III. EXPERIMENTAL PROCEDURE

A. Alloy Preparation

The 2½ pound ingot of copper- (nominally) 2 wt % cobalt used in this investigation was prepared from 99.999 copper cathode plate obtained from Cominco Products Inc. and 99.9 reactor grade cobalt rod 1/4 inch in diameter obtained from Kulite Tungsten Co. A typical analysis of the cobalt rod is given below.

Co	99.9 wt % including Ni
Ni	0.2-0.3
Cu	0.005
Fe	0.002
S	0.001
C	0.012

The copper plate was vacuum induction melted in a graphite crucible and then rod rolled and swaged into 1/2 inch diameter rods. Three of these rods were then bundled together with a cobalt rod having the proper diameter to yield a Cu-2 wt % Co alloy. The bundle, in the position of the electrode in a consumable electrode arc melting furnace, was melted into a graphite crucible under a static atmosphere of argon. The resulting ingot was rod rolled and swaged into a 3/4 inch

diameter rod which was then cut into four 1/2 inch long pieces. The pieces were homogenized for 7 days at 950°C under flowing dried nitrogen and quenched in water. All steps in the above procedure were preceded with a thorough cleaning in 50% nitric acid and water followed by a water and acetone rinse. It will be shown in Section IV that the actual composition of the alloy was Cu-1.9 wt % Co.

B. Specimen Preparation

1. Polycrystalline tensile specimens

All tensile testing of polycrystalline material was performed on wire specimens having a nominal diameter of 0.060 inches. To form the specimens the 3/4 inch diameter, homogenized Cu-1.9 wt % Co rod was swaged to 0.300 inches diameter, bright dipped in 50% nitric acid and water, and vacuum annealed at 600°C for 1 hour. It was then swaged to 0.065 inch diameter wire and cut into 2 inch long pieces for subsequent testing.

The specimens were solution treated and recrystallized at 970°C $\pm$ 10°C under flowing, dried nitrogen and quenched in iced brine. The furnace contained a graphite block with holes in it for the wires which decreased any temperature gradients and facilitated quenching. Timing was started when, following loading of the furnace, the cold graphite block reached 950°C.

Typically the block temperature reached 980°C one hour after it passed 950°C. For this reason, the solution temperature is quoted as 970°C.

The solution treated wires were cleaned in a 25% nitric acid and water etch to remove the oxidation picked up during the quench and then either prepared for testing or aged. All aging was carried out under flowing, dried nitrogen at 600°C in a furnace identical to the one used for solution treating. The specimens were also placed in holes in a graphite block in the aging furnace but, in this case, the graphite block was always kept at 600°C to shorten the heat up time following loading which was, typically, 5 minutes. Both furnaces were controlled with proportioning controllers.

In order to prepare the heat treated 0.065 inch diameter wires for testing, 1/2 inch lengths at each end were coated with a non-conducting lacquer. This left a one inch gauge length exposed. The wires were then electropolished in a well stirred solution of 1/3 nitric acid and 2/3 methyl alcohol maintained at about 0°C by a bath containing methyl alcohol and ice. Polishing was carried out at a current density of 1/2 amp/cm^2. The wires were continually rotated and periodically turned end for end during polishing to eliminate any

taper in the gauge length. Following electropolishing the gauge lengths typically measured 0.060 ± .0002 inches.

2. Single crystal tensile specimens

a. Growth In order to prepare single crystals for subsequent tensile testing the 3/4 inch diameter Cu-1.9 wt % Co rod was swaged to a 0.300 inch diameter, cleaned in 50% nitric acid and water, and vacuum annealed at 600°C for one hour. It was then swaged to a 0.113 inch diameter and cleaned again in nitric acid and water. Pieces of this rod 9-1/2 inches long were then placed in a 12 inch long 1/8 inch diameter cavity in a split graphite mold along with a 2-1/2 inch long seed crystal. The seed crystal was necessary to insure that all crystals tested were of a similar orientation, namely an easy glide orientation. There were two cavities in the mold which enabled two crystals to be grown simultaneously during each run.

The crystals were grown from the melt by a modified Bridgman technique in the apparatus shown schematically in Figure 2. The split graphite mold was screwed to a vertical water cooled stainless steel pedestal attached to a brass base plate and then covered with a closed end alumina tube attached to the base plate by a water cooled brass flange. All runs

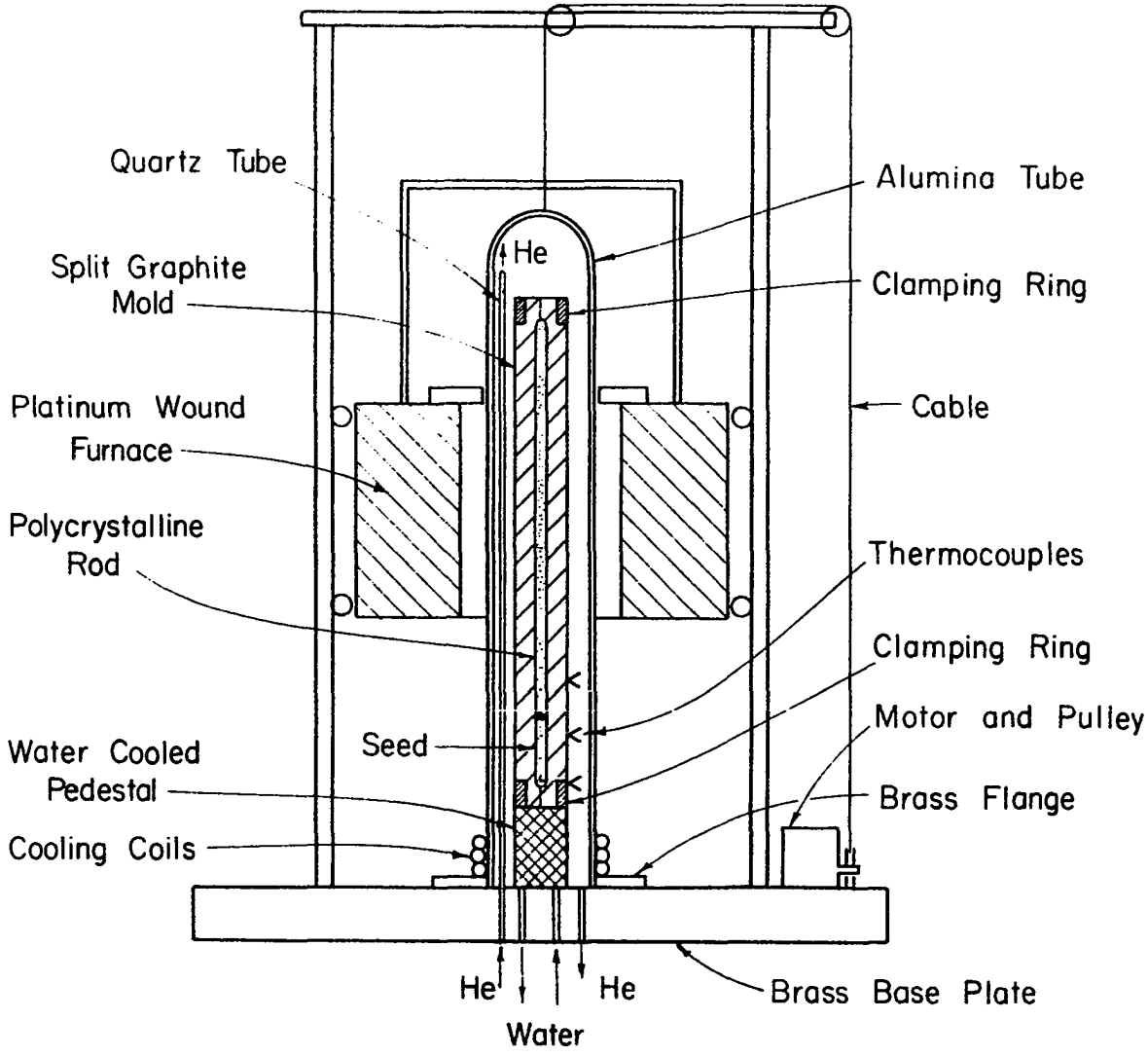

Figure 2. Schematic of crystal growing apparatus

were made under flowing helium which entered near the top of the mold through a quartz tube and exited through a hole in the base plate. To start a run the platinum-13% rhodium wound furnace was lowered to a position near the bottom of the mold and then heated to around 1400°C. When approximately one-half of the seed crystal melted, as noted by thermocouples placed in holes in the graphite mold at 1 inch intervals, the furnace was pulled upward by the motor and pulley system thus starting growth. The water cooled pedestal provided a steep temperature gradient in the vicinity of the seed and prevented its complete melting. The temperature in the mold away from the seed was typically about 1250°C. Most crystals were grown at a rate of 100 mm/hr although some were grown at 33 mm/hr. No differences in mechanical behavior were noted that could be attributed to growth rate.

Each run yielded two 1/8 inch diameter crystals about 9-1/2 inches long[1]. The bottom 2-1/2 inches of each was cut off to seed subsequent runs. Two 3 inch long sections were cut from the middle portion of each for tensile specimens and the

---

[1]Following each crystal run, prior to cutting, the as-grown crystals were etched in a 50% HCl-50% saturated $FeCl_3$ in water solution to reveal grain boundaries. All crystals showing grain boundary formation were discarded.

remainder discarded. Each run, therefore, yielded four 3 inch long, oriented single crystals. All cutting was done with a Servomet spark cutter using a wire electrode.

The crystals were then given a bright dip in 50% nitric acid and water and homogenized for 7 days at $1025^{o} \pm 10^{o}C$ under flowing dried nitrogen. The same graphite block and furnace used for the solution treatment of the polycrystalline material was used for the single crystals. Following the homogenization and solution anneal the crystals were quenched in iced brine. Aging was carried out under the same conditions as those used for the polycrystalline material; namely $600^{o}C$ under flowing, dried nitrogen followed by an iced brine quench.

One-half inch sections at each end of the crystals were masked with non-conducting lacquer and the 2 inch gauge lengths electropolished in the manner used for the polycrystals. Electropolishing was continued until the diameters of gauge lengths were typically 0.100 inches. Frequent end for end reversing of the specimens in the polishing bath kept the variation in diameters along the gauge lengths to less than 0.002 inches in all cases.

The orientations of the polished crystals were checked

by standard Laue X-ray techniques. A Laue photograph was made of every crystal grown to insure that the orientations were uniform.

C. Optical Metallography

Prior to metallographic examination specimens were ground on 600 grit paper and then electropolished in a 1-2% by volume solution of sulphuric acid in ethyl alcohol maintained at dry ice and acetone temperature. They were then etched in Girards No. 2 reagent (24 parts $FeCl_3$, 25 parts HCl, and 100 parts water by volume) and examined.

Grain size determinations were made at 50X on cross sections taken in the grip sections of the tested polycrystalline wires.

D. Particle Size Measurements

1. Polycrystals

To determine the average sizes of the cobalt rich precipitates in the aged material it was first necessary to determine the initial susceptibilities and saturation magnetizations corresponding to each aging time of interest. Initial susceptibilities were measured at 33 cps in a low field mutual inductance apparatus designed by Gerstein (66). Measurements

were made at 300°K in a field of approximately 10 gauss. It was further determined that the susceptibilities so measured were not frequency dependent. The samples were 1/2 inch long pieces taken from the gauge lengths of untested wire tensile specimens. Measurements were made on solution treated specimens aged 30, 50, 100, 300, 500 and 1000 min. at 600°C.

Saturation magnetizations were determined from high field magnetization curves run on 1/8 inch long pieces of the same specimens. Measurements of the induced moments were made in fields ranging from 1 to 16 kilogauss in a vibrating specimen magnetometer designed and constructed by Miller (67). All measurements were taken at room temperature. The saturation magnetization was determined by plotting the magnetization vs. the reciprocal of the applied field and extrapolating to infinite field. The apparatus was calibrated with a nickel sample at saturation.

2. Single crystals

The particle sizes in aged single crystals were measured by the same equipment and methods as given above. Measurements were made at 300°K on samples aged 5, 30, 50, 100, 300, 500, and 1000 min. at 600°C.

E. Tensile Testing

1. Polycrystals

a. Stress-strain tests All tensile testing was carried out with an Instron Model TTC floor model testing machine. The polycrystalline wire specimens were held in pin vise grips with serrated collets to prevent slipping. The unpolished portion at each end of the specimens was gripped thus leaving the electropolished one inch gauge length exposed. A Polanyi-type cage fastened to the crosshead of the Instron enabled the specimens to be immersed in suitable low temperature baths during testing. The constant temperature baths used and their nominal temperatures are shown below.

Methyl alcohol and ice	247°K[1]
Dry ice and acetone	200°K[1]
Frozen acetone	178°K[1]
Frozen 2-chloropropane	156°K[1]
Liquid nitrogen	77°K

Although some testing was carried out in the constant temperature baths at temperatures above 77°K, it was felt that

---

[1]These baths gave some variation in testing temperatures from those given above but during any single test the temperature remained constant to ± 1°C.

a better spread of testing temperatures could be obtained in cold isopentane. For this reason, most tests carried out at temperatures above 77°K were run with the specimen immersed in a dewar of isopentane that was cooled by liquid nitrogen being blown through copper tubing coiled around the inside of the dewar. During cooling stirring was accomplished by bubbling the exit gas from the copper coil through the isopentane. Once the desired temperature was reached the bath was quite stable and the drift in testing temperature was less than $\pm$ 1°K during the course of a run. The isopentane bath was used for all tests run at 133, 188, and 244°K.

Temperatures were measured with a copper-constantan thermocouple placed 1/2 inch from the center of the specimen. In all cases temperatures were maintained to $\pm$ 1°K in both the constant temperature baths and the cooled isopentane bath.

Constant strain rate tests were run on the polycrystalline specimens at strain rates of 8.33×10^{-5} sec^{-1} and 1.67×10^{-4} sec^{-1}. In all tests a stepped zero suppression control on the Instron enabled the load scale to be expanded thus increasing the sensitivity of the load readings on the load-elongation trace. The load elongation data were transformed into true stress-true strain data through the use of an IBM

7094 computer which both tabulated and plotted the data. Since an extensometer was not used the deflection of the machine had to be subtracted from the extension indicated on the load-extension trace. For this reason the load-deflection curve of the machine was determined and periodically checked. This curve was then incorporated into the computer program used for the true stress-true strain data computation. Generally the machine deflection curve was determined before each series of tests. It was found that it was adequate to determine the machine calibration only at room temperature because machine deflection curves obtained with the Polanyi cage at $77^{o}K$ were essentially identical to those obtained at room temperature.

b. Strain rate change tests Strain rate change tests were made in this investigation to study the strain rate sensitivity of the flow stress. In a strain rate change test the specimen was typically extended to one percent strain at a base strain rate of 8.33×10^{-5} sec^{-1} at which time the strain rate was increased by a push button cross-head speed control on the Instron. After extension at the higher strain rate exceeded about one percent strain the cross-head speed was reduced to the base strain rate by the push button control.

This alternating process was then continued until uniform elongation was reached. All strain rate change tests made in this investigation on polycrystals used a strain rate ratio of 20:1. Since the quantity of interest in these experiments is the instantaneous change in load accompanying a change in strain rate, the load scale was expanded by use of the stepped zero suppression control thus increasing the sensitivity of the load change measurement. Since a typical load change accompanying a twenty fold increase in strain rate is 1 pound for an age hardened 0.060 inch diameter Cu-1.9 wt % Co polycrystalline wire, the zero suppression was set for 20 pounds full scale. The Instron uses a 10 inch chart so the sensitivity of the load reading is $\pm$ .05 lb. This means the changes in loads were typically measured to 5% which was quite adequate in this case.

In order to maintain the same ratio of chart speed to cross-head speed the chart speed and cross-heat speed were changed simultaneously during the experiments.

c. Temperature change tests Changes in flow stress accompanying changes in temperature at constant strain rates were measured to allow calculations of apparent activation energies. These measurements were carried out at a strain

rate of 8.33×10^{-5} sec^{-1}. All tests were started with the specimen immersed in a stirred alcohol bath maintained at $300^{o}K \pm .5^{o}K$ by a Philadelphia Micro-Set mercury contact control that actuated an immersion heater in the bath. Overshoot was minimized by the presence of copper cooling coils carrying a continual flow of cold water.

In a typical test the specimen was extended about 1.5 percent strain at $300^{o}K$ at which point the test was stopped and the specimen unloaded to 5 pounds to maintain axial alignment of the loading fixtures. The testing temperature was then changed by quickly replacing the alcohol bath with a dewar containing an appropriate bath (e.g. dry ice and acetone). When equilibrium was reached, testing was resumed and the specimen was extended about 1.5 percent strain at the lower temperature and then unloaded to 5 pounds again. The low temperature bath was then quickly replaced by the $300^{o}K$ alcohol bath and, when the heaters in the alcohol bath shut off, testing was resumed at $300^{o}K$ for another 1.5 percent strain. This process was repeated until uniform elongation was reached.

A typical cooling time from $300^{o}K$ to a lower testing temperature was 5 minutes. When the baths were changed the rapid

temperature changes caused the applied 5 lb. load to fluctuate wildly due to expansions and contractions occurring in the Polanyi cage members and pull rod. These were counteracted by the continual adjustment of the cross-head position with a manual control located on the Instron control panel. In this way it was possible to maintain the 5 lb. load during the change.

In many cases the load extension curve following a decrease in temperature exhibited a yield point. When this occurred the recorded change in load was taken to a point on the load-extension curve extrapolated through the yield point and intersecting the elastic portion of the reloading curve.

2. Single crystals

a. Stress-strain tests The crystals were held with split jaw grips having serrated faces to prevent slipping. One-half inch at each end was gripped leaving the 2-inch electropolished gauge length exposed. The grips were attached to yokes on the pull rod and Polanyi cage by pins. The top yoke threaded into the pull rod and the bottom one was secured to the bottom plate of the Polanyi cage by a spherical nut which sat in a spherical depression in the plate. This provided better axial alignment of the testing assembly and lessened

the chance of introducing bending moments in the crystal during testing.

A mounting jig was used when the crystals were affixed to the grips to prevent accidental damage while the grip faces were tightened. After mounting the grips, the crystals were carefully inserted in the machine. Prior to testing the slack was always taken up and a small load on the order of 1 to 2 lbs. applied. The cage was then lightly tapped to set all load bearing surfaces while the small pre-load was maintained. This insured axial alignment during the early part of the test. For the single crystal tests, temperatures above 77°K and below 300°K were all obtained with the isopentane bath described previously. All constant strain rate tests were run at a strain rate of 4.17×10^{-4} sec^{-1}.

b. Tensile axis orientations The crystals were all seeded to give easy glide orientations of the tensile axes, i.e. all in the center of the [001], [011], [$\bar{1}$11] stereographic triangle. Although the orientations varied slightly from crystal to crystal all had a tensile axis orientation near 23° from [001] and 27° from [011]. The orientations of all crystals tested will be given in the Results in both graphical and tabular form.

c. Calculation of stress-strain curves All stress-strain data obtained on single crystals is reported as resolved shear stress on the slip plane in the slip direction versus glide strain in the slip direction. The crystals were assumed to slip on the (111) plane in the $[\bar{1}01]$ direction for purposes of computation. As will be shown later this assumption appears to be valid along most of the stress-strain curve since extensive overshoot was encountered in all tests and conjugate glide, if present, did not occur to the extent that the tensile axis deviated from the great circle connecting its initial position and the $[\bar{1}01]$ direction during a test.

Resolved shear stress-glide strain curves were obtained from load-elongation data according to the well known derivation of Schmid and Boas (68). The equations used are given below.

$$\tau = \frac{P}{A_o} \cos\phi_o \cos\left[\sin^{-1}\left(\frac{\sin\lambda_o}{d}\right)\right]$$

$$\gamma = \frac{1}{\cos\phi_o}\left[(d^2 - \sin^2\lambda_o)^{\frac{1}{2}} - \cos\phi_o\right]$$

where τ = resolved shear stress

γ = resolved shear strain

P = tensile load

A_o = original cross sectional area

ϕ_o = initial angle between slip plane normal and tensile axis

λ_o = initial angle between slip direction and tensile axis

$d = 1 + \epsilon = l_1/l_o$ where ϵ = engineering tensile strain,

l_1 = instantaneous length and

l_o = initial length.

All resolved shear stress-glide strain calculations were carried out on an IBM 7094 computer which both tabulated and plotted the data. Since crosshead motion was used to measure specimen extension, the machine extension curve was incorporated into the program which then subtracted it from the measured total elongation to give the correct specimen elongation at all values of loads. The load-deflection curve of the machine was determined before each series of runs using a non-deforming specimen.

d. Strain rate change tests Strain rate sensitivity parameters were determined on the single crystals using a base strain rate of 1.67×10^{-6} sec^{-1} and a strain rate ratio of 25:1 during the strain rate changes. It will be seen in Section IV that the age hardened crystals yielded discontinuously for about 10% glide strain. When this occurred strain

rate changes were always made after this region of the stress-strain curve was passed.

F. Resistivity Measurements

Measurements on the electrical resistivity of Cu-1.9 wt % Co polycrystalline wires were made at temperatures ranging from 77° to 300°K as a function of aging time in order to clarify some anomalies in the temperature dependence of the strain rate sensitivity. The specimens were 12 inches long, 0.020 inch diameter wires that were drawn down from 0.065 inch diameter tensile specimen blanks. They were solution treated 1/2 hour at 950° ± 5°C under flowing, dried argon and quenched in iced brine. Aging was accomplished in the same furnace under flowing argon at 600° ± 5°C and was followed by an iced brine quench. The heat treated wires were cleaned in 30% nitric acid and water and soldered to the current and potential leads of a specimen holder which enabled the specimens to be immersed in a dewar of stirred isopentane cooled by passing liquid nitrogen through copper coils lining the dewar.

Resistance measurements were made by standard potentiometric techniques using a Leeds and Northrup Type K-3 potentiometer and null detector. The specimen current was typically 1.06 milliamps and was supplied by an ordinary automobile

storage battery. Measurements of voltage drop were made with the current flowing in both the forward and backward directions in order to cancel any effects caused by the presence of thermal and contact emfs. The two readings were then averaged. Generally about four readings were taken at each temperature. Temperatures were measured to the nearest degree Kelvin by a copper-constantan thermocouple placed near the specimen.

At least 35 measurements were made of the diameter at 1/4 inch intervals along the specimen with a micrometer to accurately determine its cross sectional area. The potential leads were typically 11-1/2 inches apart.

Each run was started at $300^{o}K$. The temperature was periodically lowered in about $10^{o}K$ intervals by allowing liquid nitrogen to be blown through the coils for a short period of time. After the nitrogen was turned off the temperature dropped some more, leveled off for a while, and then started to rise again. All measurements were made on the "plateau" of the cooling curve.

IV. EXPERIMENTAL RESULTS

A. Chemical Analyses and Grain Sizes

1. Chemical Analyses

a. Polycrystals Random samples taken from tensile tested polycrystalline wires were analyzed for C, O, H, N, and Co. These results are given in Table 1.

Table 1. Chemical analyses of Cu-Co polycrystalline wires

Specimen	O ppm	H ppm	N ppm	C[a] ppm	Co[a] (wt %)
1000-3	35	1	<1		
300-5	48	1	<1		
50-5	38	<1	<1		
STDA-12	51	1	<1		
STDA-12	28	<1	<1		
STB-10	22	<1	<1		
STB-4	20	<1	<1		
STA-8	15	<1	<1		
STA-2	19	<1	<1		
ST-12	27	1	<1		
100-2				60	
STDA-6				22	
STB-11				20	
ST-10				68	
STA-10				15	
STDA-7					1.92
STDA-2					1.93
1000-4					1.90
300-4					1.93
100-1					1.96
30-1					1.94
STB-19					1.86
STB-13					1.92

[a]Averages of two readings.

Table 1. (Continued)

Specimen	O ppm	H ppm	N ppm	C[a] ppm	Co[a] (wt %)
STB-7					1.91
STB-1					1.98
STA-14					1.93
STA-8					1.91
STA-2					1.90
ST-12					1.92
ST-6					1.93
ST-3					1.91

It is apparent that the preparation and handling of the polycrystalline wires did not introduce any serious amounts of impurities (30 ppm O average and 37 ppm C average). The Co analyses show the alloy to be Cu-1.9 wt % Co. The Co analyses show that the ingot was quite homogeneous.

A qualitative spectroscopic analysis was also run on a piece of the polycrystalline ingot to check for the presence of metallic impurities. These results are given in Table 2.

Table 2. Qualitative spectroscopic analysis of Cu-Co polycrystal

Element	Analysis	Element	Analysis
Ag	not detected	Pb	faint trace
As	not detected	Sb	not detected
Bi	faint trace	Si	trace
Fe	trace	Sn	not detected
Mn	very weak trace	Te	trace
Ni	very weak	Zn	not detected
P	not detected		

Evidently the ingot was fairly pure and free from metallic impurities.

b. Single crystals Table 3 shows similar results of analyses on tested single crystal tensile specimens.

Table 3. Chemical analyses of Cu-Co single crystals

Specimen	O ppm	H ppm	N ppm	C[a] ppm	Co[a] (wt %)
X-0-3	10	1	N.D.	24	1.92
X-0-6	7	<1	<1	18	2.00
X-5-1	7	<1	N.D.	27	1.94
X-30-1	8	<1	N.D.	41	1.91
X-100-1	14	1	N.D.	31	1.84
X-300-b	6	<1	N.D.	42	2.03
X-500-3	17	2	N.D.	27	1.98
X-1000-1	12	1	N.D.	32	1.92
X-1000-6	41	N.D.	N.D.	65	1.93

Except for slightly less oxygen probably resulting from better handling during loading and quenching from the annealing furnaces, the chemical analyses on single crystals gave essentially identical results to those obtained on polycrystals namely 1.9 wt % Co and 34 ppm C. The average oxygen content for the single crystals analyzed was 13 ppm.

To determine the homogeneity of the crystals being grown, a 7-1/2 inch long as-grown crystal was cut into 1/2-inch long pieces each of which was analyzed for Co. The average Co con-

tent was 1.92 wt % and the largest deviation from this value was 0.13 wt % Co. In other words the as-grown crystals were quite homogeneous along their length.

2. Grain sizes

Grain size determinations were made on a number of transverse cross-sections of wires. The grain sizes were determined by a standard intercept method and are given below.

Specimen	Grain size (mm)	Specimen	Grain size (mm)
ST-1	.19	STDA-8	.13
ST-15	.25	STDA-13	.11
ST-9	.13	100-4	.28
STA-1	.10	500-4	.32
STA-8	.16	STB-4	.28
STA-15	.14	STB-10	.28
STDA-1	.17	1000-5	.18
		Average	.19

The grain size can be typically taken to be $\approx$ 0.2 mm.

B. Particle Size and Volume Fraction Measurements

1. Polycrystalline material

Since the precipitates in an age hardened Cu-1.9 wt % Co alloy are small enough, the alloy behaves as a superparamagnet which allows the particle sizes to be determined by magnetic measurements. The method followed in this investigation is the one described by Becker (53) and used by Livingston (16)

and Livingston and Becker (57). Briefly, the initial susceptibility is used to determine the particle size and the saturation magnetization gives the volume fraction of precipitate. The equations used are given below.

$$X_i = \frac{MI_o}{3kT}$$

and

$$M = I_s V$$

where X_i is the initial susceptibility

M is the magnetic moment of a single particle

I_o is the saturation magnetization of the sample

k is Boltzman's constant

T is the absolute temperature

I_s is the saturation magnetization of the particle

V is the particle volume.

Since the particles are Co containing about 10% Cu, the saturation magnetization of the particles is close to 90% that of pure Co (53) or,

$$I_s = 1264 \text{ emu/cm}^3$$

The volume fraction, f, of precipitate is determined from the saturation magnetization of a sample as follows.

$$f = \frac{I_o}{I_s}$$

In addition, the weight percent of Co precipitated can be found from the following:

$$\text{wt \% Co} = \frac{m_{Co}}{m_{alloy}} \quad \frac{\rho_{Co} I_o}{\rho_{alloy} I_s}$$

where m_{Co} is the mass of Co precipitated

m_{alloy} is the mass of specimen

ρ_{Co} is the density of Co = 8.71 gm/cm^3

ρ_{alloy} is the density of Cu + 2 wt % Co alloy = 8.95 gm/cm^3 assuming Vegard's Law holds.

In this way the equilibrium solubility of Co in Cu at the aging temperature can be determined.

The initial susceptibilities, saturation magnetizations, particle sizes and spacings, volume fractions, and percent Co precipitated in the polycrystals are shown in Table 4.

Table 4. Summary of magnetic data, particle sizes, and volume fractions taken on polycrystals solution treated at 970°C and aged for various times at 600°C

Specimen	Aging time (min)	X_i $\left(\frac{\text{emu}}{\text{cm}^3\text{gauss}}\right)$	I $\left(\frac{\text{emu}}{\text{cm}^3}\right)$	r (Å)	f	wt % Co
--	5	--	--	20[a]	--	--
30-6	30	0.0376	21.3	34.5	0.0168	1.48
50-6	50	0.0651	22.9	40.5	0.0181	1.59
100-6	100	0.112	22.5	48.8	0.0178	1.56
300-6	300	0.339	23.9	69.8	0.0185	1.63
500-6	500	0.411	23.0	80[a]	0.0181	1.60
1000-6	1000	0.263	23.0	99[a]	0.0181	1.60

[a]Particle sizes taken from extrapolated aging curve.

It is evident from the table that the volume fraction of precipitate is constant throughout aging in agreement with other studies on the same system (53,57). This allows the aging process to be described as a coarsening of a nearly constant amount of precipitate.

The particle sizes are shown as a function of aging time in Figure 3. The log particle size vs. log aging time curve is a straight line up to a particle size of about 70Å and has a slope of 1/3. At larger particle sizes the alloy is not superparamagnetic and the methods used do not apply (16,53, 57). For this reason the particle sizes given in Table 4 corresponding to aging times greater than 300 minutes were taken from the extrapolated straight line of Figure 3. Livingston's (16) data on Cu-2 wt % Co polycrystals solution treated 1/2 hour at 1000°C and aged at 600°C are also included on the curve. The agreement is quite good and it should be noted that, although the particle sizes differ somewhat, the aging kinetics are identical. Support of the validity of the magnetic method of determining particle sizes is given by the inclusion of three data points taken from Bonar's (29) particle size measurements in which transmission electron microscopy was used. The equations used in this investigation to

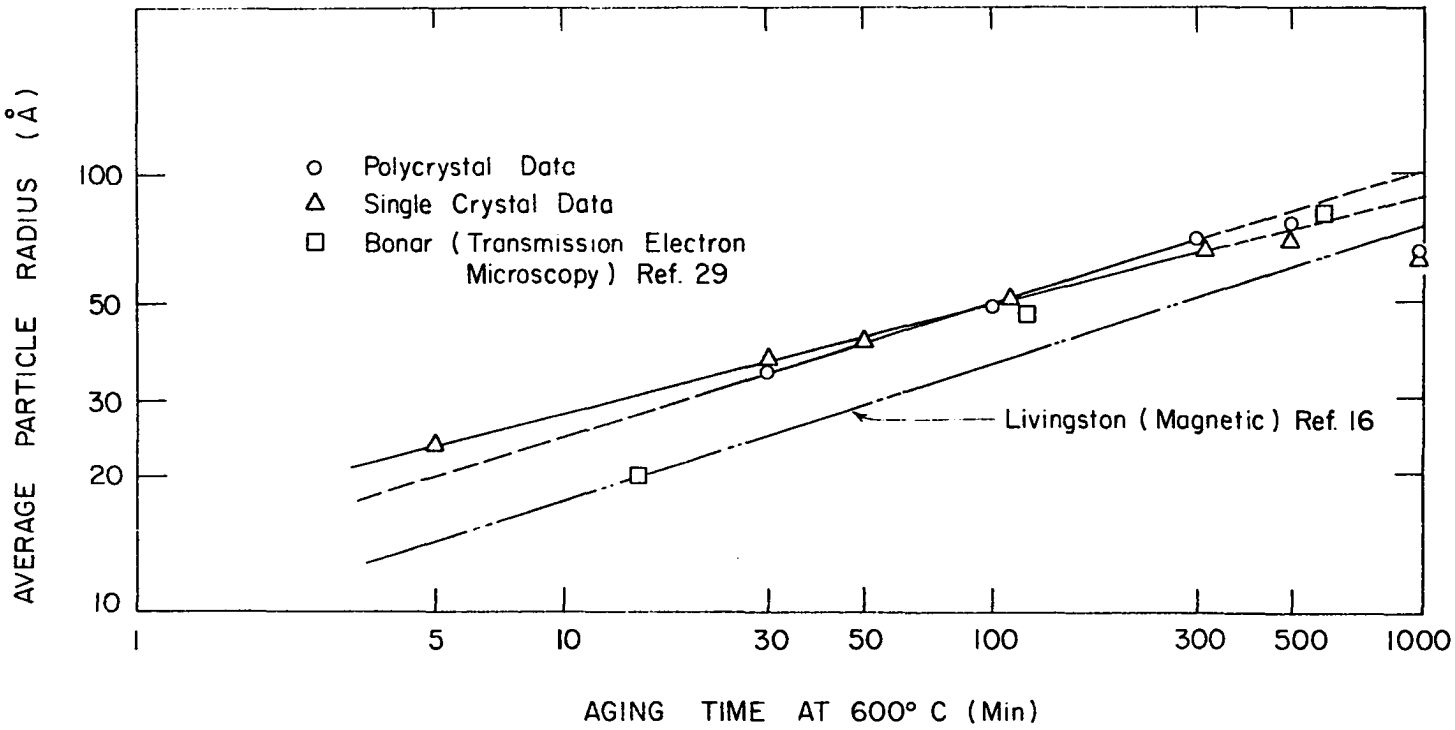

Figure 3. Log mean particle radius vs log aging time at 600°C for Cu-1.9 wt % Co single and polycrystals

determine the average particle size included the assumption of a volume distribution that was a constant over all particle sizes. The average particle sizes determined magnetically are then actually one-half of the maximum particle sizes if the smallest particles are taken to be infinitesimal. It has been found, in fact, that the particle size distribution in aged Cu-Co alloys is roughly symmetrical about a mean size (29,69) although not a constant. It appears, however, from the agreement between the magnetic determinations and the transmission electron microscopy determinations that the exact form of the particle size distribution does not affect the results to any great extent, i.e., to within 20%.

The differences between Livingston's (16) data and the present data are not evident but could be attributed to the difference in solution anneals or slight differences in alloy composition. The data taken in the present investigation indicate that the coarsening of the Co-rich precipitates at 600°C can be described by the following equation,

$$r = At^{1/3}.$$

This is in accord with Livingston's (16) data at 600°C as shown by the replots of his data by Ardell and Nicholson (70). Ardell and Nicholson (70) point out that these coarsening

kinetics are predicted by the Lifshitz-Wagner theory (71,72) if coarsening is assumed to take place at the onset of aging.

The percent Co precipitated indicates that the solubility of Co in Cu at 600°C is about 0.40% which is close to Livingston's value of 0.35%.

2. Single crystals

Particle sizes and volume fractions in single crystals aged at 600°C were measured by identical means to those used for the polycrystals. The results of magnetic determinations of particle size, volume fraction, etc. in the single crystals are summarized in Table 5.

Table 5. Summary of magnetic data, particle sizes, and volume fractions taken on single crystals solution treated at 1025°C and aged for various times at 600°C

Specimen	Aging time (min)	X_i $\left(\frac{\text{emu}}{\text{cm}^3 \text{ gauss}}\right)$	I_o $\left(\frac{\text{emu}}{\text{cm}^3}\right)$	r (Å)	f	wt % Co
x-5	5	1.06×10^{-2}	19.1	23.5	0.0151	1.32
x-30	30	4.45×10^{-2}	21.2	36.6	0.0167	1.47
x-50	50	6.37×10^{-2}	23.0	40.2	0.0181	1.60
x-110	110	12.3×10^{-2}	22.0	50.8	0.0174	1.53
x-315	315	25.9×10^{-2}	22.1	65.0	0.0174	1.54
x-500	500	31.4×10^{-2}	22.1	74[a]	0.0174	1.54
x-1000	1000	24.3×10^{-2}	22.7	88[a]	0.0179	1.58

[a]Particle sizes taken from extrapolated aging curve.

The particle sizes as a function of aging time for the single crystals are included in Figure 3. It is evident that the aging kinetics of both the polycrystals and single crystals are almost identical. The single crystal curve is slightly above the polycrystal curve at lower aging times and has a slightly lower slope. Since the single crystals were solution treated at 1025°C and the polycrystals at 970°C, the as-quenched vacancy concentration of the single crystals would be expected to be larger for similar quenching rates. This would cause an increased rate of precipitation at low aging times in the single crystals and result in larger particle sizes at similar aging times. The similarity between the two curves indicates that the presence of grain boundaries has a negligible effect on the aging kinetics. Particle size as a function of aging time for the single crystals can be described by the following equation

$$r \approx Bt^{\frac{1}{2}}$$

As was found for the polycrystals, the volume fraction of precipitate in the single crystals was fairly constant after short aging times. This is evident in Table 5 and is shown in Figure 4 in which the volume fraction of precipitate, f, is plotted as a function of aging time for both the polycrys-

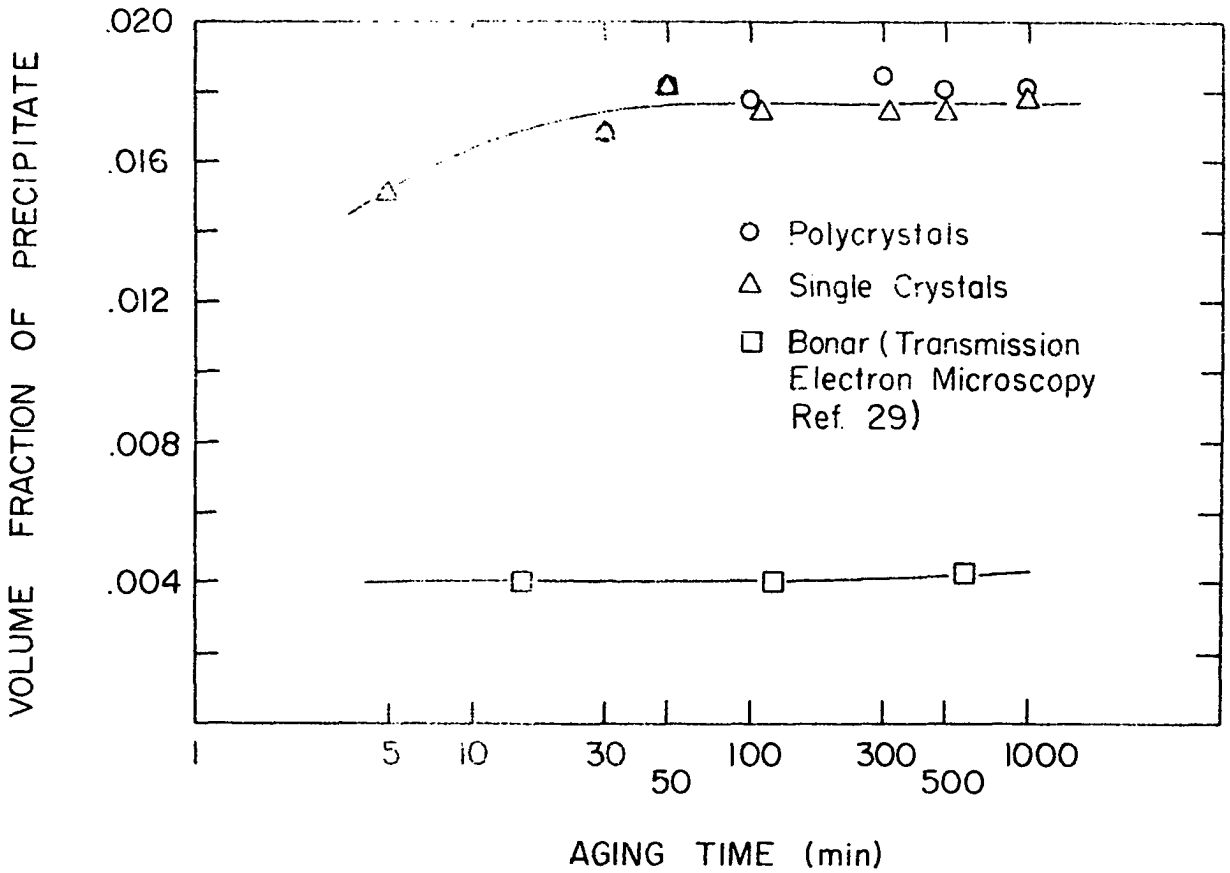

Figure 4. Volume fraction of precipitate vs. aging time at 600°C for Cu-1.9 wt % Co single and polycrystals

tals and single crystals. Included on the curve are Bonar's data (29) obtained by transmission electron microscopy. Since it was found in this study that the aging kinetics of single and polycrystals of Cu-1.9 wt % Co are quite similar and can be taken to be identical to within experimental scatter, Bonar's observations on large grained polycrystalline foils afford a valid comparison between the magnetic methods used here and direct observation methods.

Although the volume fraction data obtained by direct observations of thin foils (29) appear constant up to 1000 minutes aging time the volume fractions reported are lower than the present magnetic data by a factor of 4.5. Bonar explains this by stating that the matrix is not a truly random solid solution and contains clusters of Co atoms less than 20Å in diameter. These are certainly invisible in the electron microscope, but will be detected by magnetic measurements. These "clusters" are in reality coherent precipitates and must be counted as such. If the presence of invisible particles were the only cause of low observed volume fractions it is expected that Bonar's data would show a definite upward trend in f with aging time because of the increased number of visible particles. It is apparent from Figure 4 that this is

not the case. Two possible explanations are given below.

1) The alloy is not truly homogeneous and the small areas of foils examined by transmission electron microscopy are not representative of the bulk alloy.

2) The scatter in the average size determined by direct observation is large enough to mask the expected upward trend in f with aging time and the invisible 20Å radius particles do have a significant effect on the determination of f even up to 1000 minutes aging time. It is puzzling, however, that the values of f determined by direct observation are so low since even at 2 hrs aging time approximately symmetrical particle size distributions are attained by Bonar. In any case the reasons for the discrepancy are, at present, not immediately obvious especially since the particle size determinations by both methods correlate so well (see Figure 3).

C. Mechanical Properties of Polycrystals

1. Stress-strain behavior

a. Stress-strain curves — True stress-true strain curves obtained on polycrystals aged for various times at 600°C and tested at room temperature are shown in Figure 5. The large increase in strength that occurs when the solution treated alloy is aged even 5 minutes at 600°C is evident.

Figure 5. Typical true stress-true strain curves of Cu-1.9 wt % Co polycrystals solution treated at 1243°K, aged for various times at 873°K, and tested at 298°K

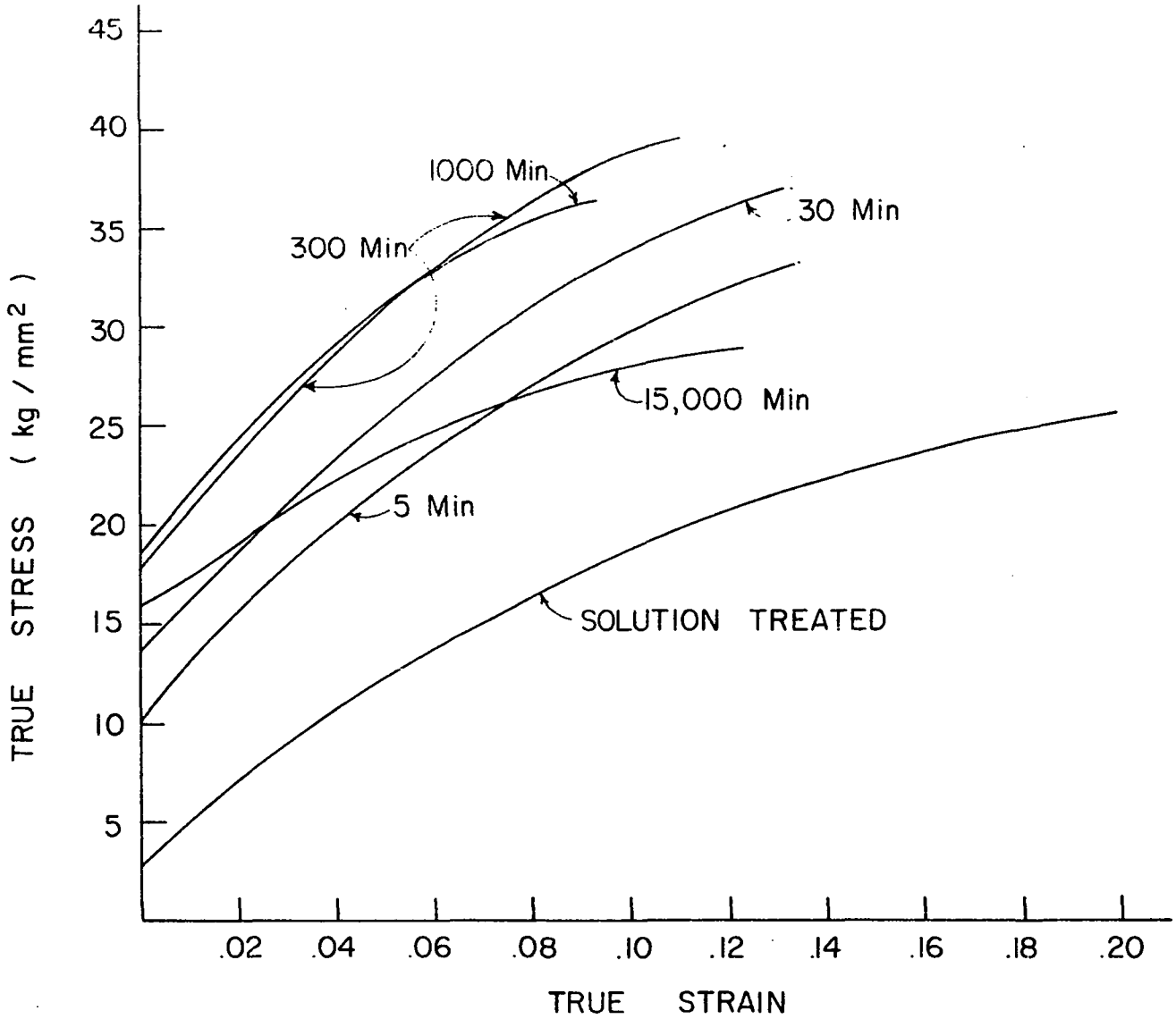
45
40
35
30
25
20
15
10
5
TRUE STRESS (kg / mm2)
1000 Min
300 Min
30 Min
15,000 Min
5 Min
SOLUTION TREATED
.02
.04
.06
.08
.10
.12
.14
.16
.18
.20
TRUE STRAIN

The work hardening behavior of all specimens aged up to 1000 minutes is essentially identical. Both the solution treated specimen and the overaged specimen had slightly lower work hardening rates. True stress-true strain curves obtained at testing temperatures extending down to 77°K were similar to those shown in Figure 5 and are not presented here because they are quite similar to those found elsewhere (73).

b. Aging curves The changes in strength that occur in the Cu-1.9 wt % Co alloy during aging are probably best illustrated by plots of yield and tensile strength versus aging time as shown in Figures 6a, b, and c, for tests run at 298, 188, and 77°K respectively. The curves are dotted where the mechanical behavior is uncertain due to insufficient data. The yield strength data at all temperatures had less scatter than the tensile strength data. This is especially true at 77°K where the scatter in the tensile strength data was quite large. Peak yield strength was reached at all temperatures after about 1000 minutes aging time. This is shown very clearly at 298°K in Figure 6a. Similar results were obtained by Livingston (16) whose yield strength data for the same alloy solution treated at 1000°C and aged at 600°C are included in Figure 6a. Although his results deviate from the

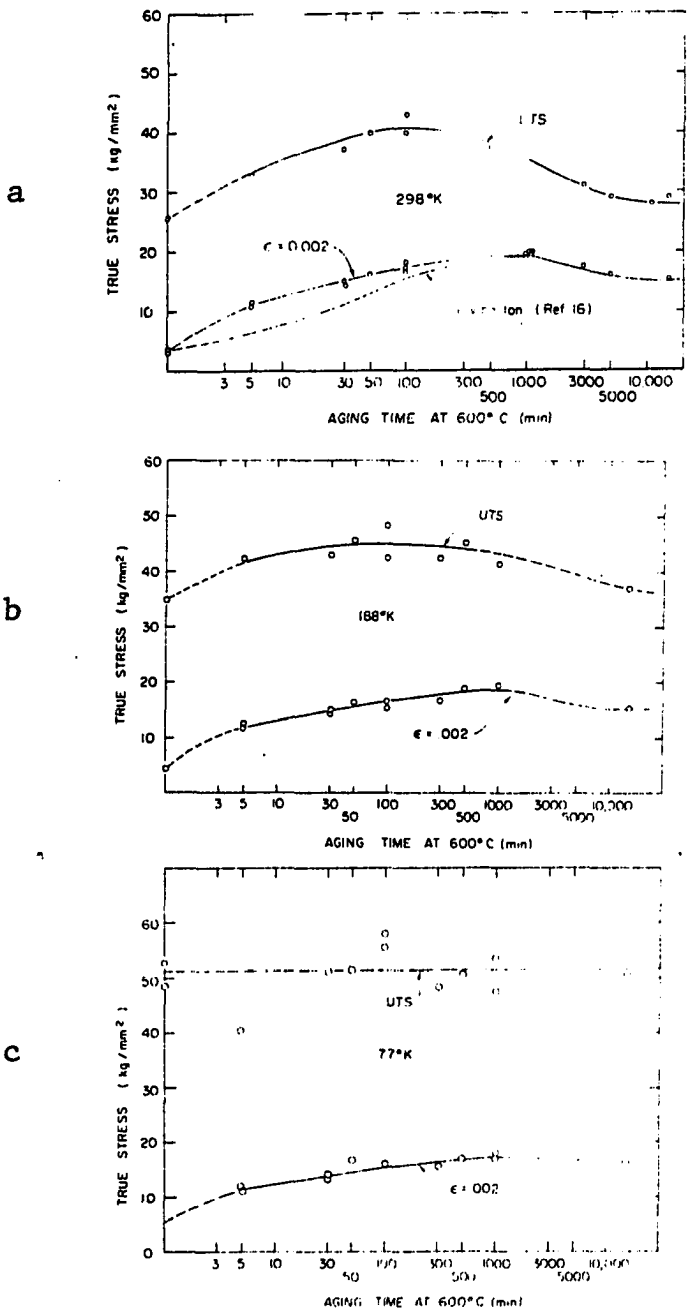

Figure 6. 0.2 percent offset yield strength and ultimate tensile strength vs. aging time at 600°C for polycrystals tested at 298, 188, and 77°K

present results at low aging times, possibly due to differences in heating rates during aging, both sets of data peak at about 1000 minutes aging time.

Figures 6a and 6b show that the tensile strengths at 298 and 188°K peak after about 100 minutes aging time. The scatter in the 77°K data shown in Figure 6c prevents further comment. The early peaks in the tensile strengths at 298 and 188°K with respect to the yield strength peaks indicate that the work hardening rates, at least at higher strains, decrease with increased aging past 100 minutes. This behavior is also evident in the stress-strain curves taken at 298°K shown in Figure 5.

c. Temperature dependence of the flow stress The temperature dependence of the flow stress of f.c.c. metals at temperatures ranging up to their melting points has been studied extensively[1]. It is generally recognized that, as the temperature is lowered (e.g. 300°K to 4.2°K) the flow stress increases. Furthermore the temperature dependence of the flow stress of f.c.c. metals is an increasing function of strain because a decrease in temperature results in an increase in work hardening rate. For this reason the yield

[1]See for example Reference (3).

strengths of f.c.c. metals and solid solution alloys increase slightly while the tensile strengths increase quite drastically as temperature decreases.

Flow stress-temperature curves taken from tensile tests of solution treated polycrystalline specimens are shown in Figure 7. The solution treated material behaves as a typical f.c.c. solid solution, exhibiting a slight increase in yield strength at $77^{o}K$ over that at $300^{o}K$. The large increase in tensile strength with decreased temperature is also evident from the curve. There are more data points on the yield strength curve because additional yield strength values were taken, when possible, from the initial portions of the load elongation curves used in the strain rate sensitivity tests.

Flow stress-temperature curves of material solution treated at $970^{o}C$ and aged at $600^{o}C$ for 5, 30, 50, 100, 300, 500, 1000, and 15,000 minutes are shown in Figures 8 through 15 respectively. These curves show one of the surprising aspects of the mechanical behavior of aged Cu-Co alloys. The flow stresses at 0.2, 5, and 10 percent strain in specimens aged up to 1000 min. decreased as the testing temperature was decreased. The similarity between the flow stress-temperature curves at 0.002, 0.05, and 0.10 strain for each aging time

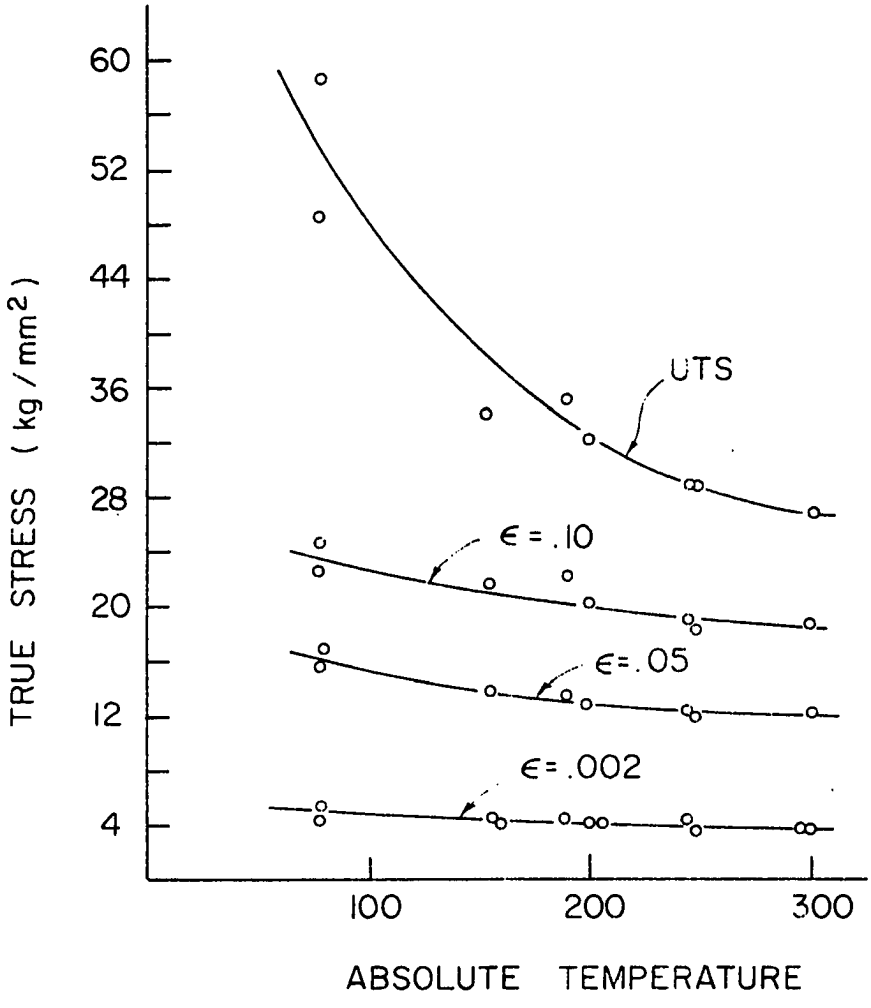

Figure 7. The temperature dependence of the flow stress at various strains for solution treated Cu-1.9 wt % Co polycrystals

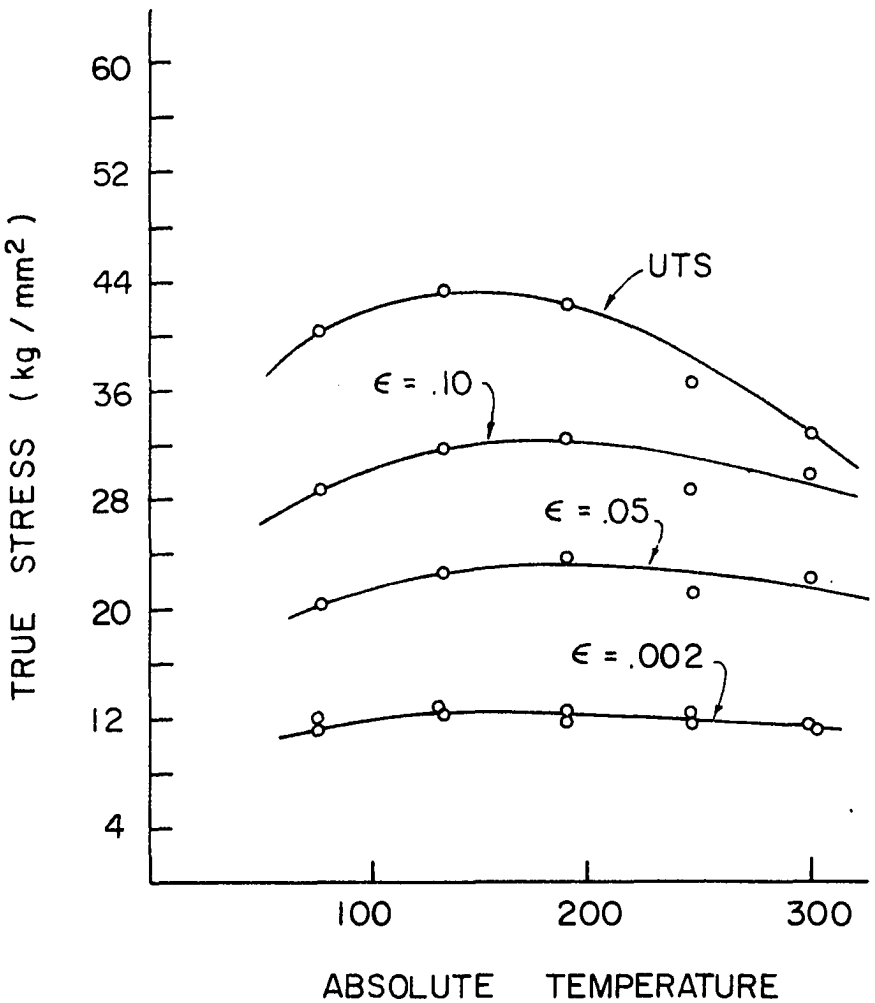

Figure 8. Flow stress at various strains vs test temperature for solution treated Cu-1.9 wt % Co polycrystals aged 5 min. at 873°K

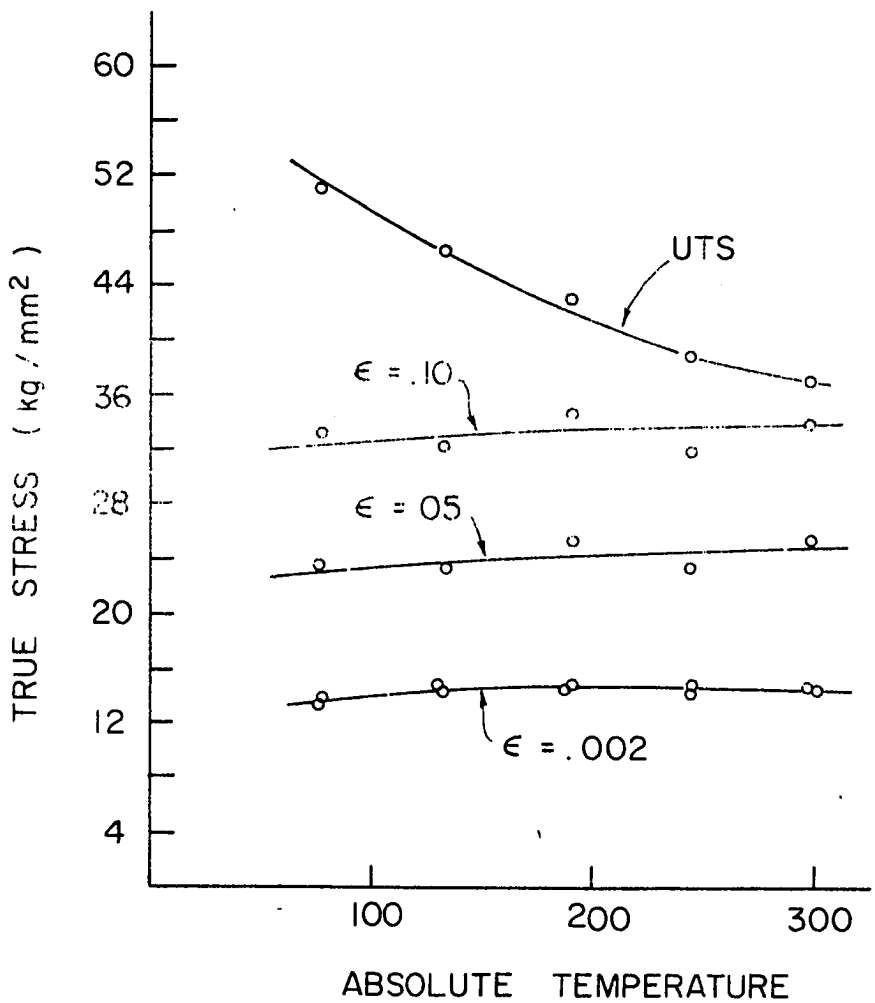

Figure 9. Flow stress at various strains vs. test temperature for solution treated Cu-1.9 wt % Co polycrystals aged 30 min. at 873°K

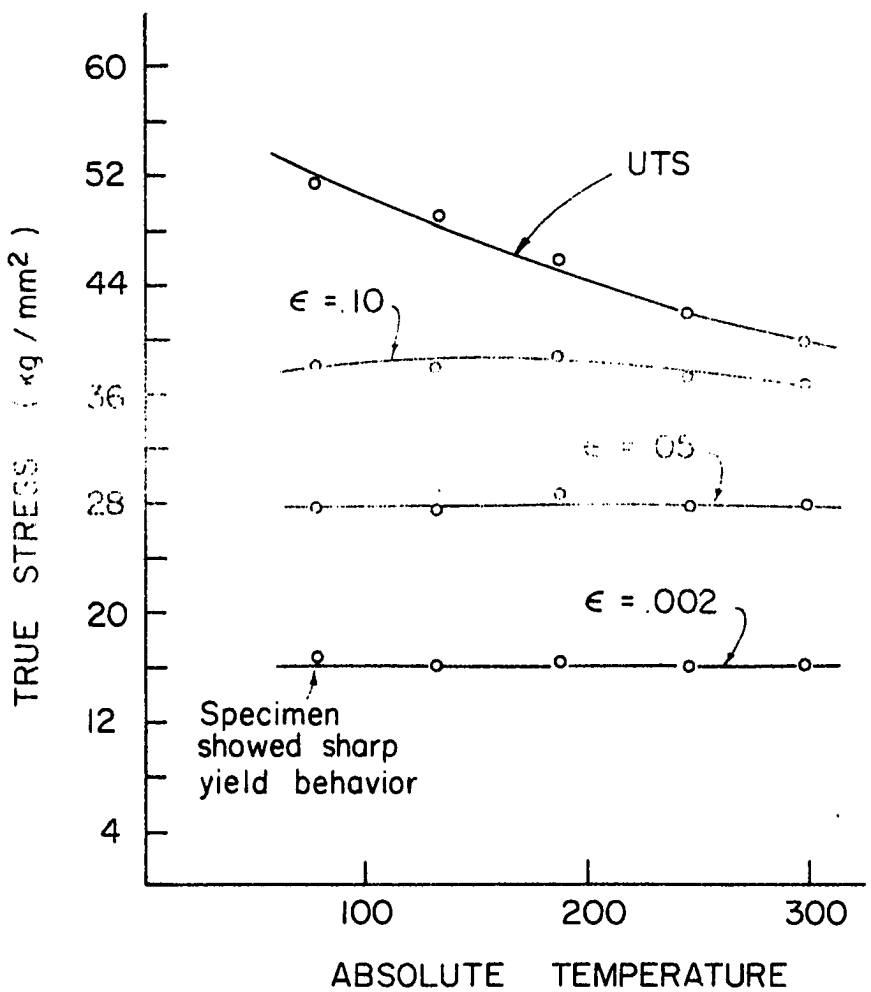

Figure 10. Flow stress at various strains vs. test temperature for solution treated Cu-1.9 wt % Co polycrystals aged 50 min. at 873°K

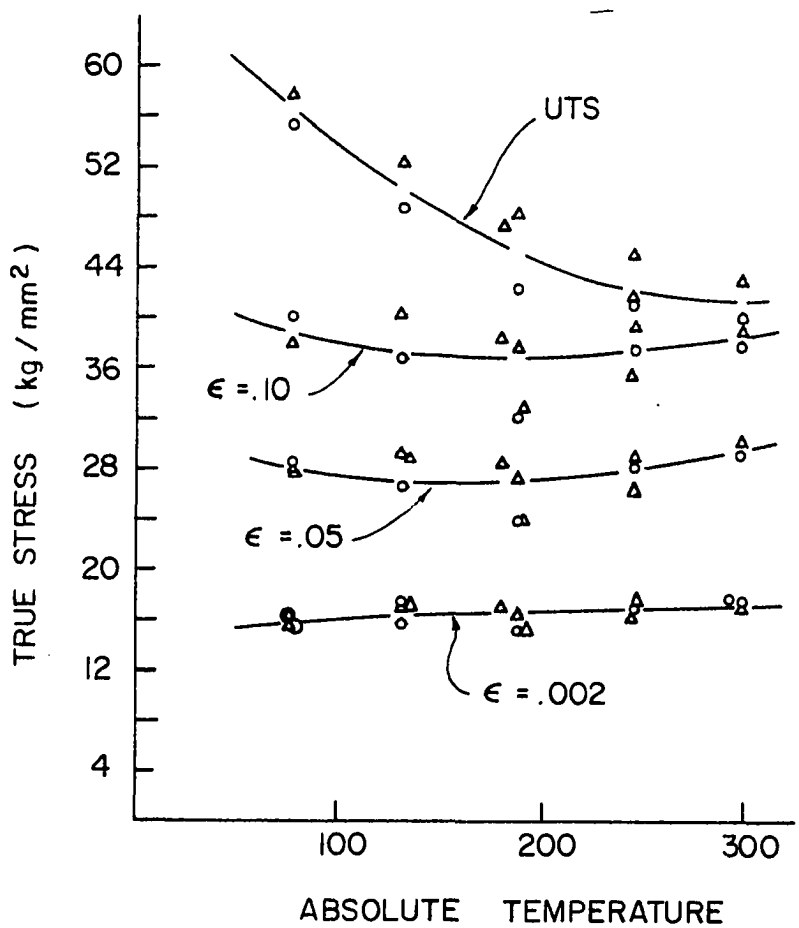

Figure 11. Flow stress at various strains vs. test temperature for solution treated Cu-1.9 wt % Co polycrystals aged 100 min. at 873°K

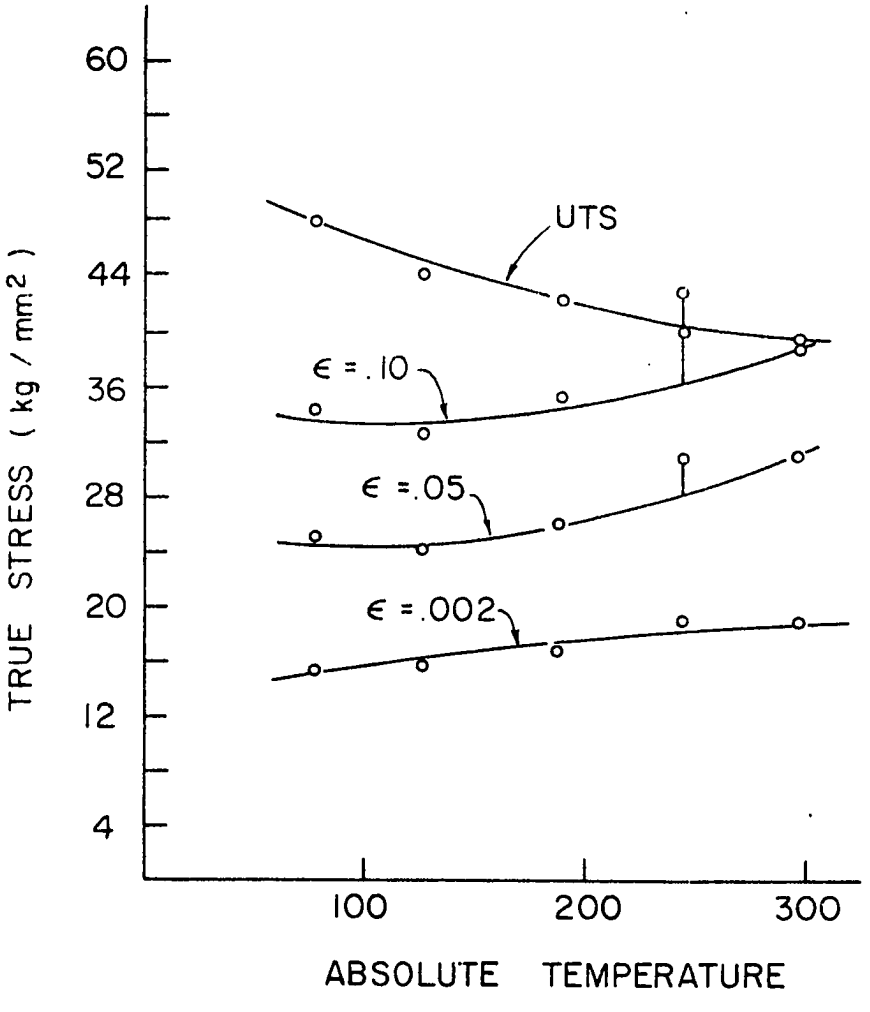

Figure 12. Flow stress at various strains vs. test temperature for solution treated Cu-1.9 wt % Co polycrystals aged 300 min. at 873°K

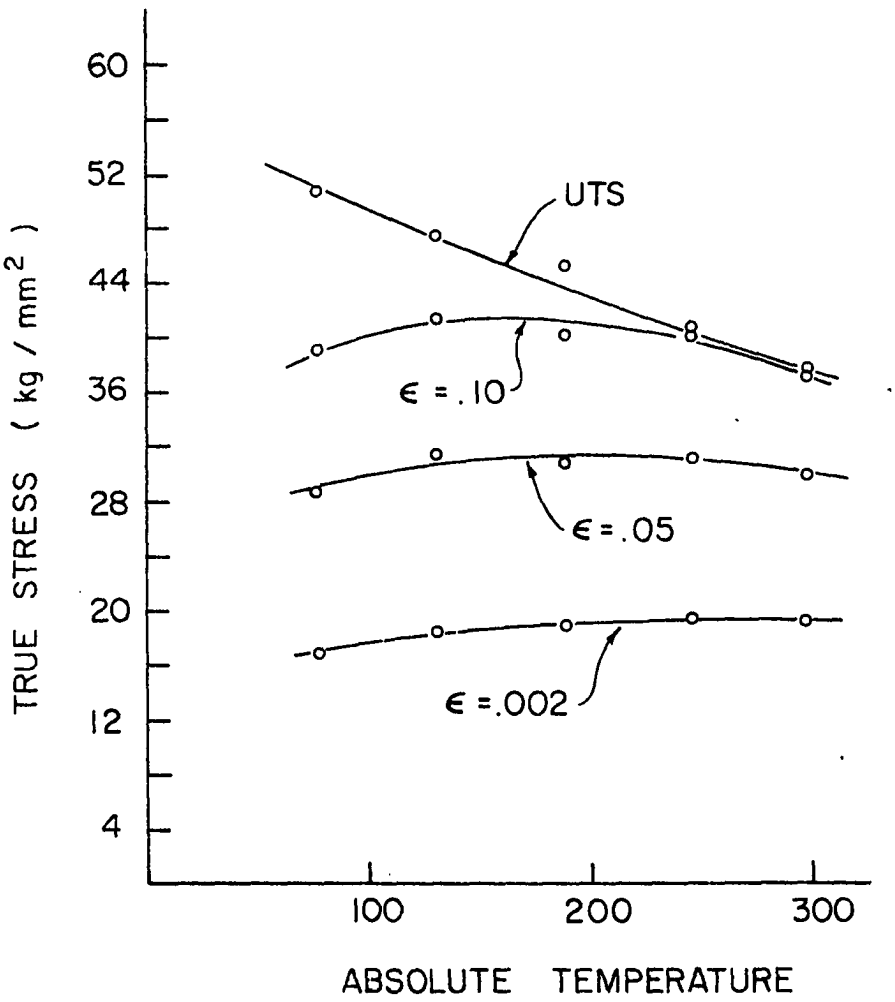

Figure 13. Flow stress at various strains vs. test temperature for solution treated Cu-1.9 wt % Co polycrystals aged 500 min. at 873^{o}K

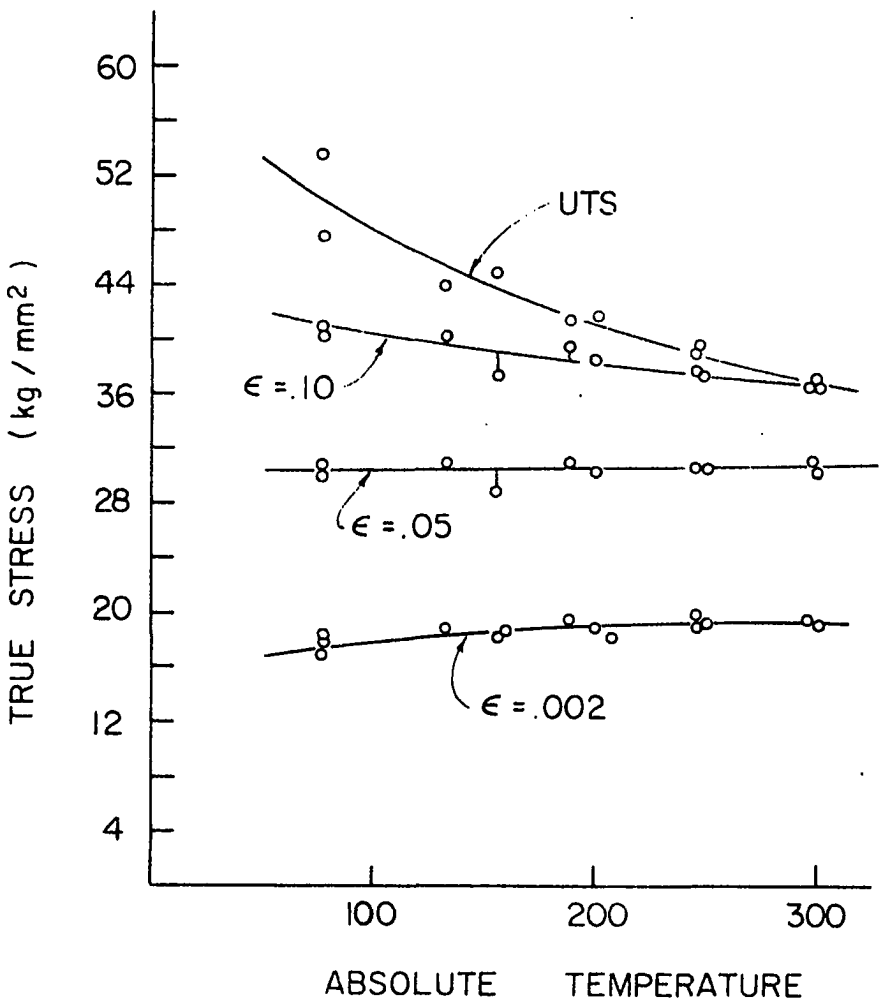

Figure 14. Flow stress at various strains vs. test temperature for solution treated Cu-1.9 wt % Co polycrystals aged 1000 min. at 873°K

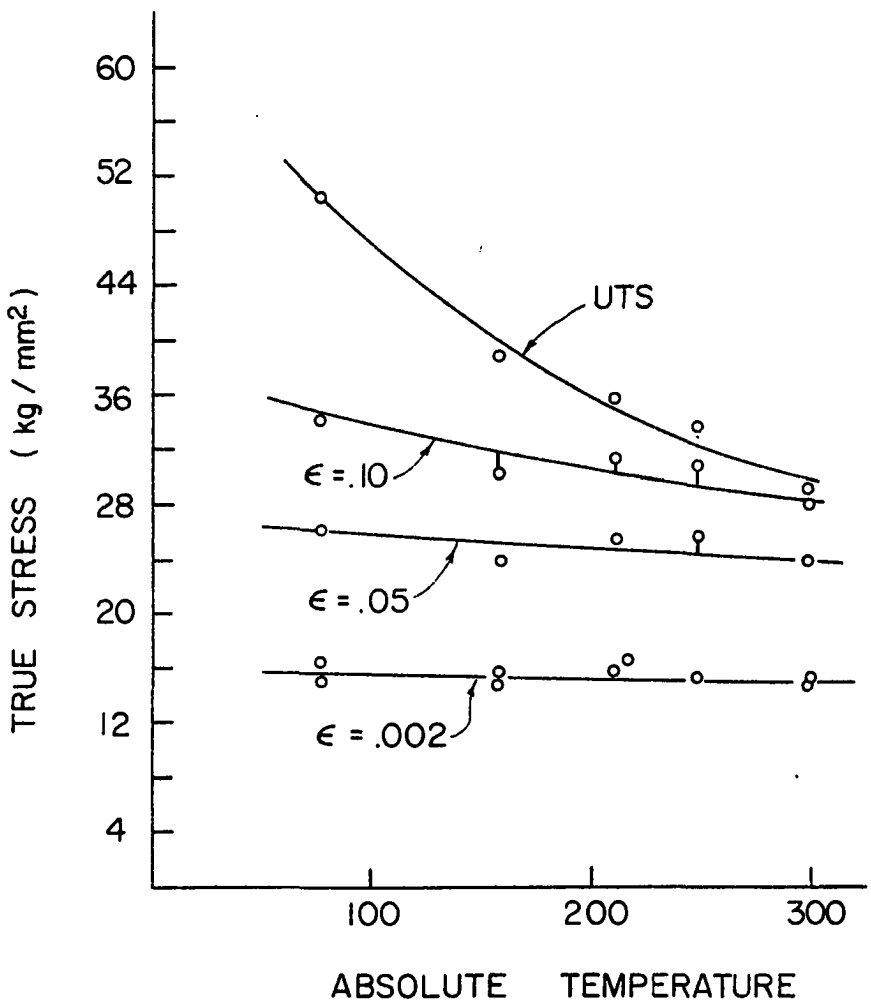

Figure 15. Flow stress at various strains vs. test temperature for solution treated Cu-1.9 wt % Co polycrystals aged 15,000 min. at 873°K

indicates that the work hardening characteristics of the aged alloys were not a strong function of temperature at least up to 0.10 strain. In all figures except that for the 5 minute aging time, the tensile strength increased as the testing temperature decreased in a manner similar to the solution treated series although not as markedly.

In some cases, e.g., the 100 min. and 300 min. aging times, the flow stresses at 5 and 10 percent strain decreased and then tended to increase with a decrease in temperature while the flow stress at 10 percent strain in the 1000 minute specimens appeared to increase in a manner similar to the tensile strengths. This behavior cannot be discussed at length in view of the scatter observed in the data, especially in the 100 min. series in which many duplicate runs were made. It is evident from several of the curves, however, that scatter in the yield strength data was slight and seemed to increase with strain.

The decrease in flow stress accompanying a decrease in temperature at low values of true strain has been observed by others (28,73) and has been attributed to the decrease in elastic strain fields surrounding the coherent cobalt-rich precipitates (28) as noted in Section II.

The amount of observed decrease in yield strength with temperature appears about the same in specimens aged from 5 min. to 1000 min. at 600°C and no indications of any trends with aging time are evident.

In contrast to the behavior of the materials aged up to peak strength (1000 min.) the flow stress-temperature curves of the overaged series (15,000 min. at 600°C) appear similar to those of the solution treated series. These are shown in Figure 15.

2. Strain rate sensitivity data

Strain rate change tests can yield valuable information about the rate controlling dislocation mechanisms operating during deformation[1]. Since the effects of precipitate size and spacing on deformation are a major consideration in this dissertation, the strain rate sensitivity of the flow stress has been extensively studied in Cu-1.9 wt % Co as a function of both test temperature and aging time. As mentioned in the section on experimental procedure, strain rate change tests on polycrystalline wires were run at a base strain rate of $8.33 \times 10^{-5} sec^{-1}$ with excursions to a strain rate of 1.67×10^{-3} to obtain the strain rate sensitivity data. Before discussing

---

[1]See for instance Conrad (3).

the results of these experiments, a discussion of the tests and data would be profitable.

A schematic of a portion of a typical strain rate change test is shown in Figure 16. Two features commonly seen in the strain rate-change tests run in this investigation are evident: (i) The appearance of a small yield point accompanying the stress increase associated with an increase in strain rate. Generally the yield point was not present at the early stages of a test and developed only after a few percent elongation. (ii) The large transient associated with a decrease in strain rate after which the work hardening rate was quite high and decayed gradually to a constant value. As noted by Thornton et al. (74) even if the data obtained during a strain rate decrement were valid, the large transient makes extrapolation difficult and leads to scatter in the data. For this reason, only positive strain rate changes have been considered here. Following the notation of Orava et al. (75), it is evident that two values can be taken for the stress increment associated with a positive strain rate change. The stress increment, $\Delta \sigma_p$, is determined by the yield point while the value of $\Delta \sigma_e$ is obtained from the extrapolated line through the yield point. Thus an ambiguity

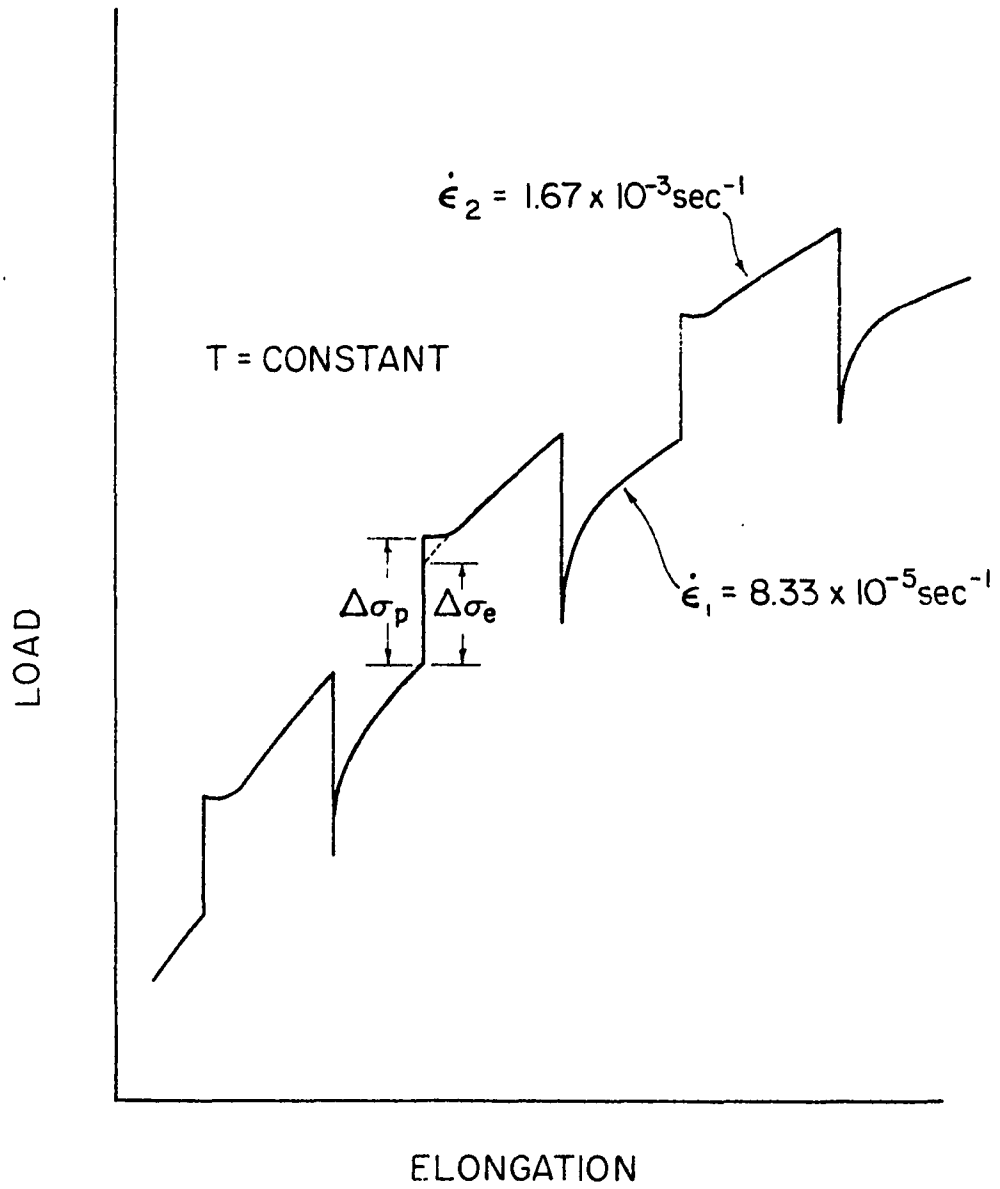

Figure 16. Schematic of a portion of a load-elongation curve from a strain-rate change test.

exists in the interpretation of the data. It is important, in these measurements, to measure the stress increment accompanying a strain rate change that is representative of the structure existing before the strain rate change. In other words, a key assumption in the application of strain rate change data to the determination of dislocation mechanisms responsible for the temperature and strain rate dependent portion of the flow stress is that the mobile dislocation density remain constant during the strain rate change. Clearly this is not the case when the strain rate is decreased because of the recovery that takes place (76). In fact Thornton et al. (74) showed that strain rate changes in the vicinity of the reverse yield point gave values of $\Delta\sigma$ quite different from those taken after sufficient strain had occurred to remove the irreversible effects associated with the yield point transient.

In keeping with the constant structure philosophy noted above, stress values immediately adjacent to the strain rate change (i.e., $\Delta\sigma_p$) were used throughout this investigation. It is felt that this value of $\Delta\sigma$ most faithfully represents the state of deformation existing just prior to the strain-rate change. Basinski (43) has made similar comments.

a. $\Delta\sigma$-σ curves An intriguing aspect of the strain rate sensitivity (SRS) of the flow stress in f.c.c. metals is that when the change in stress $\Delta\sigma$ accompanying an instantaneous change in strain rate is plotted against the flow stress, σ, that prevailed immediately preceding the change, the results are a straight line that often goes through the origin. This behavior is quite general and is observed in most f.c.c. metals (3). When the $\Delta\sigma$-σ line passes through the origin the material is considered to behave according to the Cottrell-Stokes law. The behavior was first noted by Cottrell and Stokes (65) for Al single crystals. They found that the ratio of flow stresses, $\sigma_{T_2}/\sigma_{T_1}$, obtained during tensile tests by periodically changing temperature between T_1 and T_2, was approximately constant independent of strain for strains greater than 10%. As mentioned above this constancy is also found during strain rate change tests at constant temperature. For this reason linear $\Delta\sigma$-σ plots are also taken as evidence that the material follows the "Cottrell-Stokes law". A $\Delta\sigma$-σ plot following true Cottrell-Stokes behavior is of the form

$$\Delta\sigma = A\sigma$$

$$\text{i.e.:} \quad \sigma_{\dot{\varepsilon}_2} - \sigma_{\dot{\varepsilon}_1} = A\sigma_{\dot{\varepsilon}_1}$$

where $\sigma_{\dot{\epsilon}_2}$ is the flow stress at strain rate $\dot{\epsilon}_2$ and temperature T.

$\sigma_{\dot{\epsilon}_1}$ is the flow stress at strain rate $\dot{\epsilon}_1$ and temperature T.

so that

$$\frac{\sigma_{\dot{\epsilon}_2}}{\sigma_{\dot{\epsilon}_1}} = (1 + A) = \text{constant} .$$

Since the flow stress change due to a change in strain rate or temperature reflects the magnitude of the strain rate and temperature dependent component of the flow stress it is easily seen that the Cottrell-Stokes relation in the temperature change tests is equivalent to the above relation derived from strain rate change tests namely,

$$\frac{\sigma_{T_2}}{\sigma_{T_1}} = C$$

In many cases the Cottrell-Stokes law is only partially followed and the $\Delta\sigma$-σ plots have the form -

$$\Delta\sigma = D + E\sigma$$

$$\text{i.e.} \quad \sigma_{\dot{\epsilon}_2} - \sigma_{\dot{\epsilon}_1} = D + E\sigma_{\dot{\epsilon}_1}$$

In this dissertation, the linearity of $\Delta\sigma$-σ plots will still be referred to as "Cottrell-Stokes behavior" but it should be kept in mind that the Cottrell-Stokes law is only rigidly

followed when the intercept of the $\Delta\sigma$-σ plot goes through the origin, i.e., when D = 0 in the above equation.

That Cottrell-Stokes behavior is followed in both solution treated and aged polycrystalline specimens of Cu-1.9 wt % Co is illustrated in Figures 17 and 18. These figures exhibit $\Delta\sigma$-σ plots at different temperatures for polycrystals in the solution treated condition and in the solution treated and aged for 5, 30, 100, 300, 1000, and 15,000 minutes conditions respectively. At each aging condition, the plots representing different test temperatures have been displaced along the σ axis for clarity.

The linearity of the $\Delta\sigma$-σ plots is evident for the alloy at all states of aging up to 15,000 min. When the early portions of the curves for the solution treated series are discounted, it is apparent that the Cottrell-Stokes law is exactly obeyed. The slopes for all the curves above $77^{o}K$ are approximately equal as will be shown below. The slopes for the $77^{o}K$ curves are all slightly less than the others.

The averages of the slopes of the four curves above $77^{o}K$ in each series were taken and a standard deviation computed. The standard deviations for each series ranged from 3.2% to 10% of the value of the average slope for each series.

Figure 17. $\Delta\sigma$-σ curves at different test temperatures of Cu-1.9 wt % Co polycrystals solution treated at 1243°K and aged 0, 5, 30, and 100 min. at 873°K. The origins have been displaced along the σ axis for clarity

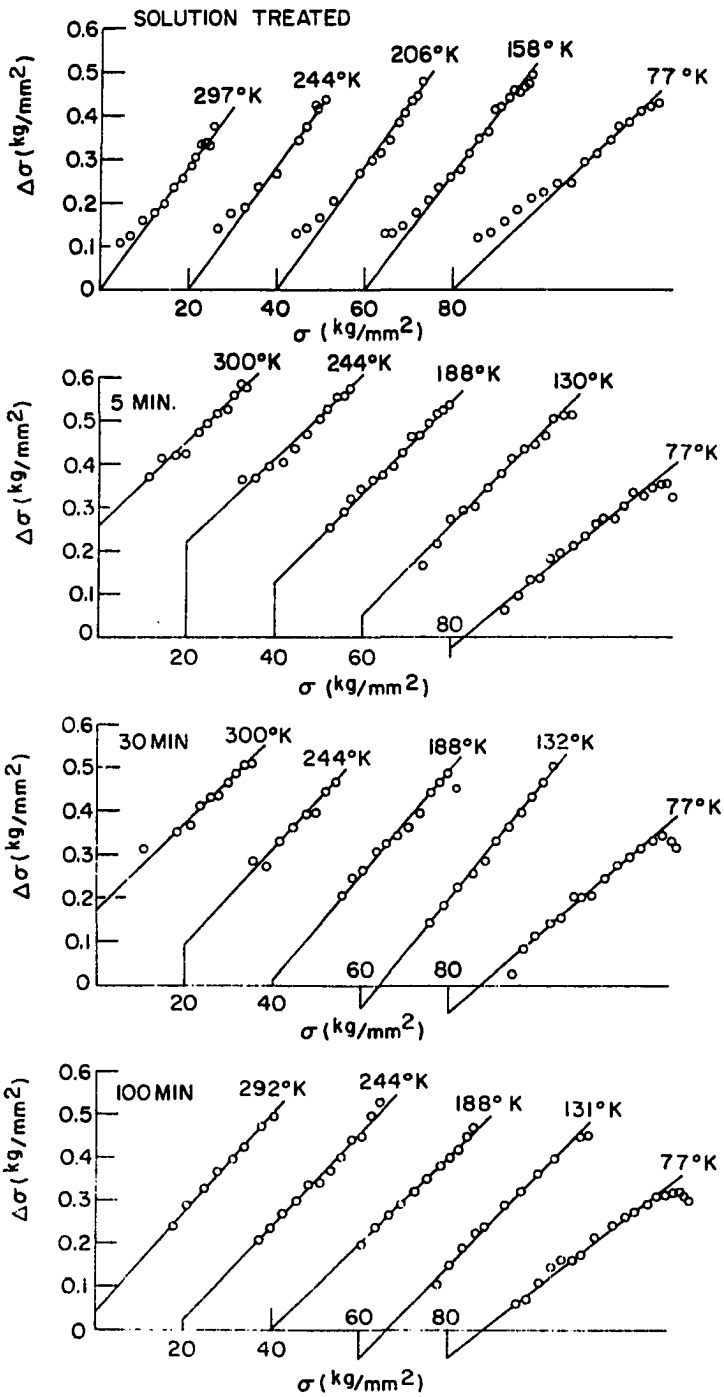
SOLUTION TREATED
297°K
244°K
206°K
158° K
77 °K
5 MIN.
300°K
244°K
188°K
130°K
77°K
30 MIN
300°K
244°K
188°K
132°K
77°K
100 MIN
292°K
244°K
188° K
131°K
77°K
Δσ (kg/mm2)
σ (kg/mm2)
0.6
0.5
0.4
0.3
0.2
0.1
0
20
40
60
80

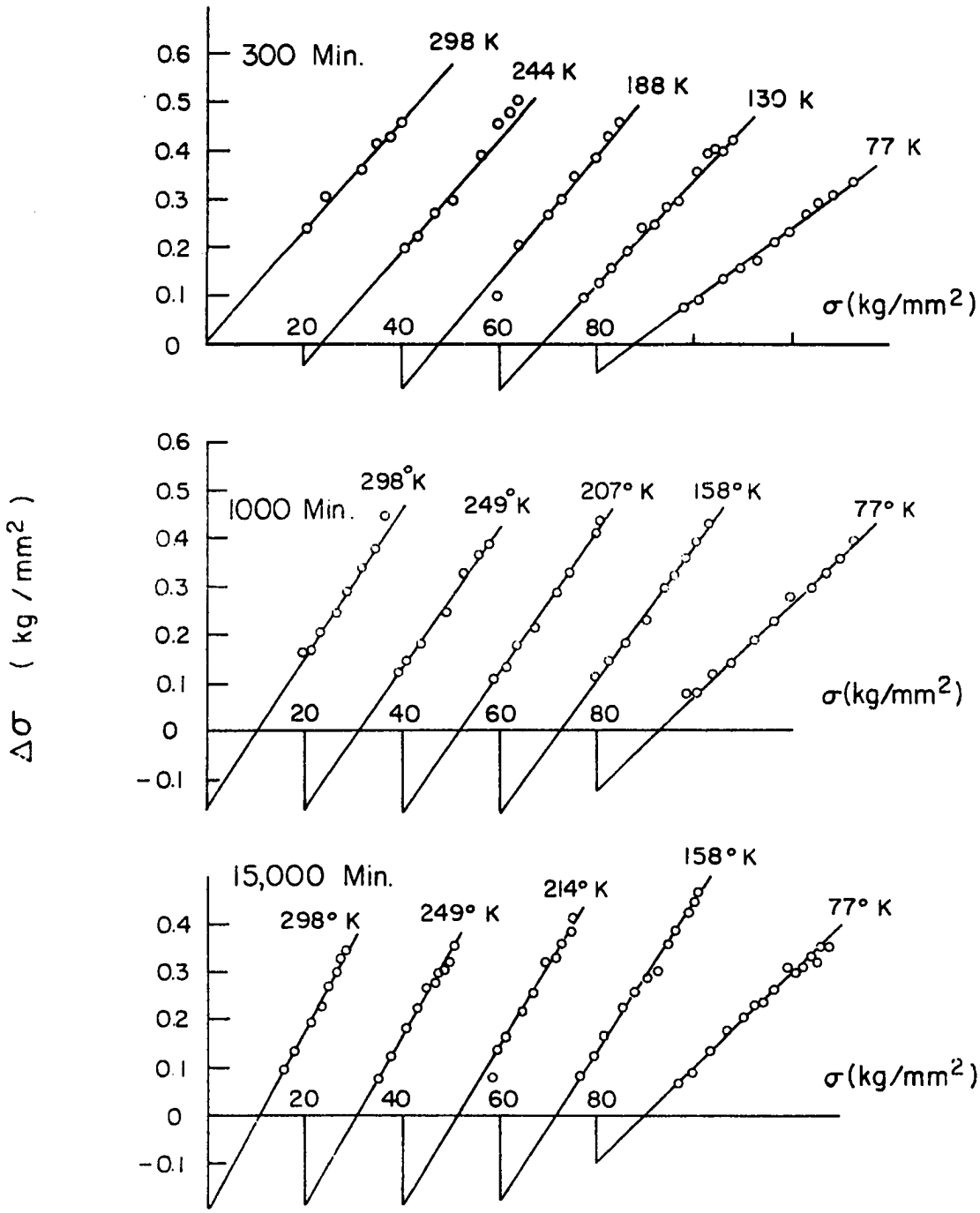

Figure 18. $\Delta\sigma$-σ curves at different test temperatures of Cu-1.9 wt % Co polycrystals solution treated at 1243°K and aged 300, 1000, and 15,000 min. at 873°K. The origins have been displaced along the σ axis for clarity

Although a sample population of 4 makes any standard deviation calculated almost meaningless, the results are taken to show that the slopes of the four $\Delta\sigma$-σ curves for $T > 77^{o}K$ in each series can be approximated by the average value which will be given in Table 6.

Table 6. Values of D and E for polycrystalline Cu-1.9 wt % Co in the solution treated condition and aged for various times at 600°C

Condition	Temp. (°K)	D	E	
Pure Cu[a]	375		0.0160	
	295		0.0130	
	175		0.0100	
	77		0.0072	
Solution treated	297	0.07	0.0088	
	244	0.08	0.0098	
	206	0.08	0.0100	0.0094 ± .0006
	158	0.075	0.0092	
	77	0.07	0.0078	
Aged 5 min. at 600°C	300	0.26	0.0097	
	244	0.22	0.0097	
	188	0.13	0.0103	0.0100 ± .0003
	130	0.05	0.0105	
	77	-0.03	0.0070	
Aged 30 min. at 600°C	300	0.18	0.0097	
	244	0.09	0.0113	
	188	0.02	0.0117	0.0112 ± .0011
	132	-0.05	0.0123	
	77	-0.07	0.0088	

[a]Data for pure polycrystalline copper taken from Thornton *et al.* (74).

Table 6. (Continued)

Condition	Temp. (°K)			
Aged 100 min. at 600°C	292	0.045	0.0113	
	244	0.020	0.0180	
	188	0	0.0098	0.0106 ± .0006
	131	-0.07	0.0105	
	77	-0.07	0.0080	
Aged 300 min. at 600°C	298	0	0.0116	
	244	-0.05	0.0120	
	188	-0.10	0.0122	0.0117 ± .0009
	130	-0.10	0.0110	
	77	-0.06	0.0076	
Aged 1000 min. at 600°C	298	-0.16	0.0155	
	249	-0.16	0.0145	
	207	-0.17	0.0145	0.0146 ± .0007
	158	-0.17	0.0138	
	77	-0.13	0.0098	
Aged 15,000 min. at 600°C	298	-0.21	0.0193	
	249	-0.19	0.0180	
	214	-0.19	0.0167	
	158	-0.18	0.0157	
	77	-0.10	0.0100	

The intercepts of the $\Delta\sigma$-σ curves on the $\Delta\sigma$ axes showed definite trends both with aging time and testing temperature. The intercepts for the solution treated, 1000 min., and 15,000 min. series were approximately constant with temperature at all testing temperatures. The intercepts for the 5, 30, and 100 min. series all decreased as the testing temperature decreased while those for the 300 min series decreased and

then increased. In fact the changes in intercepts for the above maintained series were approximately linear functions of temperature as shown in Figure 19. Although the slopes of the $\Delta\sigma$-σ curves for any given testing temperature were approximately constant, their intercepts on the $\Delta\sigma$ axis decreased as aging time increased. In other words, as aging time increased the $\Delta\sigma$-σ curves were shifted toward higher values of σ at any one temperature.

It is apparent that aged Cu-1.9 wt % Co obeys Cottrell-Stokes behavior in strain rate change tests since the $\Delta\sigma$-σ curves are straight lines that can be represented by

$$\Delta\sigma = D + E\sigma$$

where D and E are constants.

The values of the constants corresponding to the curves shown in Figures 17, 18, and 19 are given in Table 6.

To summarize, the $\Delta\sigma$-σ behavior of solution treated and aged Cu-1.9 wt % Co polycrystals can be represented by

$$\Delta\sigma = D + E\sigma$$

in which D has the values given in Table 6 and E has the following average values for aging times up to 100 min.:

$300^{\circ}K > T > 130^{\circ}K \qquad E = 0.0112$

$T = 77^{\circ}K \qquad E = 0.0081$

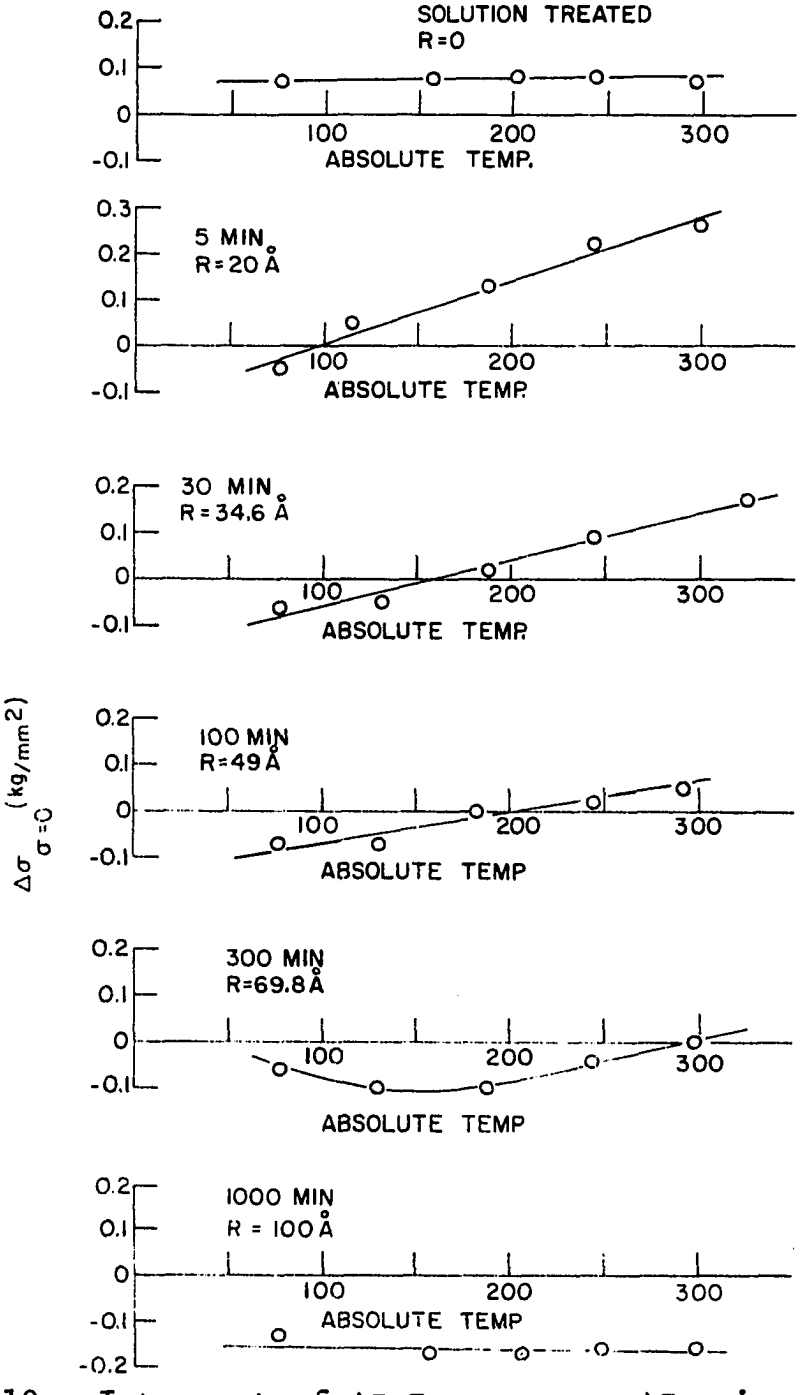

Figure 19. Intercept of $\Delta\sigma$-σ curves on $\Delta\sigma$ axis vs. temperature for Cu-1.9 wt % Co polycrystals aged 0, 5, 30, 100, 300, and 1000 min. at 873°K

Both values are quite similar to that for pure copper as shown in Table 6.

Figure 20 shows schematically the trends in the $\Delta\sigma$-σ behavior with aging time and testing temperature.

b. Strain rate sensitivity parameter n The strain rate sensitivity of a material is commonly defined by -

$$n = \frac{\Delta \ln \sigma}{\Delta \ln \dot{\epsilon}} = \frac{\ln \sigma_2/\sigma_1}{\ln \dot{\epsilon}_2/\dot{\epsilon}_1}$$

where σ_2 = stress immediately following a strain rate change from $\dot{\epsilon}_1$ to $\dot{\epsilon}_2$.

σ_1 = stress immediately preceding the change.

The parameter, n, directly reflects the change in flow stress accompanying a change in strain rate. The change in n with aging time and test temperature for Cu-1.9 wt % Co polycrystals is shown in Figure 21 as a function of temperature at true strains of 0, 0.05, and 0.10. The value of n at $\epsilon = 0$ denoted n* was obtained by extrapolation. First $\Delta\sigma$ was plotted as a function of strain and extrapolated to zero strain to give $\Delta\sigma^*$. The values of the flow stress corresponding to the base strain rate σ_1, were then plotted as a function of strain and extrapolated to zero strain to give σ_1^*, permitting n* and other SRS parameters to be calculated for the zero strain state. This method was used because

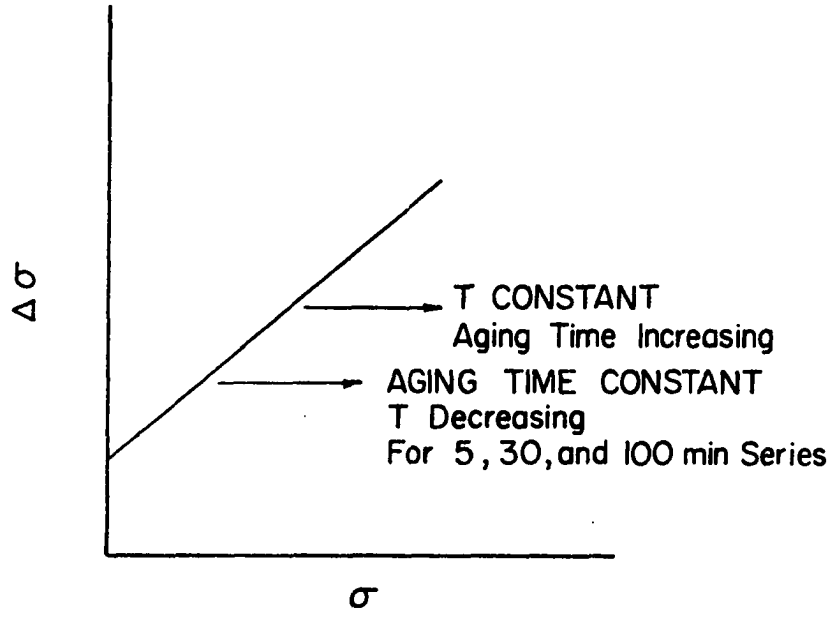

Figure 20. Schematic $\Delta\sigma$-σ plot showing trends in behavior as a function of aging time and test temperature. The temperature dependence of the strain-rate sensitivity parameter, n, at true strains of 0, 0.05, and 0.10 for polycrystals solution treated at 1243°K and aged for different times at 873°K

Figure 21. The temperature dependence of the strain-rate sensitivity parameter, n, at true strains of 0, 0.05, and 0.10 for polycrystals solution treated at 1243°K and aged for different times at 873°K

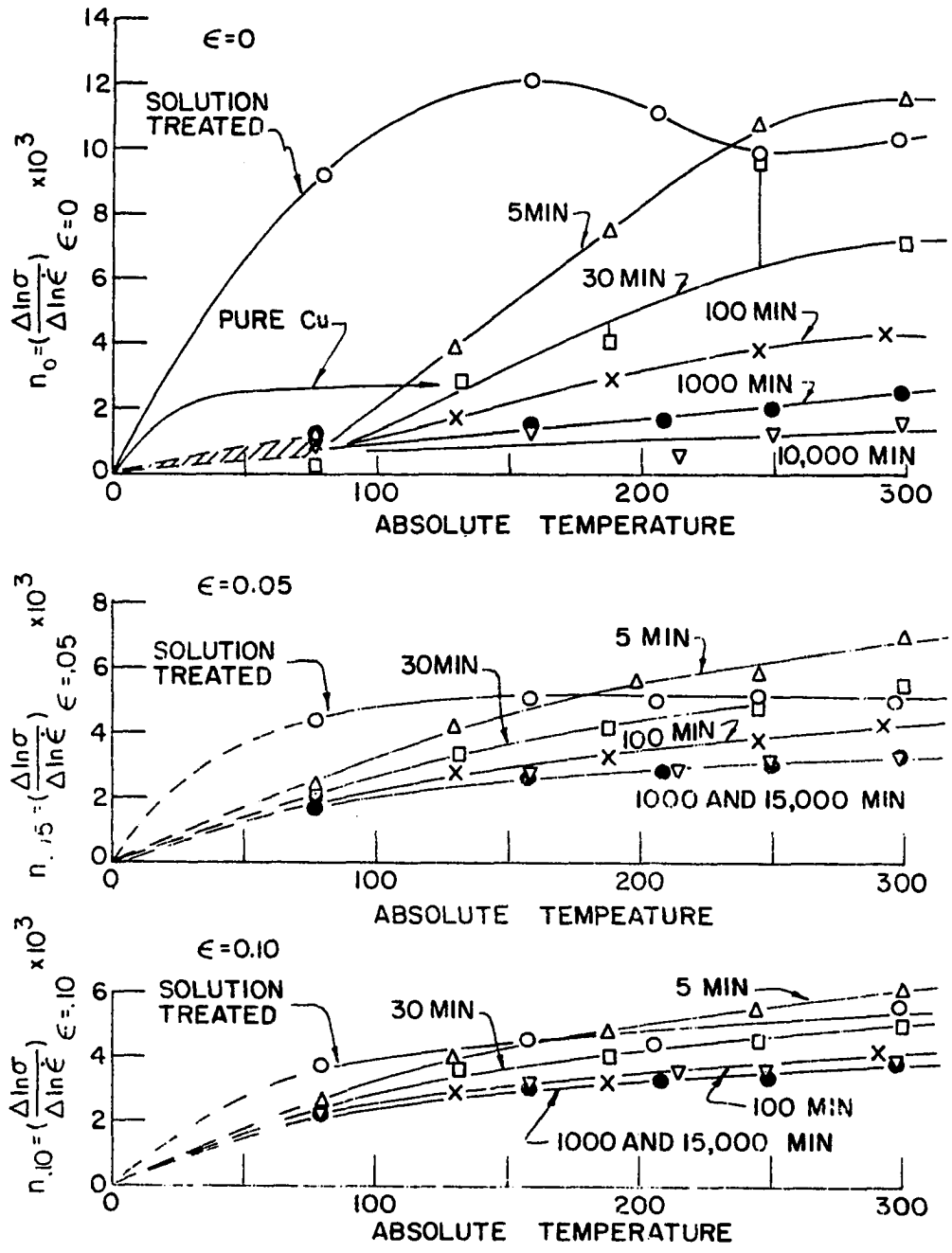
ϵ=0
SOLUTION TREATED
PURE Cu
5MIN
30 MIN
100 MIN
1000 MIN
10,000 MIN
$n_0=(\frac{\Delta \ln \sigma}{\Delta \ln \dot{\epsilon}})_{\epsilon=0} \times 10^3$
ABSOLUTE TEMPERATURE
ϵ=0.05
SOLUTION TREATED
30MIN
5 MIN
100 MIN
1000 AND 15,000 MIN
$n_{.05}=(\frac{\Delta \ln \sigma}{\Delta \ln \dot{\epsilon}})_{\epsilon=.05} \times 10^3$
ABSOLUTE TEMPEATURE
ϵ=0.10
SOLUTION TREATED
30 MIN
5 MIN
100 MIN
1000 AND 15,000 MIN
$n_{.10}=(\frac{\Delta \ln \sigma}{\Delta \ln \dot{\epsilon}})_{\epsilon=.10} \times 10^3$
ABSOLUTE TEMPERATURE

n vs ε curves undergo large curvatures at low values of strain which make extrapolation difficult. The only time that n is a constant with varying strain, of course, is when the Cottrell-Stokes law holds. It should be mentioned that throughout this dissertation, extrapolation to zero strain was accomplished when possible in order to remove the effects of deformation induced structure on the parameters under consideration.

It is apparent from Figure 21 that n* is a strong function of both aging time and temperature above 77°K but varied only slightly up to 77°K. For the solution treated material n* increased much more rapidly with temperature and was, in general, higher than that for the aged specimens. Data for pure Cu (43) were included for comparison. The rate sensitivity for copper is not strain dependent; therefore, the same curve holds for strains of 0.05 and 0.10. The curves for the aged specimens are all similar in form and generally the value of n* decreased with increased aging time. The continual decrease in the SRS parameter at zero strain with increased aging time is an indication that the precipitate particles are, at least, intimately related to short range barriers in the material.

The n vs T curves at true strains of 0.05 and 0.10 for different aging treatments have the same general relationship to each other as the n*-T curves but the changes with both temperature and aging time are much less pronounced. In fact at 0.10 strain all the curves are almost superimposed indicating that the substructure induced during deformation has a definite effect on the magnitude and, probably, type of short range dislocation mechanisms operating during deformation. This levelling off of the SRS due to plastic deformation reflects the way n, at 77°K, increases with strain and decreases with increasing strain at test temperatures greater than about 200°K. As strain increases, all the curves for the solution treated and solution treated and aged conditions seem to approach that of pure copper suggesting that the rate controlling dislocation mechanism in the deformed Cu-1.9 wt % Co alloy specimens is the same as those in deformed copper.

To determine if the strain-rate sensitivity was a function of the strain-rate ratio, a differential strain rate test was run at 300°K on a 1000 min. specimen. Strain rate ratios of 10, 25, and 50 were alternately used during the test. Values of the strain-rate sensitivity parameter n were calculated for each positive strain-rate increment and plotted

vs. elongation. The data all were on one curve within experimental scatter. It is concluded that the strain-rate sensitivity of the flow stress does not appear to be a function of the strain rate ratio in Cu-1.9 wt % Co polycrystals.

c. Strain rate sensitivity parameter m* The strain rate sensitivity of a material is frequently described by the parameter m where m = 1/n. m is of interest because the free energy of activation of the rate controlling dislocation mechanism is directly proportional to it. m* is shown versus temperature in Figure 22 for varying states of aging. Since m* and n* are inversely related, changes in n* not evident in Figure 21 are shown in Figure 22 as large changes in m*. The values of m* for the solution treated series were independent of temperature. m* generally increased with decreasing temperature in the aged specimens and was an increasing function of aging time at any single temperature excepting 77°K where the behavior was irregular. The m*-T relation of the averaged series appears to contain a well-defined peak in the vicinity of 200°K.

d. Activation volume When treating plastic deformation as a thermally activated process a quantity appears in the analysis that is equal to the total work done by external

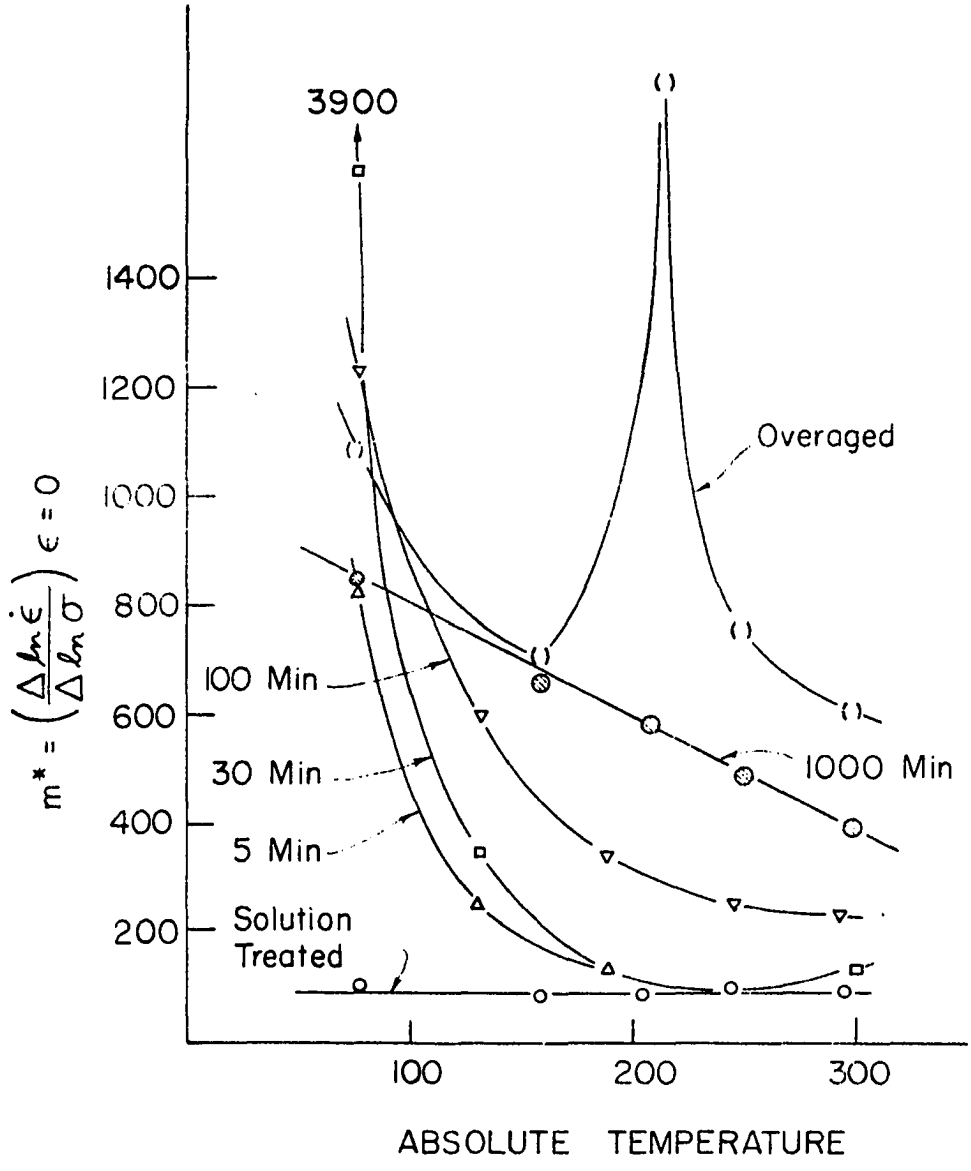

Figure 22. m* vs. temperature of Cu-1.9 wt % Co polycrystals solution treated at 1243°K and aged for different times at 873°K

forces during the activation event. This quantity, $\tau \Delta v$, defines the activation volume Δv where τ is the applied shear stress (39-42). The activation volume, Δv, at true strains of 0 and 0.05 are shown in Figures 23 and 24 respectively as a function of aging time and test temperature. In both figures Δv is normalized by b^3 where b is the Burgers vector. The activation volume varies in a regular manner with aging time, generally increasing with aging time. It is apparent in Figure 23 that the activation volume at zero strain for the solution treated series continually increases with temperature. On the other hand, the $\Delta v^*/b^3$ curves for the aged alloys are quite different. $\Delta v^*/b^3$ appears to increase with aging time at any single temperature for $T > 130^oK$. At a given aging time however, the variation of $\Delta v^*/b^3$ with temperature is unusual in that the curve appears to be composed of two portions, one existing at T greater than about 180^oK and the other at T less than 180^oK. It is also unusual that the low temperature segments of these curves tend upwards at 77^oK.

The activation volume can be considered as a measure of the amount of slip occurring during a single rate controlling activated event and is generally defined, in terms of disloca-

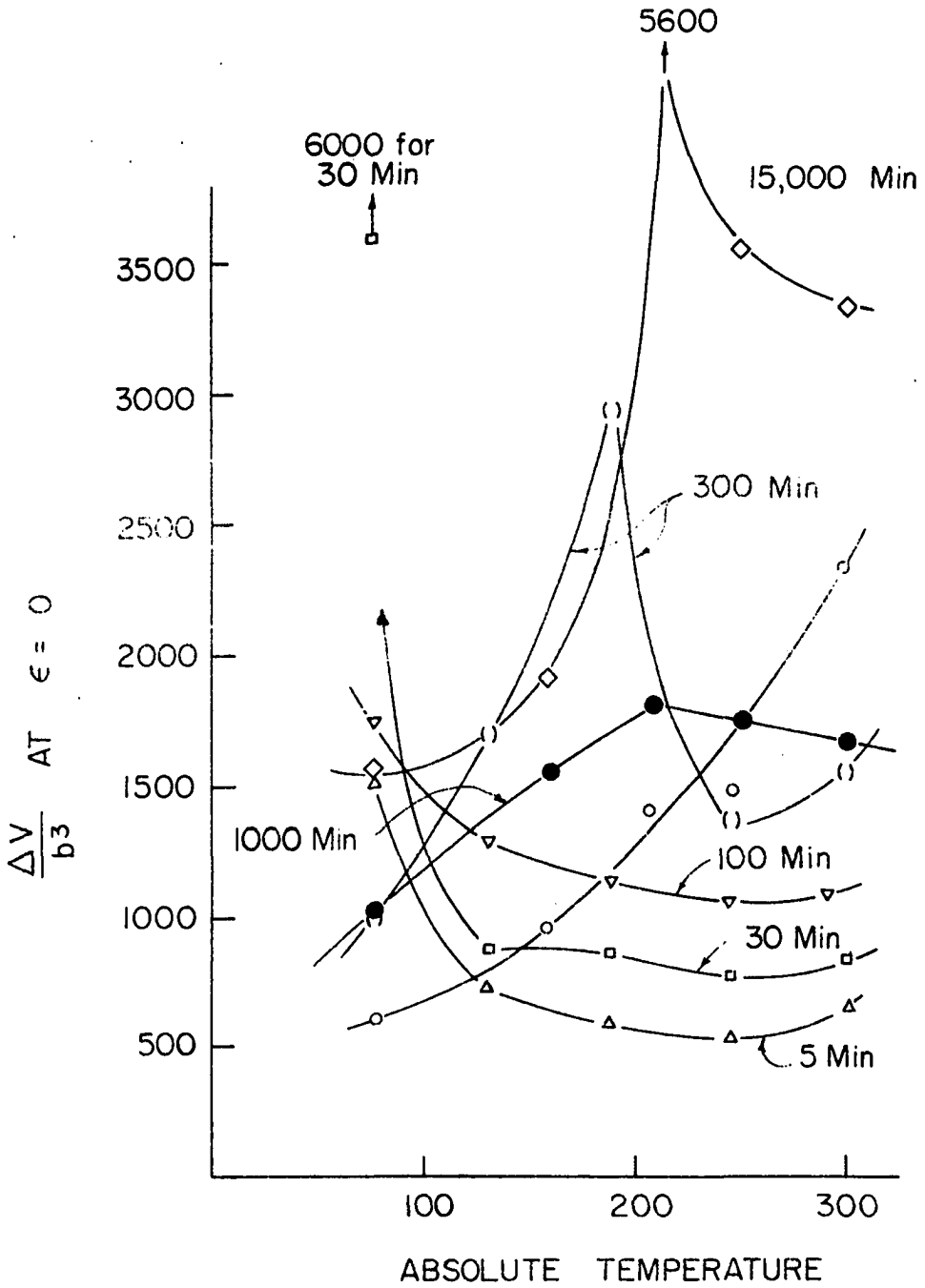

Figure 23. The temperature dependence of $\Delta V^*/b^3$ for Cu-1.9 wt % Co polycrystals solution treated at 1243°K and aged for different times at 873°K

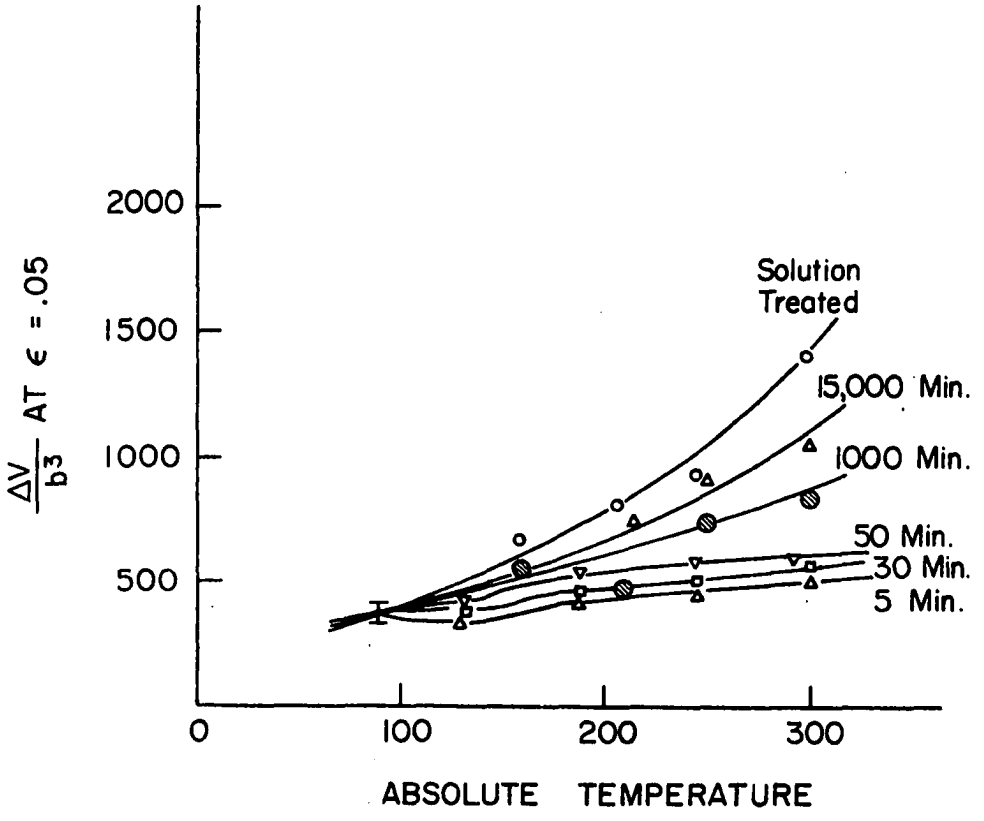

Figure 24. The temperature dependence of $\Delta V/b^3$ at 5% true strain for Cu-1.9 wt % Co polycrystals solution treated at 1243°K and aged for different times at 873°K

tions and their obstacles, as follows:

$$\Delta v = b\ l\ d$$

where b = Burgers

l = distance between obstacles

d = distance travelled by the dislocation during the activated event.

In this sense, the data in Figure 23 indicate how test temperature and aging time effect the size of the activated events responsible for the short range component of the flow stress. It is obvious that at temperatures greater than about $180^{o}K$, increased aging time increases the size of the activated event. It also appears that the mechanisms responsible for short range interactions undergo a change in the vicinity of $180^{o}K$ as shown by the development of the peak in the $\Delta v^*/b^3$ vs T curves with increasing aging time. When the effect of deformation induced structure on $\Delta v/b^3$ is removed by extrapolating to zero strain it is evident that precipitate size and spacing have a large effect on the activation volume. In other words, Figure 23 is another indication that, for low strains at least, the precipitates themselves contribute to the short range dislocation mechanisms leading to the temperature and strain rate dependent component of the flow stress.

With deformation, the picture changes drastically as shown in Figure 24. Here, $\Delta v/b^3$ at 5% true strain is plotted as a function of temperature and aging time. It is seen that the activation volume is an increasing function of aging time at all temperatures and that the solution treated condition yields the highest values of $\Delta v/b^3$. All the curves have a shape similar to that of the solution treated curve (and other f.c.c. metals) and the well defined peak of the $\Delta v/b^3$ curves is absent. Apparently deformation significantly reduces the effect of precipitates on the short range, rate controlling dislocation mechanisms. Some effect is, however, present as indicated by the regular increase in the curves with aging time.

3. Temperature change tests

In order to experimentally determine the activation energies associated with rate controlling dislocation mechanisms, the temperature dependence of the flow stress $\partial\tau/\partial T$ must be determined. For this reason temperature change tests were run on specimens in the solution treated, solution treated and aged to peak strength (1000 min. at 600°C), and solution treated and overaged (15,000 min. at 600°C) conditions.

a. Strain dependence of the flow stress ratio It was mentioned in the section on SRS data that a characteristic of f.c.c. metals is that they obey a Cottrell-Stokes relationship -

$$\Delta\sigma = D + E\sigma$$

for strain rate change tests. When the Cottrell-Stokes "law" is obeyed D = 0. It was also mentioned that this "law" is demonstrated in temperature change tests by the constancy of flow stress ratio with strain, i.e.,

$$\frac{\sigma_{T_2}}{\sigma_{T_1}} = K$$

Flow stress ratios as a function of strain for solution treated specimens are shown in Figure 25. In all cases the temperature changes were made from a reference temperature of 300°K. Yield points were generally observed in the load elongation curve proceeding a temperature change. As mentioned in Section III, the specimens were unloaded to a small load to maintain axial alignment preceding the temperature change. It is felt that the yield points are associated with the unloading and do not reflect the true temperature sensitivity of the flow stress. For this reason stresses associated with the load elongation curve extrapolated through the yield point were used. As seen in Figure 25, extrapolated

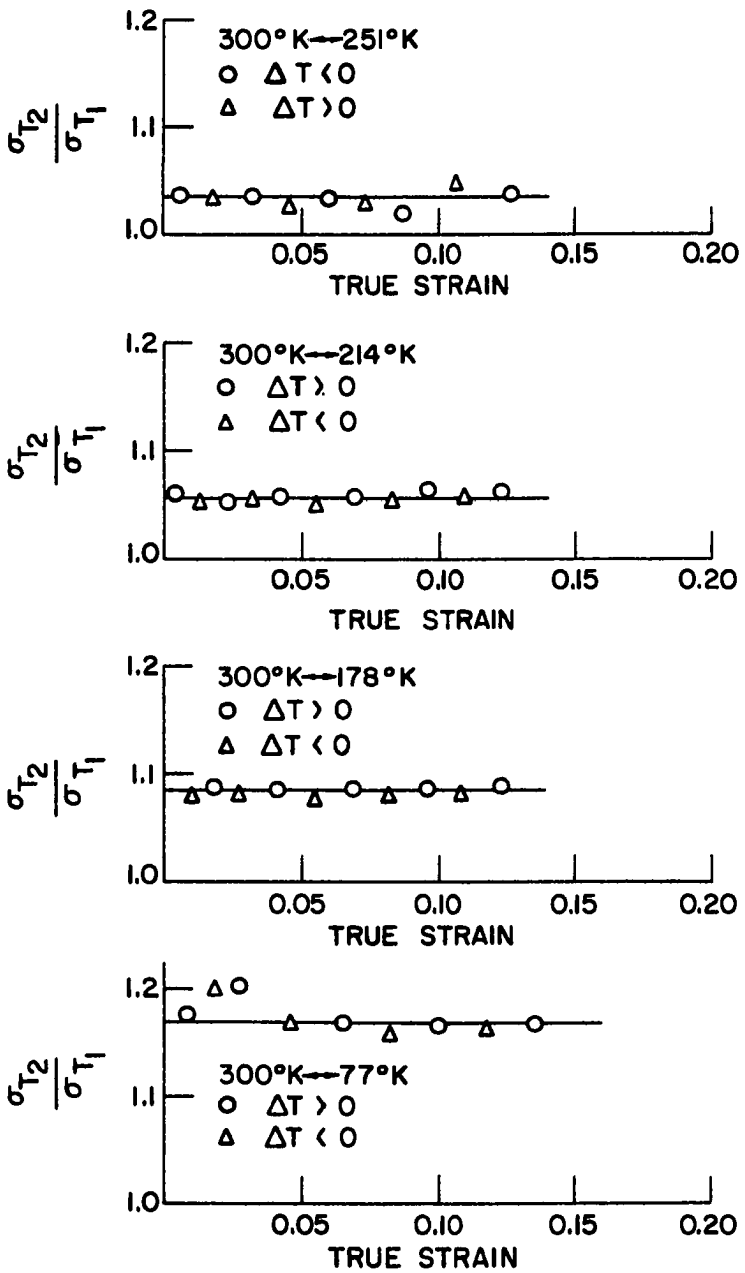

Figure 25. $\sigma_{T_2}/\sigma_{T_1}$ vs. true strain for Cu-1.9 wt % Co polycrystals solution treated at 1243°K

values of $\sigma_{T_2}/\sigma_{T_1}$ taken on both positive and negative temperature changes were equal. This reversibility of the flow stress increment accompanying a temperature change provides further justification that, in temperature change tests, the extrapolated value of $\Delta\sigma$ is most closely associated with the structure of the material existing before the change.

Clearly the flow stress ratios, $\sigma_{T_2}/\sigma_{T_1}$, are independent of strain for temperature changes from 300°K to 251°, 214°, 178°, and 77°K. In addition the Cottrell-Stokes law holds for solution treated Cu-1.9 wt % Co polycrystals. This was also shown to be true in the experiments on the strain rate sensitivity of the flow stress. Thus, in the solution treated material both the strain rate sensitivity and temperature sensitivity of the flow stress can be represented by an equation of the form

$$\frac{\Delta\sigma}{\sigma} = \text{CONSTANT} \ .$$

As mentioned above, the flow stress change accompanying a temperature change is reversible. The reversibility of $\Delta\sigma$ indicates that temperature dependent effects such as strain aging are not affecting the flow stress (77).

The failure of the Cottrell-Stokes law in aged polycrystals is shown in Figures 26 and 27. That Cu-Co specimens

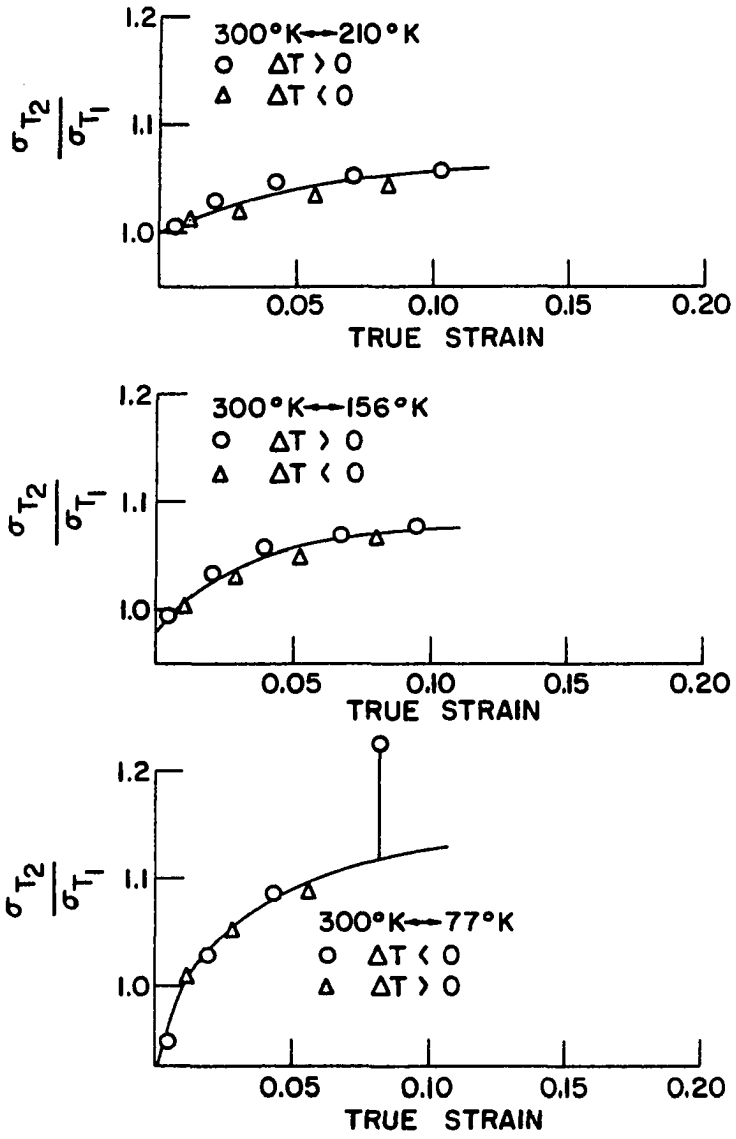

Figure 26. $\sigma_{T_2}/\sigma_{T_1}$ vs. true strain for Cu-1.9 wt % Co polycrystals solution treated at 1243°K and aged 1000 min. at 873°K

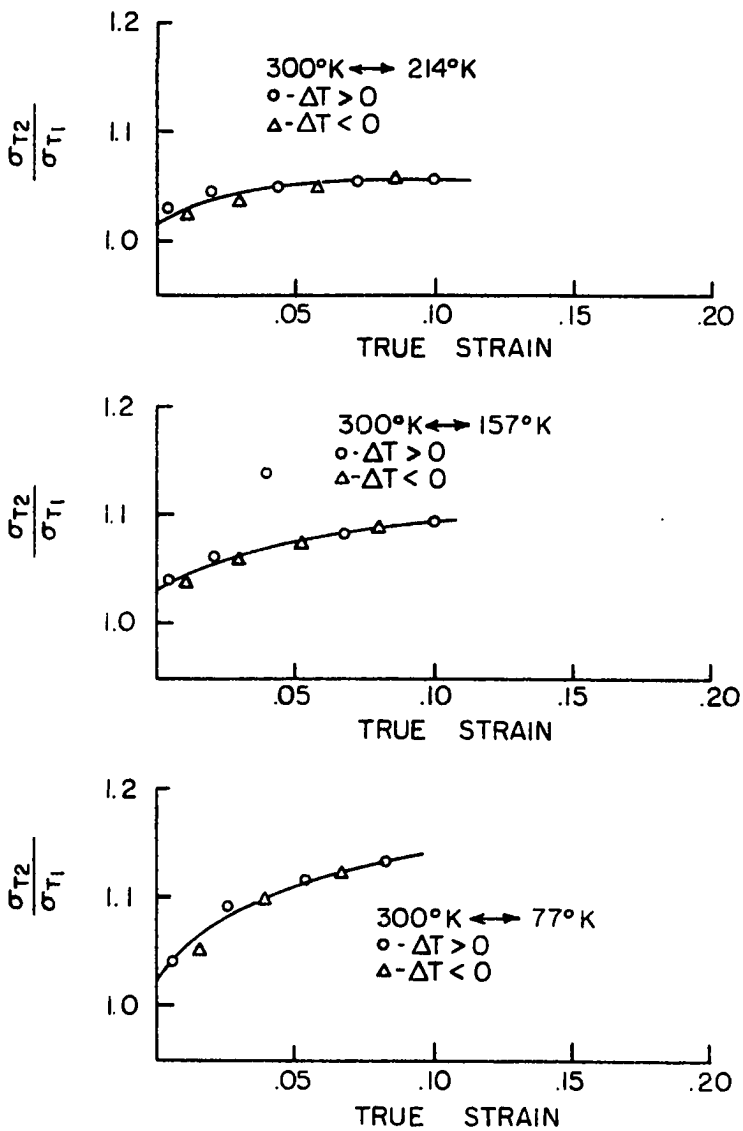

Figure 27. $\sigma_{T_2}/\sigma_{T_1}$ vs. true strain for Cu-1.9 wt % Co polycrystals solution treated at 1243°K and aged 15,000 min. at 873°K

containing coherent precipitates get softer upon cooling is quite evident. This behavior is similar to that found by Phillips (28). Phillips noted that for all aging times of a Cu-3.12 wt % Co alloy, the flow stress ratios of $\sigma_{303}/\sigma_{198}$, σ_{303}/σ_{77} and σ_{303}/σ_{20} all tended to approach that of copper at strains greater than about 10%. This tendency is also indicated in Figures 26 and 27 by the fact that, where the temperature changes are the same, the flow stress ratios of both the 1000 minute and overaged series approach the constant ratio of the solution treated series. This behavior is another indication that, at higher strains, matrix-dislocation interactions are controlling much of the deformation behavior.

The flow stress ratios for the overaged specimens increase with strain in a manner similar to the 1000 minute series. However, the temperature dependence of the flow stress was positive at all values of strain, indicating that the decrease in coherency strains due to cooling did not have as great an effect on the overaged specimens as on the peak hardened specimens. Presumably the cause of this effect is the difference in strengthening mechanisms between the two series.

4. Resistivity measurements

Electrical resistivity measurements were made on solu-

tion treated and aged polycrystalline wires in order to determine whether the discontinuous behavior observed in some of the rate sensitivity measurements (m* for example) as a function of temperature reflected temperature induced coherency losses, anomalous recovery effects, etc. The results are shown in Figure 28. It is evident that the resistivity measurements do not show any discontinuous behavior as the temperature is lowered. Since the curves appear to be a strong function of particle size, any anomalous loss of coherency, etc. that occurred should be indicated by the resistivity curves. The variation of the resistivity increment, $\Delta\rho$, due to the presence of particles as a function of particle radius was found to vary roughly as the 1/4 power of the radius at any temperature.

In other words

$$\Delta\rho = -AR^{\frac{1}{4}}$$

where $\Delta\rho = \rho_{aged} - \rho_{soln\ treated}$

A = a positive constant

R = mean particle radius

D. Mechanical Properties of Single Crystals

1. Tensile axes of all crystals

The crystals were grown from seeds in order that all had a similar orientation. The orientations of the seeds were

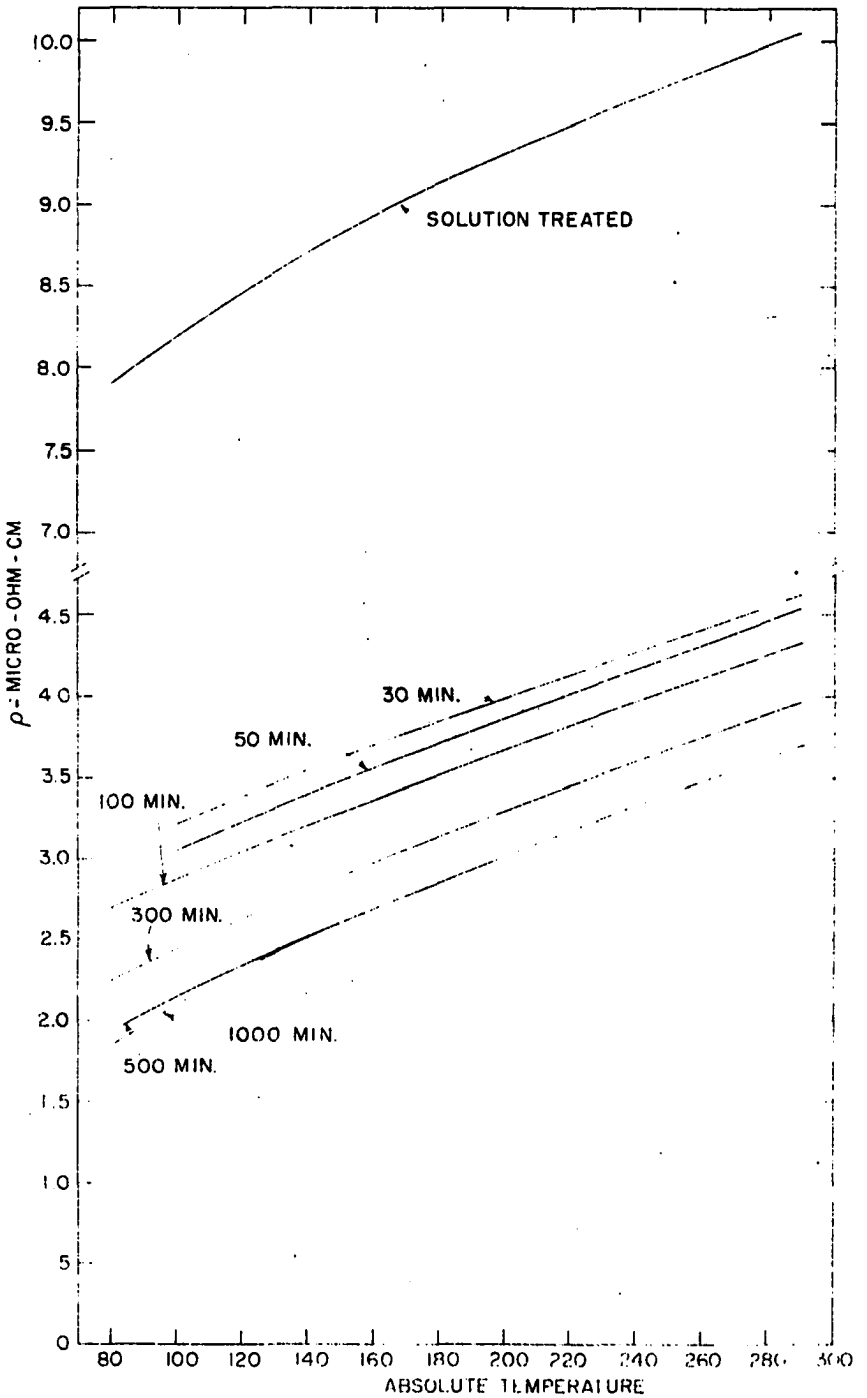

Figure 28. Resistivity vs. temperature curves for Cu-1.9 wt % Co polycrystals aged various times at 600°C

such that the tensile axis orientation lay in the center of the unit triangle to insure that the resolved shear stress was highest on one slip system. Seeds of two initial orientations that were quite close to each other were used. These seeds had their longitudinal axes 22^{o} from [001], 27^{o} from [011] and 24^{o} from [001], 25^{o} from [011] respectively. All crystals did not have exactly these orientations. In fact the orientations of all crystals grown from both seeds clustered in an area on the stereographic triangle with about a 5^{o} spread in their orientations. The spread in orientation results from the fact that the same seeds were used for all the crystal runs and were severely etched for cleaning prior to any run. The seeds thus fitted very loosely in the mold cavities and quite probably were tilted slightly with respect to the mold axis. The spread in orientations is not large however. The crystals and their initial orientations are given in Table 7. The angle between the tensile axis and the [001] direction, ρ_{001}, and the angle between the tensile axis and the [011] direction, ρ_{011}, were determined by the Laue back reflection method. Assuming (111) $[\bar{1}01]$ slip, the angles between the tensile axis and the slip direction λ_o and slip plane normal ϕ_o were determined by stereographic projection. The angles

Table 7. Orientation of Cu-1.9 wt % Co crystals solution treated at 1025° and aged at 600°C

Crystal	Aging time at 600°C (min)	Testing temp. (°K)	ρ_{001} degrees	ρ_{011} degrees	λ_o degrees	ϕ_o degrees
x-0-3[a]	0	295	22	27	39	51
x-0-6	0	243	21	28	38.5	51.5
x-0-4	0	188	21	28	38.5	51.5
x-0-7	0	126	25	25	39	51
x-0-5[a]	0	77	22.5	27	39	51
x-30-1[a]	30	295	21.5	27	39	51
x-30-3	30	244	22	27	39	51
x-30-4	30	187	22.5	26.5	39	50.5
x-30-5	30	127	22.5	27	39	51
x-30-2[a]	30	77	21	29	37.5	52.5
x-50-1	50	293	22.5	26	39.5	50
x-50-2	50	243	22	27	39	51
x-50-3	50	185	22	27.5	38.5	51.5
x-50-4	50	127	22	28	38	52.5
x-50-5	50	77	22.5	27	39	51
x-100-2	100	299	20.5	27.5	39.5	51
x-100-4	100	244	24.5	24	40.5	49
x-100-3	100	187	22	25.5	40.5	49
x-100-5	100	129	23	25	40.5	49

[a]Tensile axis rotation followed by x-rays.

Table 7. (Continued)

Crystal	Aging time at 600°C (min)	Testing temp. (°K)	ρ_{001} degrees	ρ_{011} degrees	λ_o degrees	ϕ_o degrees
x-300-3[a]	300	295	24	24	41	48.5
x-300-6	300	243	22.5	28.5	36.5	53
x-300-1	300	188	24	24.5	40	49.5
x-300-7	300	126	24	25	39.5	50.5
x-300-2	300	77	24	24.5	40	49.5
x-500-3	500	295	21.5	28.5	34	56
x-500-4	500	243	25	24	40	50
x-500-6	500	187	25	25.5	38.5	51.5
x-500-7	500	126	25	25.5	38.5	51.5
x-500-8	500	77	25	25.5	38.5	51.5
x-1000-1[a]	1000	293	22	27	39	51
x-1000-7	1000	243	25	25	39	51
x-1000-5	1000	187	22.5	27	39	51
x-1000-6	1000	127	24	25.5	39	51
x-1000-4	1000	77	22	27	39	51

ρ_{001}, ρ_{011}, λ_o, and ϕ_o are included in Table 7 as well as the temperature at which the crystal was tested.

It is estimated that the determination of ρ_{001} and ρ_{011} by the Laue technique gave the tensile axis orientation to better than $\pm 1^o$. A better idea of the range in orientations represented by the table is given in Figure 29 in which the orientations of the tensile axes of all crystals tested are plotted on one unit triangle. It is apparent that the spread in orientations is not large.

2. Stress strain behavior

a. Resolved shear stress-glide strain curves

i. Solution treated crystals Resolved shear stress-glide strain curves of solution treated Cu-1.9 wt % Co crystals tested at temperatures ranging from 295^o to 77^oK are shown in Figure 30. The curves have been displaced along the glide strain axis for clarity. Also included on the figure are the initial orientations of the crystals. The crystals all showed three stages of hardening common to f.c.c. single crystals oriented for easy glide (78,79) and are in good agreement with those obtained by Bonar (29). In fact the overall work hardening characteristics were identical to those of most f.c.c. solid solutions in that the extent of

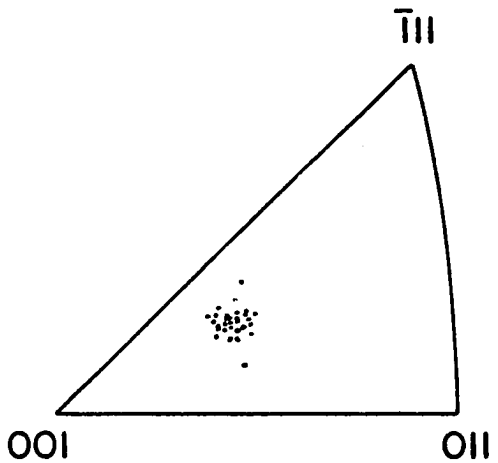

Figure 29. Orientations of the tensile axes of all single crystals tested in this investigation

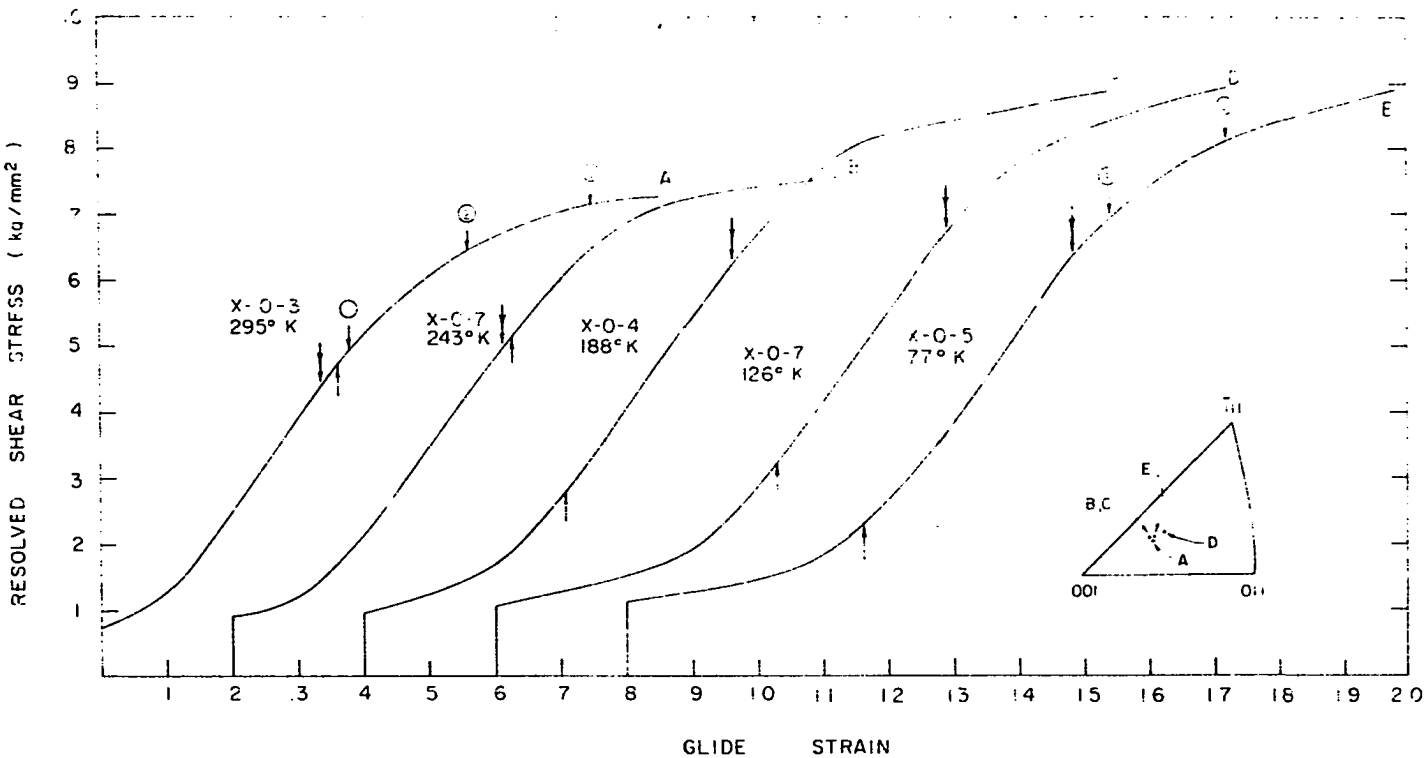

Figure 30. Resolved shear stress-glide strain curves at different test temperatures of Cu-1.9 wt % Co single crystals solution treated at 1298°K. The origins have been displaced along the glide strain axis for clarity

easy glide increased with a decrease in temperature and the slope of the linear hardening region in Stage II appeared relatively insensitive to temperature. The work hardening rate in easy glide was a decreasing function of temperature being 4.5 kg/mm^2 at 295°K and 1.64 kg/mm^2 at 77°K.

The parameter of most importance in this investigation is the critical resolved shear stress (CRSS) defined as the intersection of the extrapolated Stage I line with the elastic line. It is evident from Figure 30 that the CRSS of solution treated crystals increases with a decrease in temperature. In fact, as will be shown in a later figure, the increase in CRSS is a linear function of temperature.

The double headed arrows on the curves mark the points at which the linear hardening in Stage II starts to deviate from a straight line. This is generally taken to be the start of Stage III and the stress at which this occurs is a slowly increasing function of the decrease in temperature. This is in accord with the results of others on Cu, Cu-Zn (80), Cu-Ga, and Cu-Ge (81) alloys.

Since the initial orientations of the crystals were fairly close to the $(\bar{1}\bar{1}0)$ symmetry plane, the tensile axis crossed the plane during every test. When the tensile axis lies on

this plane (which contains the [001] and [111] directions) the resolved shear stresses on the primary slip plane, (111), and the conjugate slip plane, $(\bar{1}\bar{1}1)$, are identical and double slip can occur (68). In many cases, however, the tensile axis may overshoot the boundary while glide remains on the primary (111) $[\bar{1}01]$ system (82). For this reason it was deemed necessary to determine whether overshoot did occur in these crystals and to what extent. The orientations of the tensile axes of crystals A and E in Figure 30 were determined as a function of elongation by interrupting the tests at the points on the curves marked with single headed arrows and taking back reflection Laue x-ray patterns of the gauge lengths. The tensile axis orientations corresponding to the points marked on the stress-strain curves are shown in Figure 31. In both cases the crystals were well into Stage III and still deforming on the primary system as shown by the overshoot of the symmetry boundary that both crystals exhibited. This overshoot has been observed by Mitchell and Thornton (82,83) in Cu and α-brass, crystals who attributed it, in accord with others, (84) to hardening of secondary systems during deformation (i.e., "latent hardening"). As found by Mitchell and Thornton (82, 83) for Cu and α-brass, the amount of overshoot in solution treated Cu-1.9 wt % Co crystals increased with decreased

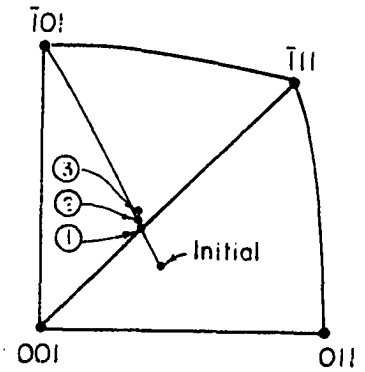

Solution Treated
Crystal A
295° K

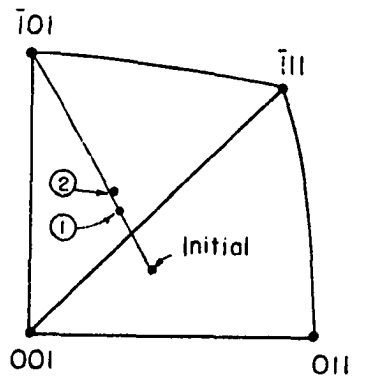

Solution Treated
Crystal E
77° K

Figure 31. Unit stereographic triangles showing rotations of the tensile axes of solution treated crystals A and E in Figure 30 during deformation. The numbers inside the triangles correspond to those marked on the shear stress-glide strain curves in Figure 30

temperature as illustrated in Figure 31. It is also apparent from the figure that the rotations of the tensile axes deviated from the great circle connecting the initial orientations and $[\bar{1}01]$. If glide was restricted to the primary system, the tensile axes would follow this great circle exactly. This deviation has also been observed by Mitchell & Thornton (83) who attributed it to the increasing contribution of secondary slip to the macroscopic deformation of the crystals with increasing strain. In fact they showed that the deviations in Cu crystals deformed at room temperature can be accounted for if 5-10% of the elongation is contributed by slip on secondary systems. Using Cu crystals oriented approximately the same as those used in this study, Mitchell and Thornton (83) further showed that deviations of the tensile axis from primary slip behavior occur even before the tensile axis reaches the symmetry plane. This is not the case with crystals of a Cu-1.9 wt % Co solid solution according to Figure 31 because the observed deviations occurred after the symmetry plane was passed. This could be attributed to solid solution hardening of the secondary systems by the Co atoms in solution.

Although the shear stress-glide strain curves in Figure 30 were computed on the basis of deformation by primary glide exclusively, which was clearly not the case, the deviations were small and it is felt that the curves give an adequate

presentation of the plastic deformation behavior of solution treated Cu-1.9 wt % Co single crystals. Activity on secondary slip systems was also demonstrated by the appearance of asterism on the Laue x-ray patterns taken during the interrupted tests.

In order to correlate overshoot with the observed deformation behavior, the strain at which the tensile axis crossed the symmetry boundary was calculated for all the crystals shown in Figure 30 and is denoted by an inverted arrow on the stress-strain curves. This was also done for all tests to be presented.

ii. Crystals aged 30 min. at 600°C The stress-strain behavior of crystals aged 30 minutes and tested at various temperatures is shown in Figure 32. Clearly aging causes a large increase in yield stress and a change in the general shape of the curves. All the crystals exhibited discontinuous yield behavior that lasted for at least 15% strain followed by a region of parabolic hardening that was terminated by a final region of increasing work hardening rate. The fracture characteristics will be discussed in a later section.

Yielding occurred in a discontinuous fashion by the

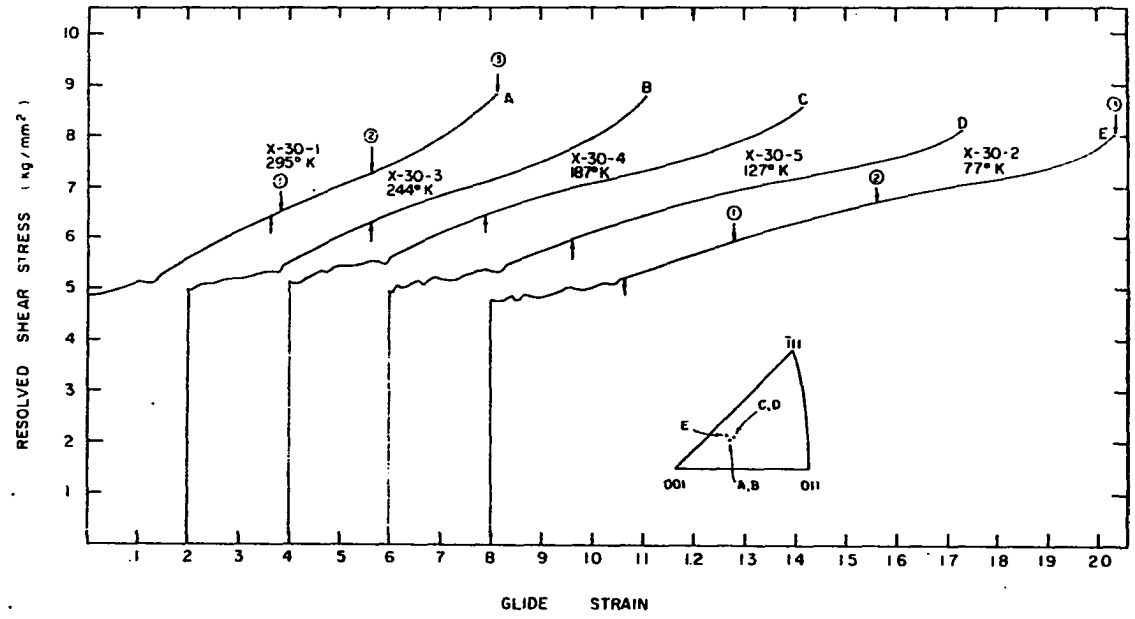

Figure 32. Resolved shear stress-glide strain curves at different test temperatures of Cu-1.9 wt % Co single crystals solution treated at 1298°K and aged 30 min. at 873°K. The origins have been displaced along the glide strain axis for clarity

formation and propagation of course slip bands concentrated in Luders-like bands. As deformation continued the Luders bands propagated along the gauge length by the nucleation of successive slip bands ahead of the front. The formation and propagation of the Luders bands was, of course, accompanied by the fluctuations in load evident on the stress-strain curves. Since the slip bands making up the Luders front nucleated in undeformed material, the overall work hardening rate during yielding is quite low even though it was high in each band. The strain during yielding is inhomogeneous since all deformation is concentrated in the Luders bands and the gauge length does not begin to deform uniformly until all the Luders bands (there may be more than one) fill the gauge length. Photographs of a Luders front in a crystal aged 300 min. are shown later.

Discontinuous yielding in f.c.c. metals and alloys has been observed by Mitchell and Thornton (82) and Piercy et al. (84) in single crystals of α-brass, by Cottrell and Stokes (65) in aluminum single crystals accompanying work softening, and by Haberkorn (20) in aged Al-Zn crystals. In the studies of α-brass the Luders yielding was clearly associated with easy glide. In the Al single crystals it was associated with

an unloading yield point following deformation at a lower temperature. In the present study the observed formation and propagation of Luders bands is a yielding phenomenon but probably is not directly related to easy glide since the hardening is parabolic immediately following the Luders deformation. Furthermore the yield stresses of crystals aged 30 min. at 600°C are about 5 times as large as those of the solution treated crystals. The large fluctuations in stress also indicate that the work hardening rate in the slip bands comprising the Luders bands is quite high; this is not characteristic of easy glide. In one way, however, the discontinuous yielding did resemble easy glide. It is apparent from Figure 32 that the extent of strain during discontinuous yielding increases as the temperature is decreased.

Values of the CRSS were obtained by extrapolating the best fit line through the fluctuating portion of the stress-strain curves to the elastic line. The intersection of these two lines was taken as the CRSS. The CRSS decreased as the temperature was lowered.

Bonar (29) tested crystals oriented for easy glide in the following conditions:

i) Solution treated

ii) Aged at 600°C for 4, 20, 90, and 66,000 min.

Tests were run at both 300° and 77°K but only the 300°K tests were presented since it was felt the differences were slight. Yield points were present in all the tests of crystals aged up to 90 min. but discontinuous yielding was not evident from his curves. Not too much can be ascertained from his tests because the discussion concerning them was quite limited and centered around the variation of the yield stress with aging time. Examination of his curves for crystals aged up to 90 min. does show, however, that parabolic hardening commenced immediately following yielding in agreement with the present results, thus adding credulance to the supposition that the observed discontinuous yielding is not associated with easy glide as commonly defined (79).

An interesting phenomenon was observed in crystals aged 30 min. and, as will be seen, in crystals aged for times up to 100 min. at 600°C. At high strains the work hardening rate increased and the stress-strain curves curved upwards until uniform elongation was reached. At that point necking and fracture commenced. This behavior is evident in Bonar's (29) curves at 300°K for Cu-2% Co crystals as well as in precipitation hardened crystals of other alloy systems oriented for

easy glide (20,85). To the author's knowledge this behavior has never been discussed in the literature. Since, as will be shown, deformation occurred mainly on the primary glide system the behavior is characteristic of an exhaustion process involving primary glide dislocations and is probably related to latent hardening on the conjugate system. This behavior and its implications will be discussed in the section on fracture. In view of the fact that Bonar's crystals never crossed the symmetry plane, the beginning of the region of increased work hardening rate does not necessarily involve the onset of conjugate slip although the results of the present study suggest that the onset of necking does.

To determine whether slip in the age hardened crystals occurred mainly on the primary system the rotations of the tensile axes accompanying extension of the 30 min. crystals A and E in Figure 32 were followed by unloading the specimens at various points along the stress-strain curves and determining their orientations by standard Laue back reflection x-ray techniques. These results are shown in Figure 33 in which the tensile axis orientations corresponding to the points marked on the stress-strain curves in Figure 32 are plotted on a standard projection along with the initial

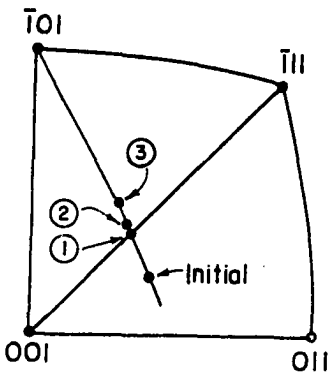

Aged 30 min
Crystal A
295° K.

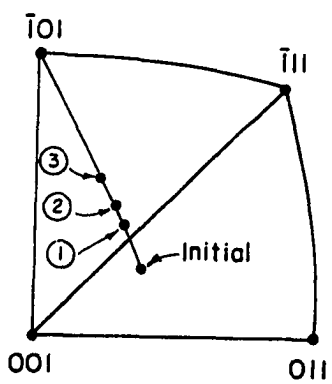

Aged 30 min
Crystal E
77° K.

Figure 33. Unit stereographic triangles showing rotations of the tensile axes of crystals A and E in Figure 32a during deformation. The numbers inside the triangles correspond to those marked on the shear stress-glide strain curves in Figure 32a

orientations. It is evident that, at both 295° and 77°K, the tensile axis overshot the symmetry plane and did not deviate from the great circle connecting the initial orientation and the slip direction up to uniform elongation. Thus, slip must have been confined to the primary system even during overshoot with the conjugate system playing a negligible role. This was also evident by the absence of asterism on the x-ray patterns. This means that the stress-strain curves of age hardened crystals of Cu-1.9 wt % Co can be calculated from the load elongation curves using the assumption of single slip which, as discussed in the experimental procedures, was done in this study. The increased elongation at 77°K of crystal E over that at 295°K of crystal A is clearly shown in Figure 33.

Finally it should be mentioned, in reference to Figure 32, that the stress at uniform elongation decreased with temperature in contrast to the solution treated crystals and f.c.c. metals in general (3).

iii. Crystals aged 50, 100, and 300 min. at 600°C

Shear stress-glide strain curves for crystals aged 50, 100, and 300 min. at 600°C and tested at various temperatures are shown in Figures 34, 35, and 36 respectively. The curves are all similar to those of the 30 min. crystals. They all

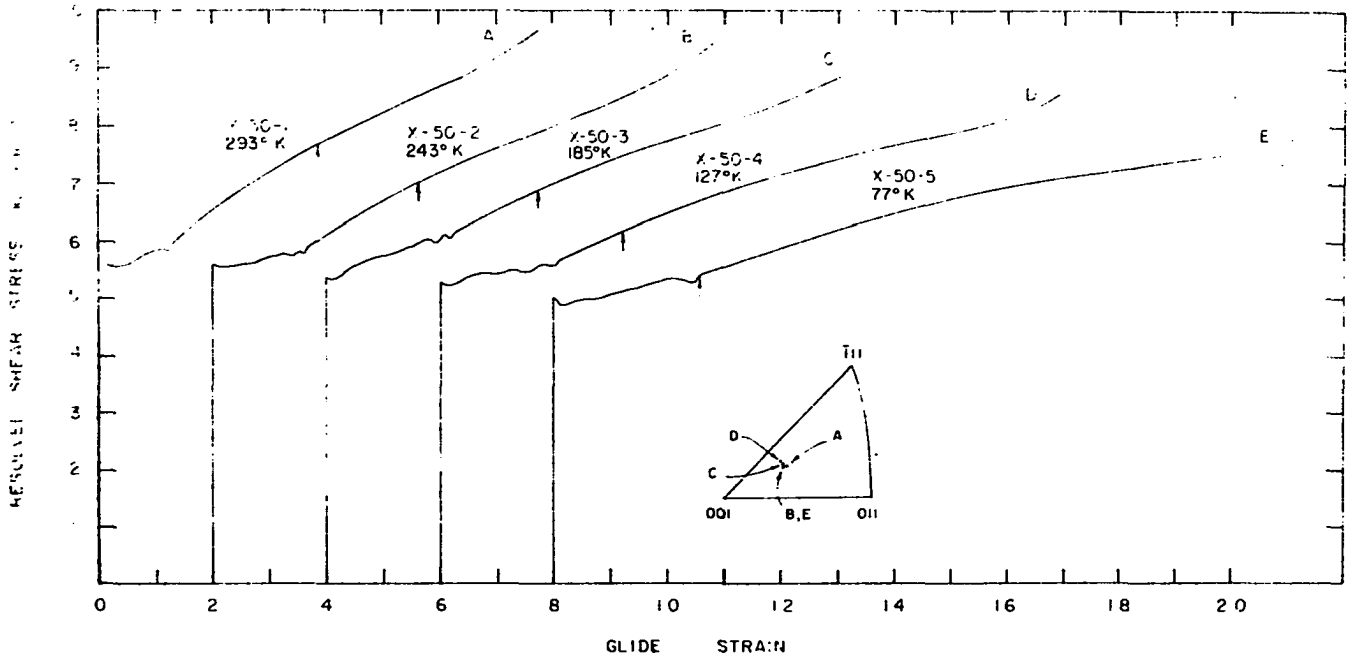

Figure 34. Resolved shear stress-glide strain curves at different test temperatures of Cu-1.9 wt % Co single crystals solution treated at 1298°K and aged 50 min. at 873°K. The origins have been displaced along the glide strain axis for clarity

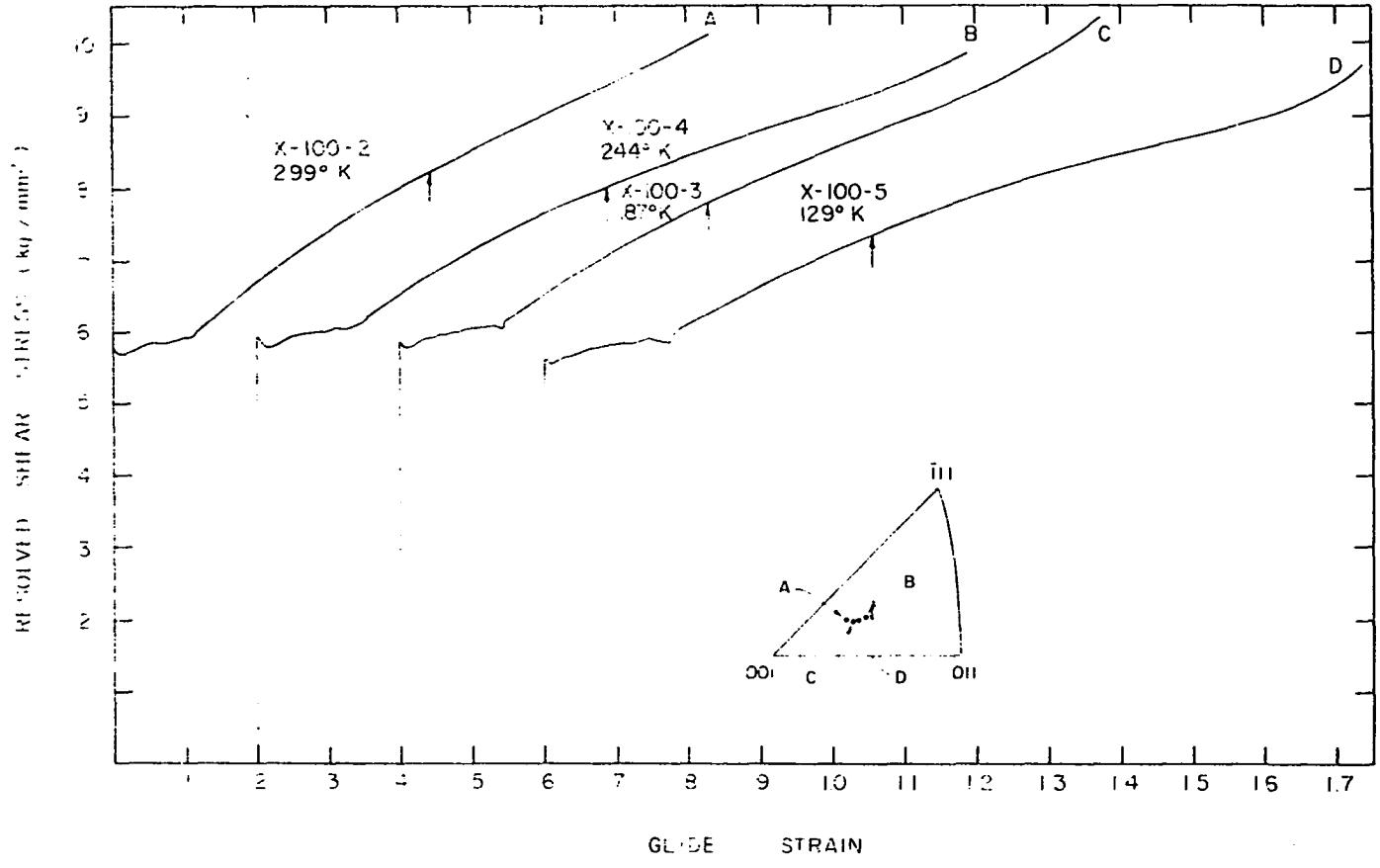

Figure 35. Resolved shear stress-glide strain curves at different test temperatures of Cu-1.9 wt % Co single crystals solution treated at 1298°K and aged 100 min. at 873°K. The origins have been displaced along the glide strain axis for clarity

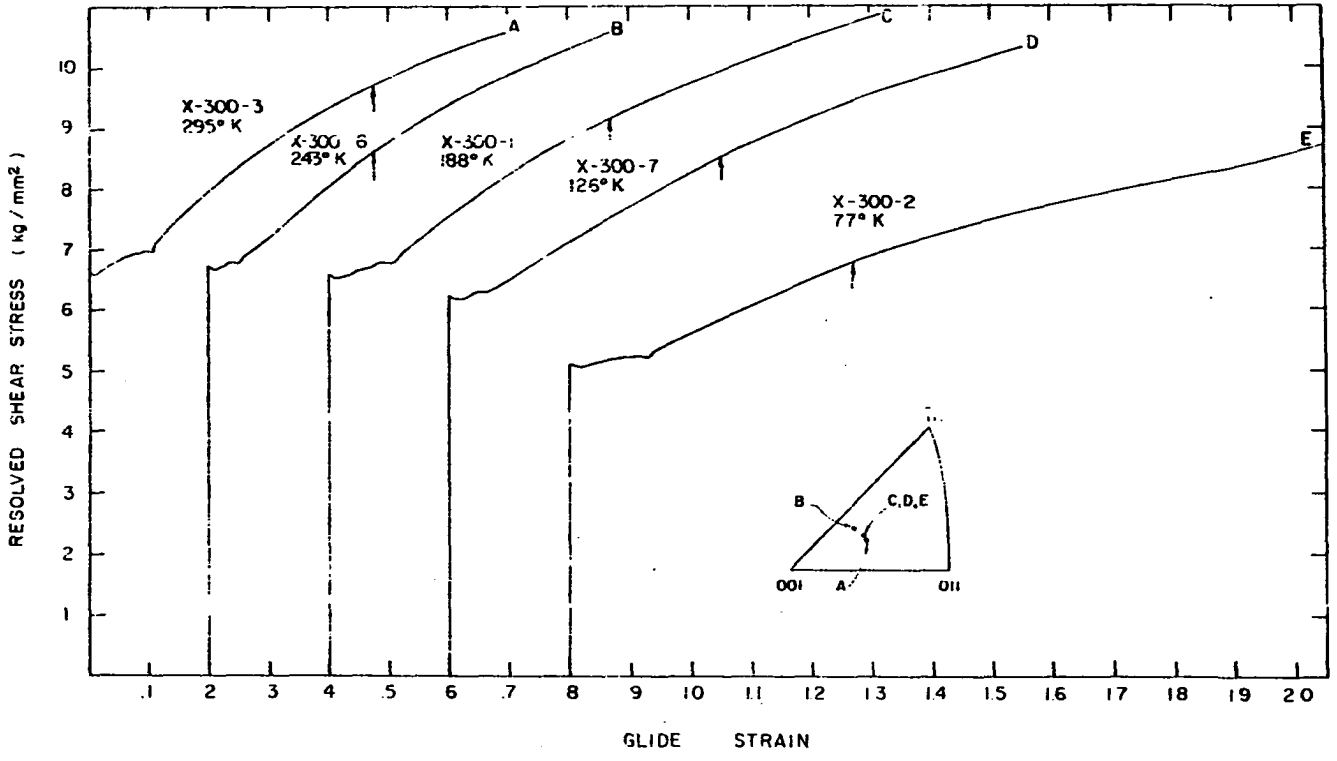

Figure 36. Resolved shear stress-glide strain curves at different test temperatures of Cu-1.9 wt % Co single crystals solution treated at 1298°K and aged 300 min. at 873°K. The origins have been displaced along the glide strain axis for clarity

show yielding by a Luders mechanism and a drop in CRSS with a decrease in temperature. Just before uniform elongation the curves of the 50 and 100 min. crystals turn up as did the 30 min. crystals. This phenomenon was not observed in most of the 300 min. crystals. The crystal tested at $77^{o}K$ did turn up before necking but the test is doubtful because of the inordinately low yield point. In regard to the increased work hardening rate just preceding uniform elongation it is interesting to note that every crystal that necked below a stress of about 10 kg/mm^2 turned upward and every one that necked at a stress over about 10 kg/mm^2 did not.

The extent of Luders yielding appeared to decrease with an increase in aging time for a given temperature and, as revealed by the 30 min. crystals, appeared to increase with a decrease in testing temperature for any single aging time.

The yield stresses increased with aging time and decreased with test temperature at any one aging time as was seen in the 30 min. crystals and the aged polycrystals.

A determination of the crystallographic orientation of the tensile axis of crystal A in Figure 36 at uniform elongation again showed that deformation occurred almost entirely on the primary slip planes because the position of the tensile

axis was on the great circle connecting the initial orientation and the slip direction. In addition little or no asterism was observed in the x-ray patterns.

It has been mentioned several times that the aged crystals yielded by a Luder mechanism. Figure 37 shows a photograph of slip bands at the front of a Luders band in a crystal aged 300 min. at 600°C and tested at room temperature. The crystal was extended to just past the yield point, unloaded, and photographed. The major characteristics of the Luders front are clearly recognizable, especially the decreasing concentration of slip bands as the front is approached. This particular Luders band nucleated away from the grips toward the center of the gauge length.

iv. Crystals aged 500 and 1000 min. at 600°C

The stress-strain curves of crystals aged 500 and 1000 min. at 600°C and tested at various temperatures are shown in Figures 38 and 39. The major differences between these curves and those of crystals aged for shorter times are the higher work hardening rates and shorter region of Luders yielding shown by these curves. During yielding there is a marked work hardening even though the load-elongation curves exhibited the discontinuous behavior characteristic of yielding. In fact,

Figure 37. Photograph of a Luders band in a crystal aged 300 min. at 600°C and extended at room temperature to just past the yield point. 50X

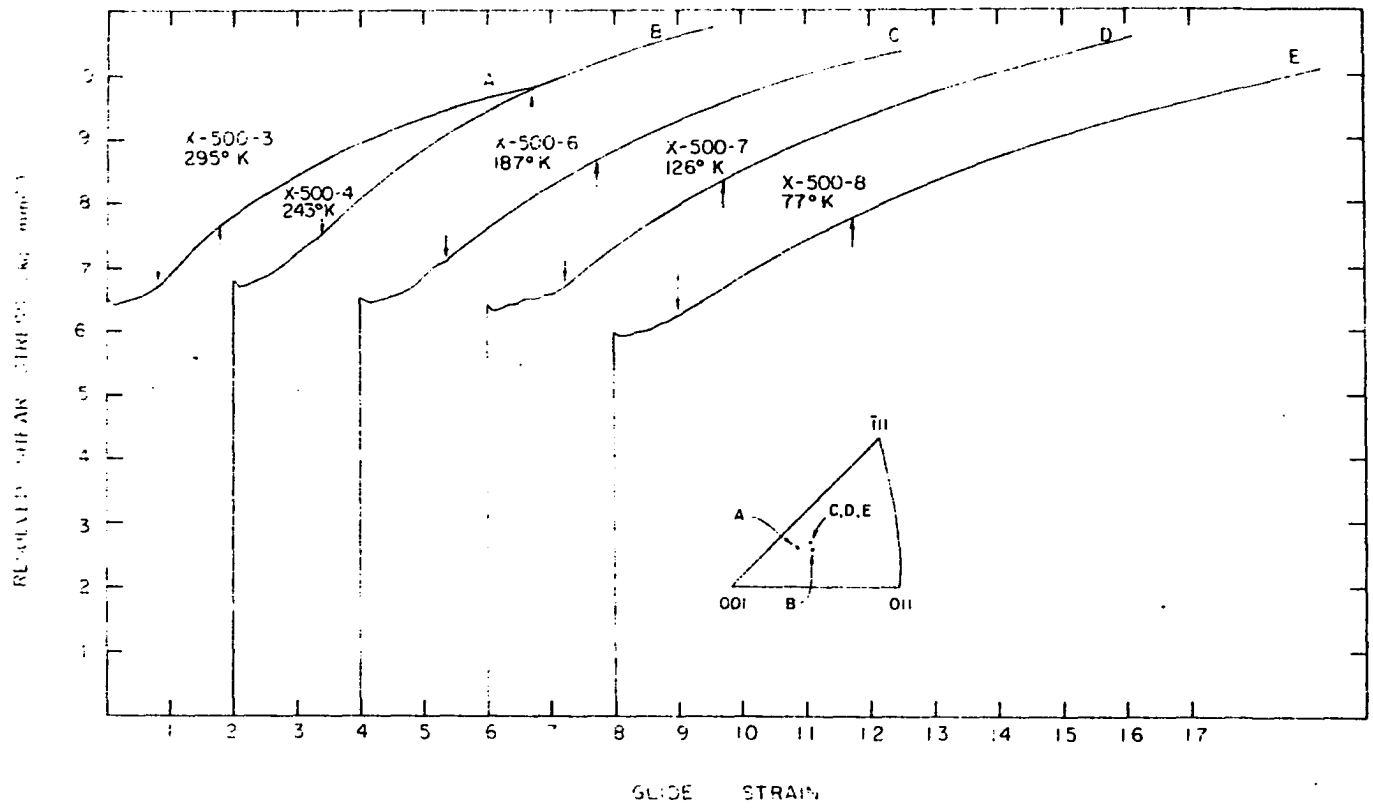

Figure 38. Resolved shear stress-glide strain curves at different test temperatures of Cu-1.9 wt % Co single crystals solution treated at 1298°K and aged 500 min. at 873°K. The origins have been displaced along the glide strain axis for clarity

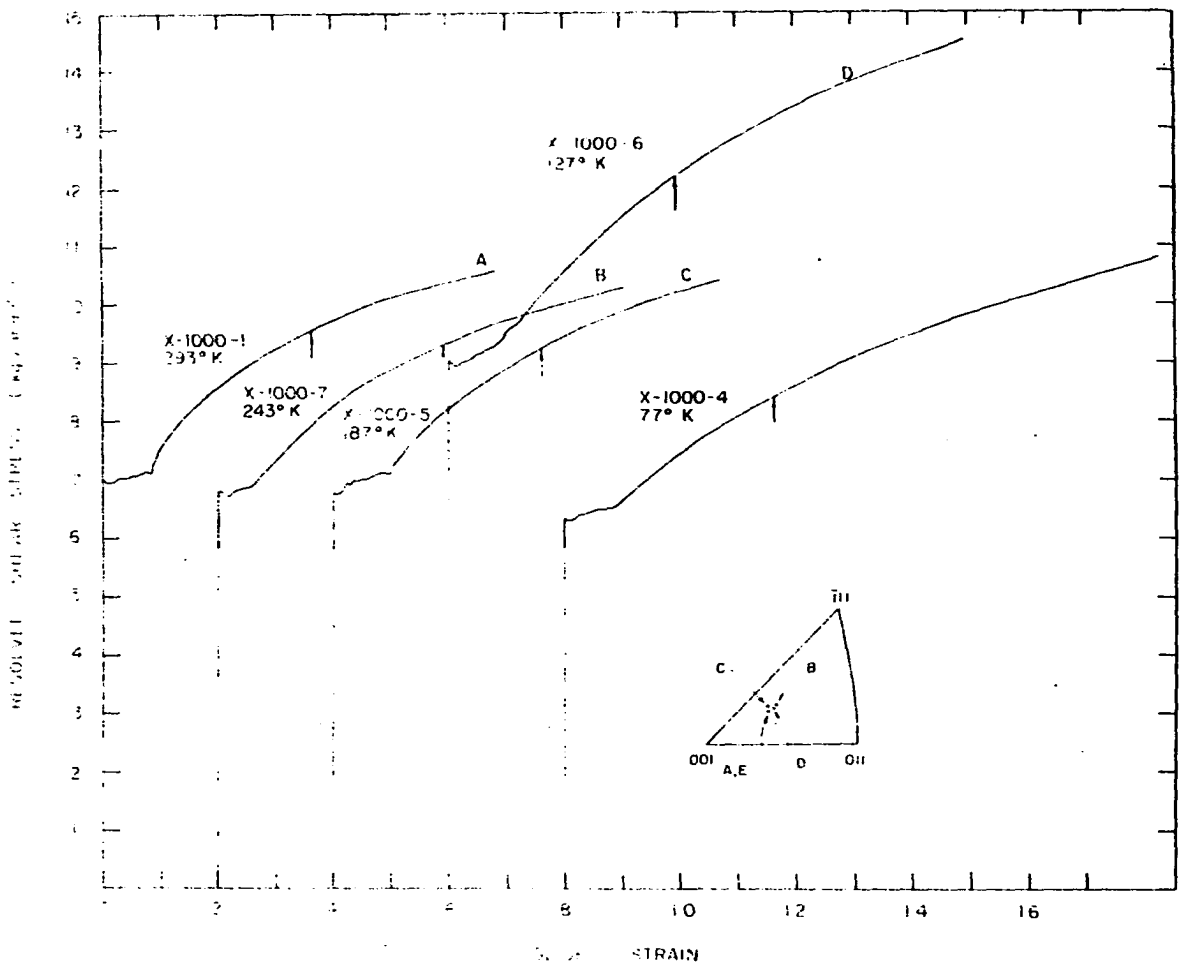

Figure 39. Resolved shear stress-glide strain curves at different test temperatures of Cu-1.9 wt % Co single crystals solution treated at 1298°K and aged 1000 min. at 873°K. The origins have been displaced along the glide strain axis for clarity

in some of the 500 min. crystals, the work hardening rate during yielding was almost the same as that during uniform elongation. For this reason the end of Luders yielding is marked with arrows in Figure 38.

The work hardening rates in the 500 min. crystals do not appear to be a function of temperature. The work hardening rates of the 1000 min. crystals, although on the average somewhat higher than those of the 500 min. crystals, also appear to have no strong relation to temperature. The unusual appearance of curve D, Figure 39 cannot be explained at present. Possibly the crystal was mishandled prior to testing.

The absence of the upswing near uniform elongation is apparent in all the 500 and 1000 min. crystals. It should also be noted that necking occurred at resolved shear stresses greater than 10 kg/mm^2 in all cases.

The CRSS was a slightly decreasing function of temperature for both the 500 and 1000 minute crystals with the exception of crystal D in Figure 39.

Laue x-ray determinations of the tensile axis orientations in 1000 min. crystals A and E in Figure 39 extended to uniform elongation showed the tensile axes in both cases to be

on the great circle connecting their initial orientations and the slip direction. No asterism was evident in either x-ray pattern. Thus, even in peak hardened crystals, the change in tensile axis orientation during deformation is that of a crystal deformed almost entirely by primary glide.

b. Critical resolved shear stress vs. temperature

The CRSS of the crystals tested is shown as a function of temperature in Figure 40. Data from differential strain tests are also included. The two tests exhibiting inordinately low and high values of CRSS (i.e., 300 minute age tested at 77°K and 1000 min. age tested at 127°K) are not included because it was felt the observed behavior was due to experimental errors and was not characteristic of the material itself. Figure 40 clearly shows that the CRSS of aged Cu-1.9 wt % Co crystals decreased with temperature for all the aging times investigated. The only exceptions are the 5 and 30 minute series in which the CRSS increased and then decreased as the test temperature decreased. This behavior is identical to that found in polycrystals and is no doubt also due to "particle shrinkage" (28). The CRSS of the solution treated crystals increased linearly with decreasing temperature.

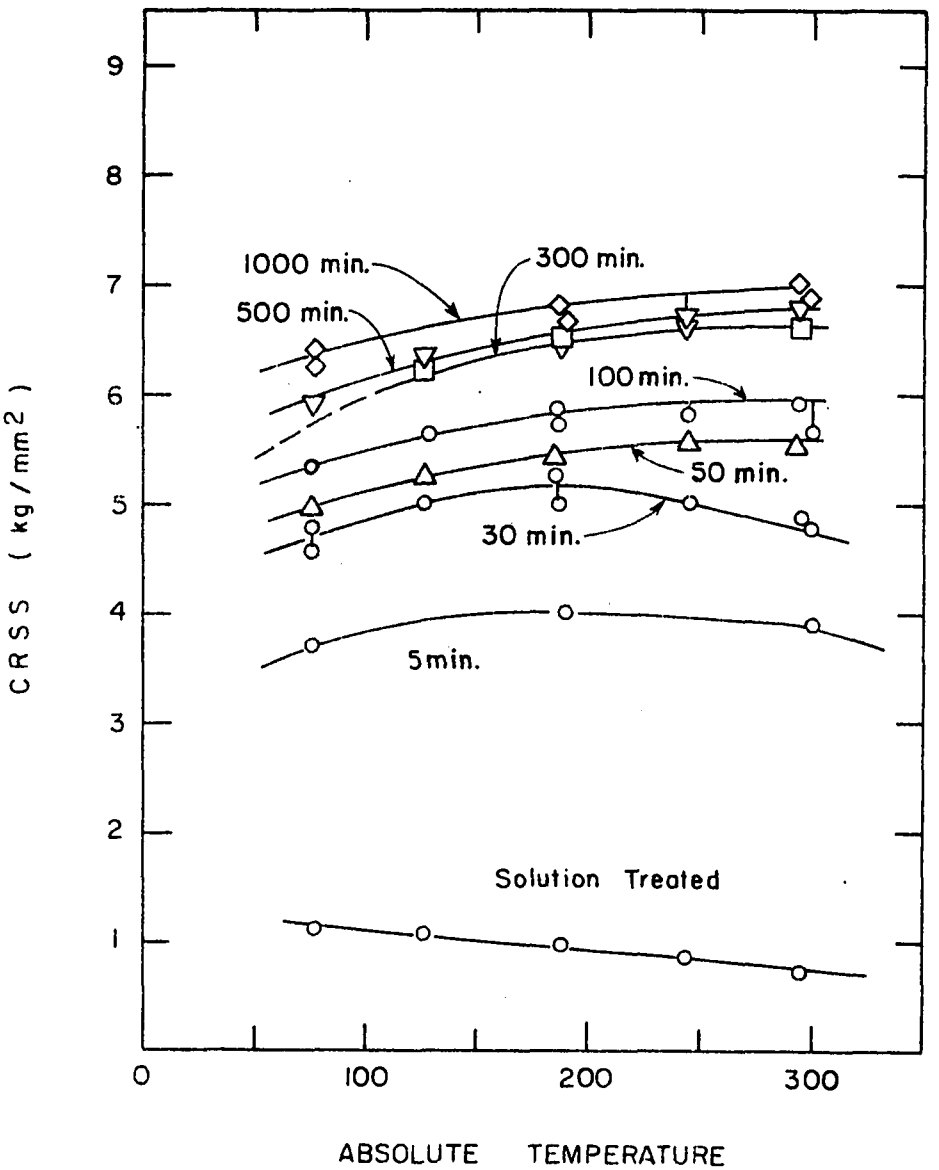

Figure 40. Critical resolved shear stress vs. temperature of Cu-1.9 wt % Co single crystals solution treated at 1298°K and aged for different times at 873°K

c. Necking and fracture of single crystals The single crystals used in this investigation all fractures by necking down to a knife-edge with reductions in area approaching 100%. The behavior accompanying the onset and early stages of necking was quite dependent on the state of aging, however, and three distinct necking "mechanisms" were observed. These will be discussed in turn below.

The solution treated crystals necked by slipping heavily on the primary and conjugate slip planes. This process continued until the crystals drew down to a knife-edge and parted. In the necked region the concentration of primary and conjugate slip bands appeared to be about equal and the coarse shear bands observed by Beevers and Honeycombe in Cu crystals (86) were absent. The necks appeared to be symmetric indicating that slip had not been preferentially restricted to one slip system. The final tear usually appeared to be at 45^{o} to the tensile axis.

The crystals aged for 30, 50, and 100 min. at $600^{o}C$ necked in quite a different manner. It should be recalled here than in all tests of the 30, 50, and 100 min. crystals, the shear stress-glide strain curves turned upward and showed a sudden increase in work hardening rate just prior to neck-

ing. Necking was accompanied by a drop in the load-elongation curves and by the formation of coarse slip bands on the conjugate slip planes. More conjugate slip bands then formed and the decrease in cross sectional area associated with the neck propagated down the gauge length in a Luders front. As the "stable neck" grew the load remained nearly constant and the load-elongation curve was reminiscent of one during yielding. A schematic of a typical load-elongation curve exhibiting this type of behavior is shown in Figure 41. The length of the "stable neck" varied from about 1/4 inch to the whole gauge length and did not appear to have any correlation with either the aging time or test temperature. Propagation of the first neck stopped when a second neck formed inside the first neck. The load then dropped continuously while the crystal necked down to a knife edge and failed. A photograph of a stable neck in a crystal aged 30 min. at 600°C and tested at 77°K is shown in Figure 42. A similar phenomenon has been shown to occur in tin crystals in some cases and Beevers and Honeycombe (86) attributed the formation of the first neck to the simultaneous operation of two slip systems. In Cu-1.9 wt % Co crystals the first neck formed due to slip only on the conjugate system. Throughout the necked region the conjugate slip

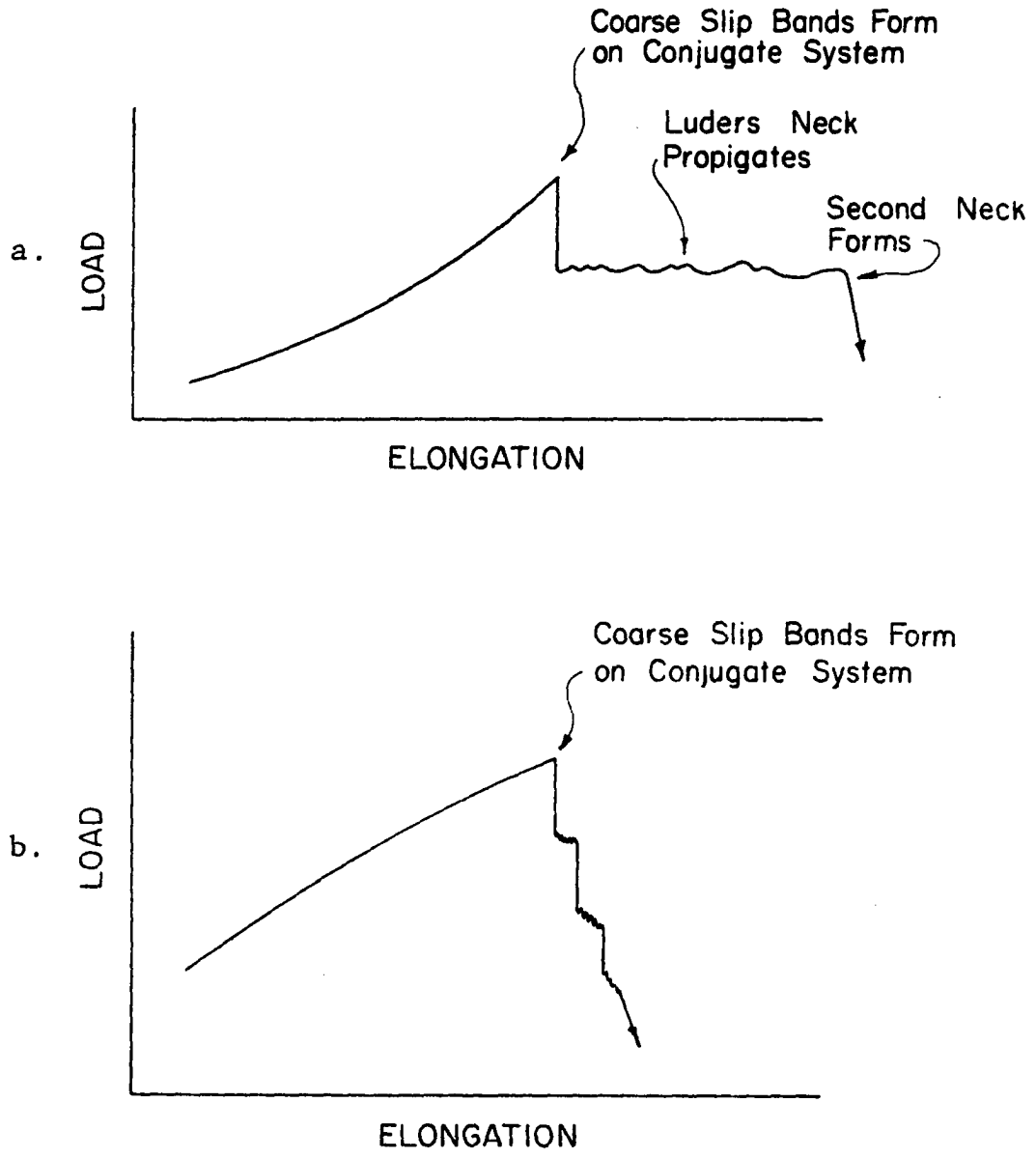

Figure 41. Schematic of single crystal load-elongation curves during necking
a. Formation and propagation of "stable neck"
b. Necking in crystals aged 300 to 1000 min. at 873°K

Figure 42. Photographs illustrating the simple slip band configurations at the ends of a stable neck and the more complex behavior at the center where an unstable neck had just begun. The sample is a Cu-1.9 wt % Co single crystal aged for 30 min. at 600°C and tested at 77°K

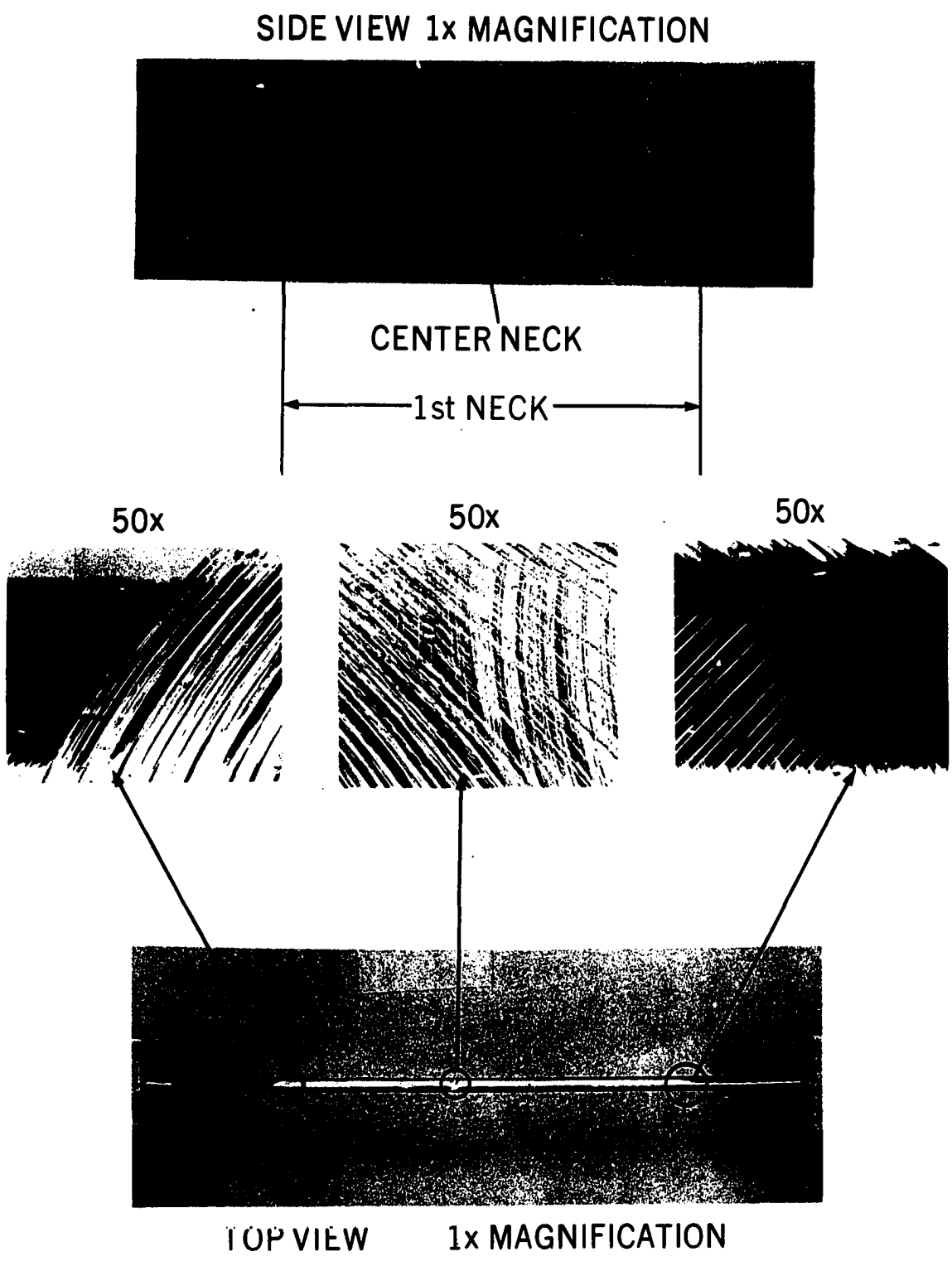
SIDE VIEW 1x MAGNIFICATION
CENTER NECK
1st NECK
50x
50x
50x
TOP VIEW
1x MAGNIFICATION

bands were quite straight and parallel to those at the Luders front. This is clearly shown in the 50X insets in Figure 42. The second neck formed by the appearance of coarse slip bands on a third set of slip planes. In this case more than one slip system operated simultaneously until fracture occurred because the third set of slip bands was jogged and wavy.

In crystals aged longer than 100 min. at 600°C the sudden increase in work hardening rate just before necking was absent and the crystals necked abruptly by the formation of coarse slip bands on the conjugate system. The formation of the coarse slip bands was accompanied by a drop in load which continued in a discontinuous manner as more slip bands nucleated. A schematic of this type of behavior is shown in Figure 41. Slip finally became confined to one set of bands and the crystals started to shear apart on a plane somewhat parallel to the conjugate slip bands. In no instance did a stable neck form when the work hardening rate did not show the increase prior to necking observed in the 30, 50, and 100 min. crystals. This point is significant because the 300 min. crystal tested at 77°K did exhibit a stable neck and the work hardening rate did increase just prior to necking.

The coarse slip bands associated with the neck of a crys-

tal aged 1000 min. at 600°C and tested at 243°K are shown in Figure 43. It is apparent that deformation in the neck is confined mainly to the coarse conjugate slip bands and that the neck is unstable. In fact the shear at the stage of necking shown in Figure 43 is confined to a relatively narrow region. When the local shear stresses in the heavily sheared region of the neck became high enough, slip on planes other than the conjugate occurred and the crystals necked down to a knife edge and ruptured. Detailed photographs of the coarse conjugate slip bands associated with necking are shown in Figure 44 for a crystal aged 500 min. at 600°C and tested at 243°K. The bands pass completely through the crystal and are relatively straight and sharp. Clearly primary slip did not occur simultaneously with the conjugate slip.

Fracture of age hardened alloy crystals containing coherent precipitates by planar localized shearing with little or no necking such as that shown in Figure 42 has been observed in Al-Cu, Al-Ag, Al-Zn, and Cu-Be alloys (2,87-90). In all cases the onset of necking (or fracture) occurred even when the stress-strain curve showed significant work hardening as observed in this study. Thus the simple explanation of plastic instability due to a low work hardening rate must be dismissed.

Top view

Side view

Figure 43. Photographs of the neck in a crystal aged 1000 min. at 600°C and tested at room temperature illuminated to show heavy conjugate slip. 3.6X

Figure 44. Photographs of coarse conjugate slip in region of neck of crystal aged 500 min. at 873°K and tested at 243°K

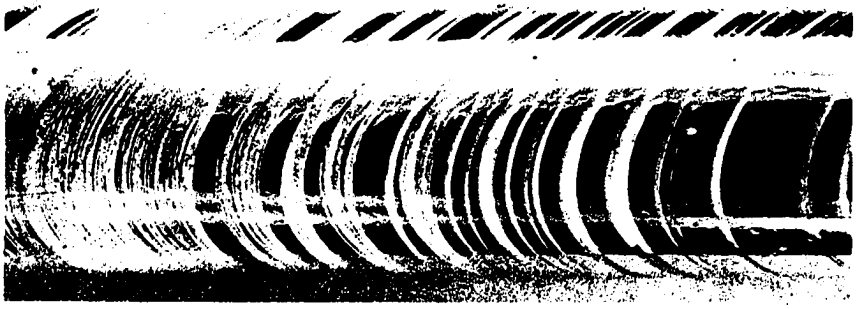

17x

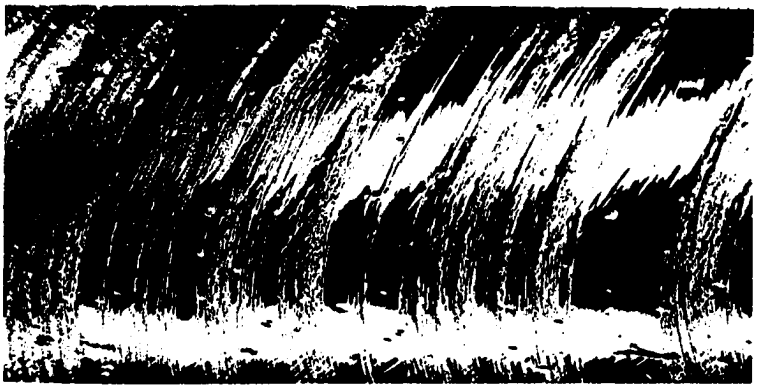

50x

DARK FIELD
ILLUMINATION

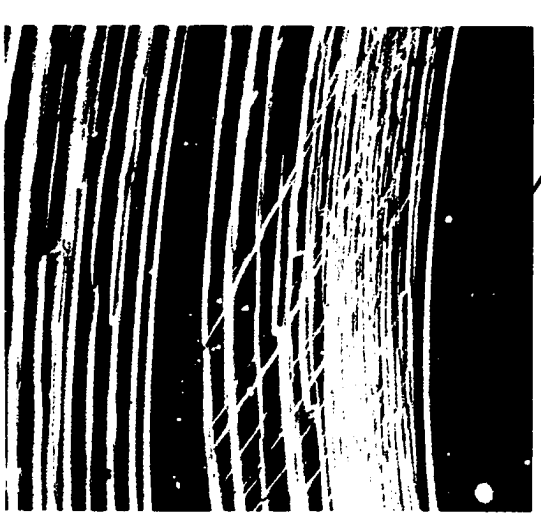

250x

DARK FIELD
ILLUMINATION

In all of the above cases it was observed (2,87) that the coarse slip associated with the onset of necking and/or fracture occurred at a specific resolved shear stress that depended strongly on temperature. In order to examine this point in the present study, the resolved shear stresses on the primary and conjugate slip planes in the primary and conjugate slip directions were compiled with the hope that a "necking criterion" based on shear stresses could be detected. Beevers and Honeycombe (86) also found in Al-Cu crystals that the resolved shear stress at fracture was a constant at a constant temperature and increased with decreasing temperature. The stress at which coarse slip was initiated in their crystals was, however, not evident from their results. It is this stress that is of most interest because it is directly related to the onset of necking and the work hardened state of the material. Table 8 includes the resolved shear stresses in the slip directions on the primary (τ^P) and conjugate (τ^C) slip planes at the onset of necking. In addition it includes the ratio of the shear stresses on the conjugate the primary systems τ^C/τ^P. This ratio is an indication of the latent hardening on the conjugate slip system in the aged crystals since no conjugate slip was observed until the onset of neck-

Table 8. Resolved shear stresses on the primary (τ^P) and conjugate (τ^C) slip systems at the onset of necking

Specimen	Aging time at 600°C (min)	Test temp. (°K)	τ^P (kg/mm^2)	τ^C (kg/mm^2)	τ^C/τ^P
x-0-3	0	295	7.25	9.09	1.25
x-0-6	0	243	7.58	9.80	1.29
x-0-4	0	188	8.86	12.40	1.40
x-0-7	0	127	8.91	12.05	1.35
x-0-5	0	77	8.90	12.13	1.36
x-30-1	30	295	8.80	10.83	1.23
x-30-3	30	244	8.76	11.22	1.28
x-30-4	30	187	8.59	11.16	1.38
x-30-5	30	127	8.14	11.07	1.36
x-30-5	30	77	8.01	11.56	1.44
x-50-1	50	293	9.69	11.44	1.18
x-50-2	50	243	9.45	11.94	1.26
x-50-3	50	185	8.87	11.35	1.28
x-50-4	50	127	8.57	11.82	1.38
x-50-5	50	77	8.27	12.36	1.49
x-100-2	100	299	10.15	12.67	1.25
x-100-1	100	243	10.01	11.87	1.18
x-100-4	100	244	9.89	12.45	1.26
x-100-3	100	187	10.36	13.10	1.26
x-100-5	100	129	9.68	12.95	1.34
x-300-3	300	295	10.59	11.77	1.11
x-300-6	300	243	10.58	12.67	1.20
x-300-1	300	188	10.88	13.32	1.22
x-300-7	300	126	10.34	13.12	1.27
x-300-2	300	77	8.73	13.78	1.58
x-500-3	500	295	9.83	12.37	1.26
x-500-4	500	243	10.75	12.50	1.16
x-500-6	500	187	10.40	12.92	1.24
x-500-7	500	126	10.57	13.96	1.32
x-500-8	500	77	10.09	13.76	1.36

Table 8. (Continued)

Specimen	Aging time at 600°C (min)	Test temp. (°K)	τ^P (kg/mm^2)	τ^C (kg/mm^2)	τ^C/τ^P
x-1000-1	1000	293	10.59	12.34	1.16
x-1000-7	1000	243	10.35	11.99	1.16
x-1000-5	1000	187	10.46	12.02	1.15
x-1000-6	1000	127	14.48	18.13	1.25
x-1000-4	1000	77	10.92	14.31	1.31

ing. The same ratio is included for the solution treated crystals but in this case the meaning is doubtful since it was observed that the unnecked portions of ruptured crystals contained an even distribution of conjugate slip bands as well as primary slip bands.

It is evident that, in general, the resolved shear stresses on the primary system at the onset of necking were below 10 kg/mm^2 for the age hardened crystals that showed a sudden increase in work hardening rate just prior to necking and were above 10 kg/mm^2 for the ones that did not. τ^P tended to increase with decreasing temperature for the solution treated crystals and decrease for the aged crystals. The decrease was not large, however, and no trends with aging time are obvious. In fact, it appears that τ^P is not a strong function of temperature in contrast to Price and Kelly's

observations on aged Al and Cu base alloys (87,88). τ^C increased with decreasing temperature for the solution treated crystals and appeared to increase with aging time but, as with τ^P, did not appear to be a strong function of temperature for the aged crystals. The shear stress ratio τ^C/τ^P was roughly the same for all crystals although a slight trend to increase with decreasing temperature is evident. If the shear stress ratio is taken to be the latent hardening ratio, as defined by Jackson and Basinski (91), the values obtained here are somewhat less than they found for conjugate slip in Cu crystals in Stage II but they did note that the ratio tended to decrease with increasing strain.

3. Strain-rate sensitivity of single crystals

Differential strain rate tests were performed on crystals in the solution treated condition and on crystals that had been aged 5, 30, 100, and 1000 min. at 600°C. Crystals in each of the above states were tested at 298, 188, and 77°K. Figure 45 shows that all the crystals exhibit Cottrell-Stokes behavior. In fact the temperature variation of the intercepts of the $\Delta\tau$-τ lines on the $\Delta\tau$ axis show trends very similar to those observed for the polycrystals. The variation in activation volume with temperature of solution treated and

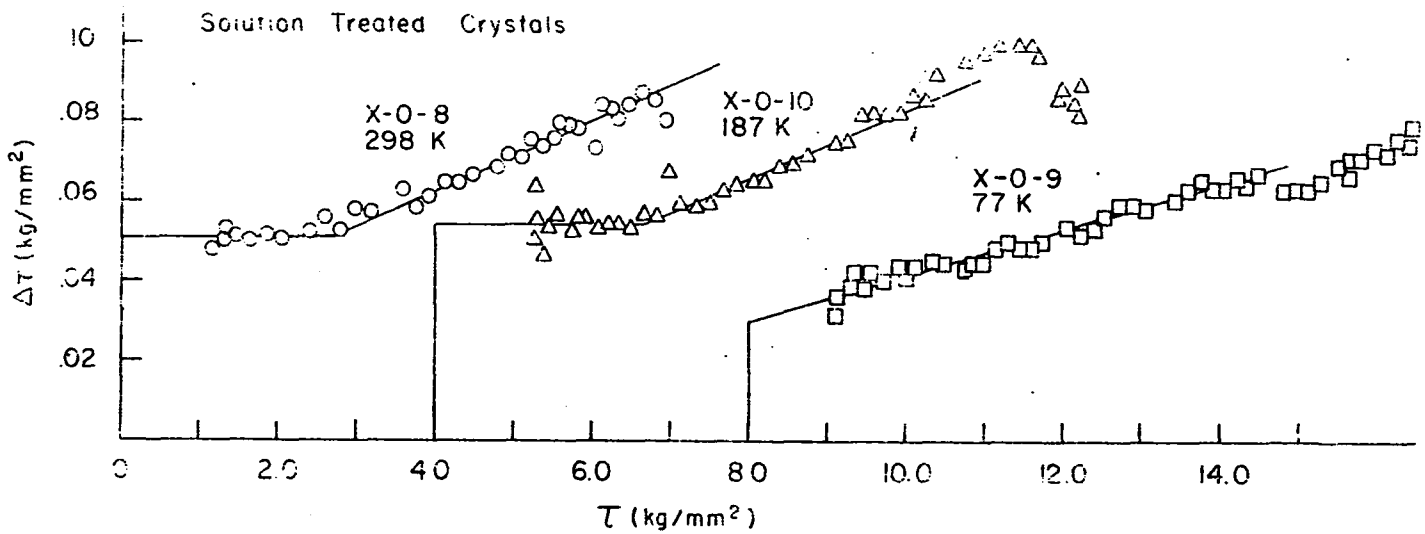

Figure 45a. $\Delta\tau$-τ curves at different test temperatures of Cu-1.9 wt % Co single crystals solution treated at 1298°K and aged 0 min. at 600°C. The curves have been displaced along the τ axis for clarity

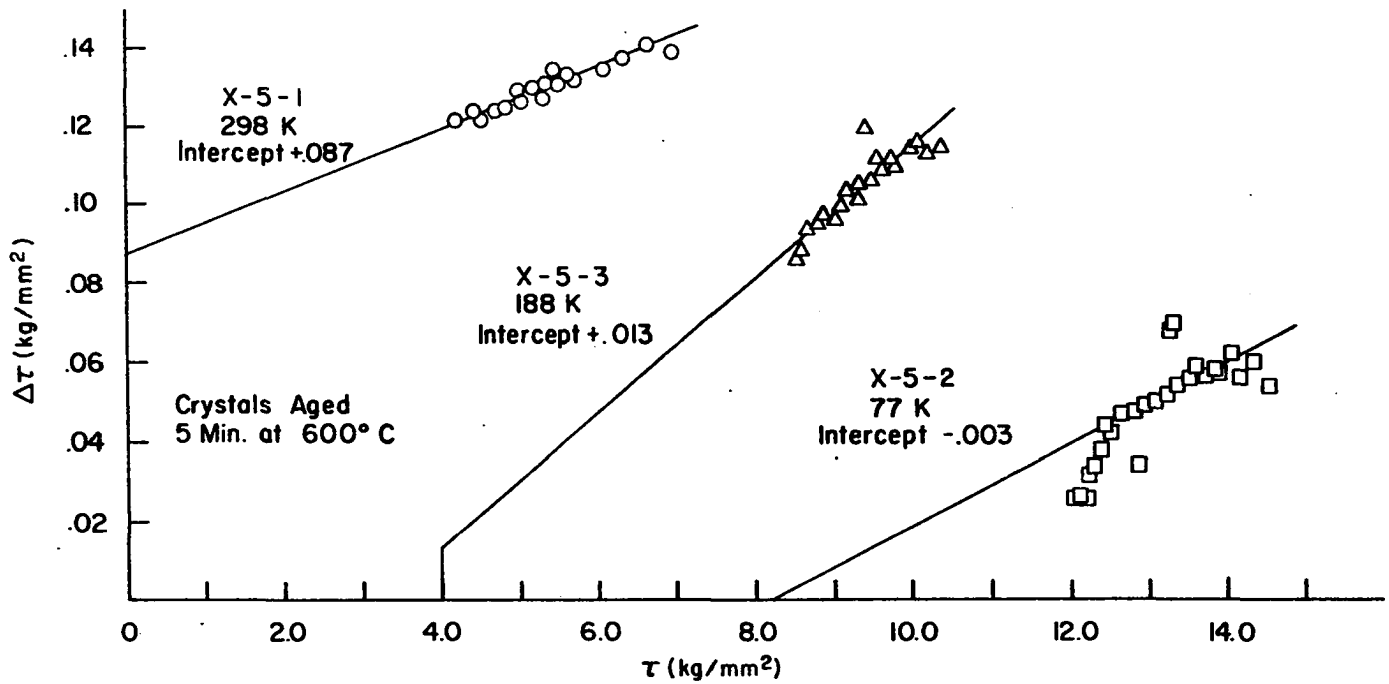

Figure 45b. $\Delta\tau$-τ curves at different test temperatures of Cu-1.9 wt % Co single crystals solution treated at 1298°K and aged 5 min. at 600°C. The curves have been displaced along the τ axis for clarity

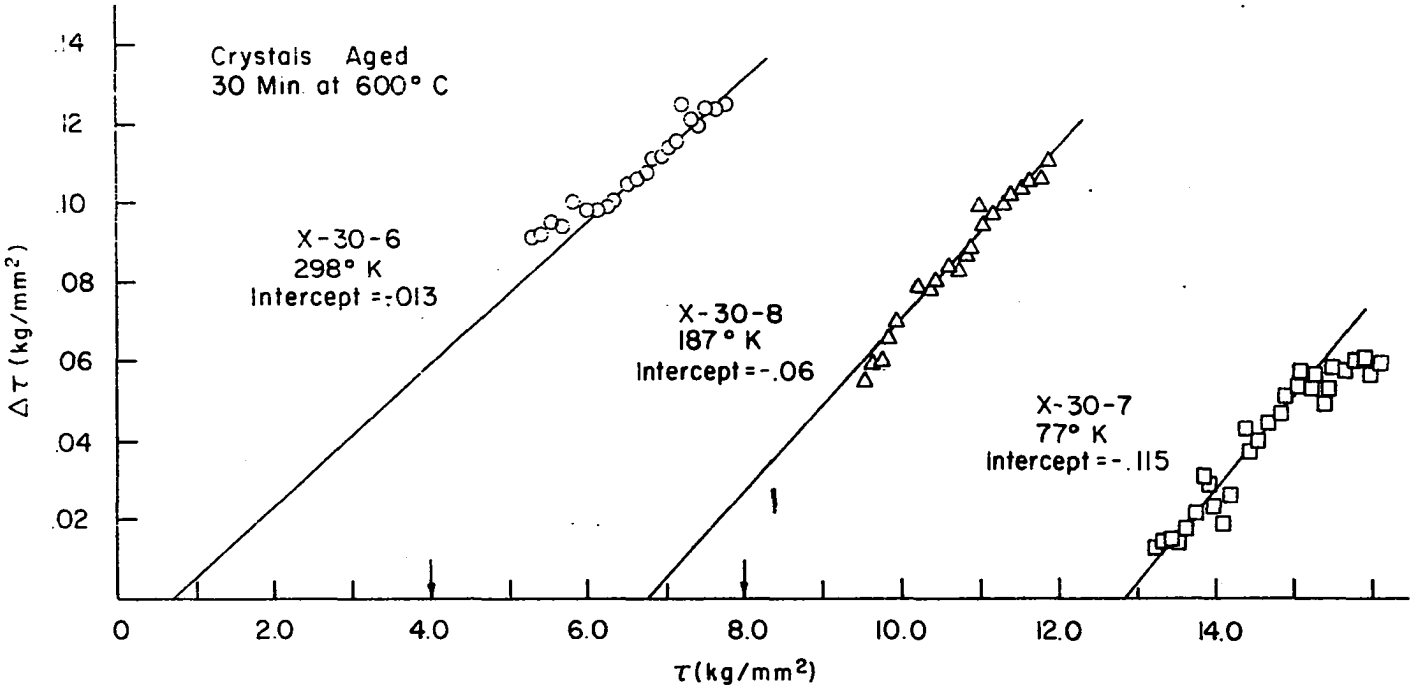

Figure 45c. $\Delta\tau$-τ curves at different test temperatures of Cu-1.9 wt % Co single crystals solution treated at 1298°K and aged 30 min. at 600°C. The curves have been displaced along the τ axis for clarity

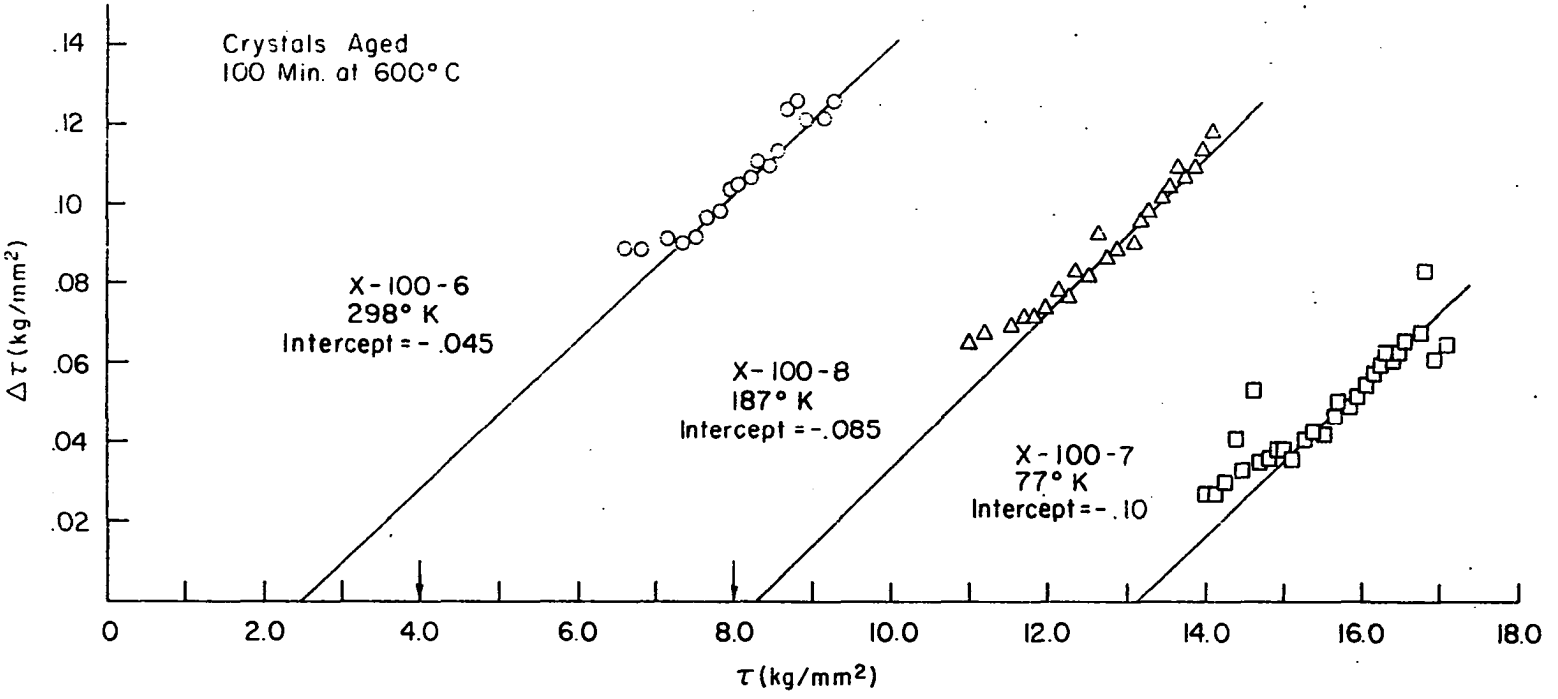

Figure 45d. $\Delta\tau$-τ curves at different test temperatures of Cu-1.9 wt % Co single crystals solution treated at 1298°K and aged 100 min. at 600°C. The curves have been displaced along the τ axis for clarity

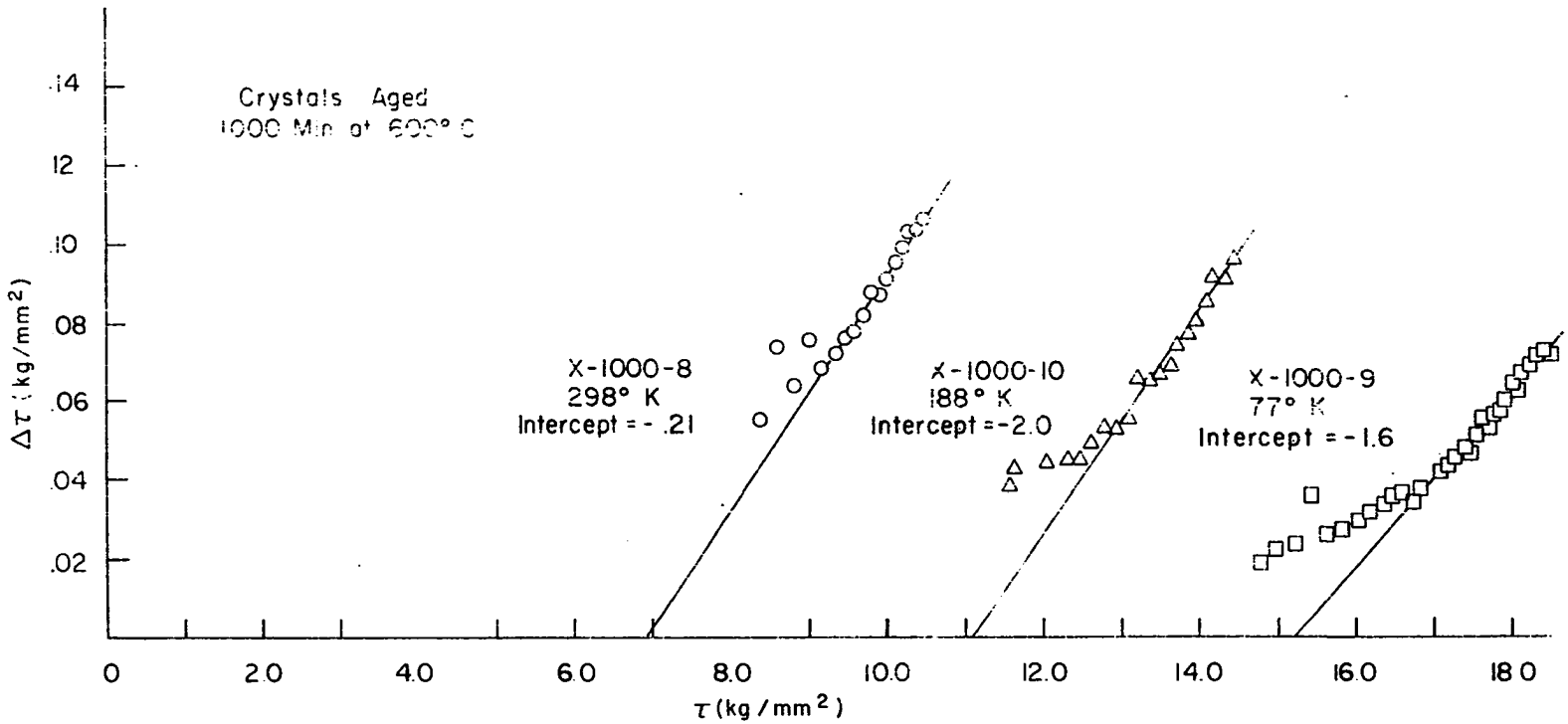

Figure 45e. $\Delta\tau$-τ curves at different test temperatures of Cu-1.9 wt % Co single crystals solution treated at 1298°K and aged 1000 min. at 600°C. The curves have been displaced along the τ axis for clarity

aged crystals is shown in Figures 46 and 47. The activation volume, $\Delta V/b^3$, at zero strain vs T is shown in Figure 46. The behavior is similar to that revealed by the polycrystals in that the solution treated curve increased monotonically with T while the curves for the aged crystals rose at both low and ambient temperatures for aging times up to 100 min. The 1000 min. curve rose and then leveled off or tended to decrease as the temperature was raised. This was observed in the polycrystals also.

It was shown that, after small amounts of strain, the activation volume-temperature relationships for the aged polycrystals closely resembled the solution treated curve. This is taken as an indication that the matrix contributed a large portion of the short range interactions leading to the thermally activated component of the flow stress. Figure 47 shows this is not exactly true in aged single crystals. It is seen that, although the activation volumes at 30% shear strain are smaller than those at zero strain, their temperature dependence still slosely resembles that of the $\Delta V^*/b^3$ curves. This implies that the particles in single crystals remain intimately associated with the mechanisms leading to ΔV even after large deformations. This is to be expected in light

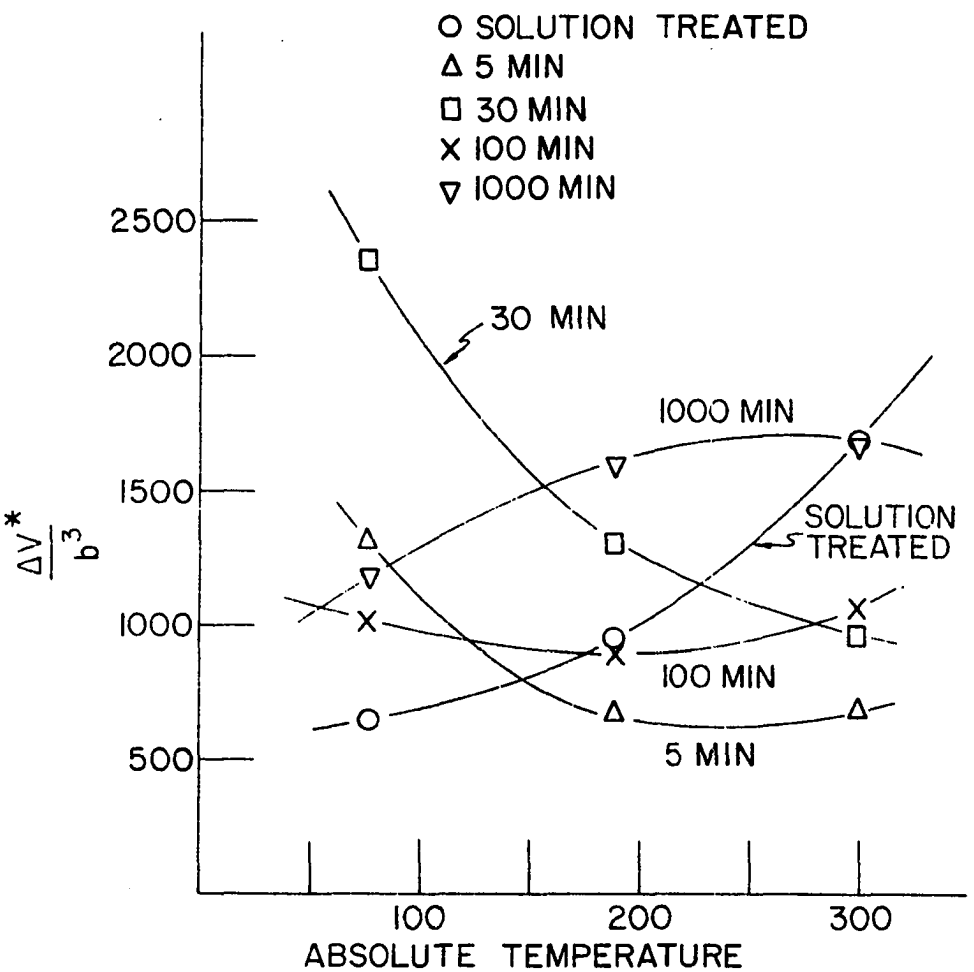

Figure 46. The temperature dependence of $\Delta V/b^3$ for Cu-1.9 wt % Co single crystals solution treated at 1298°K and aged for different times at 873°K

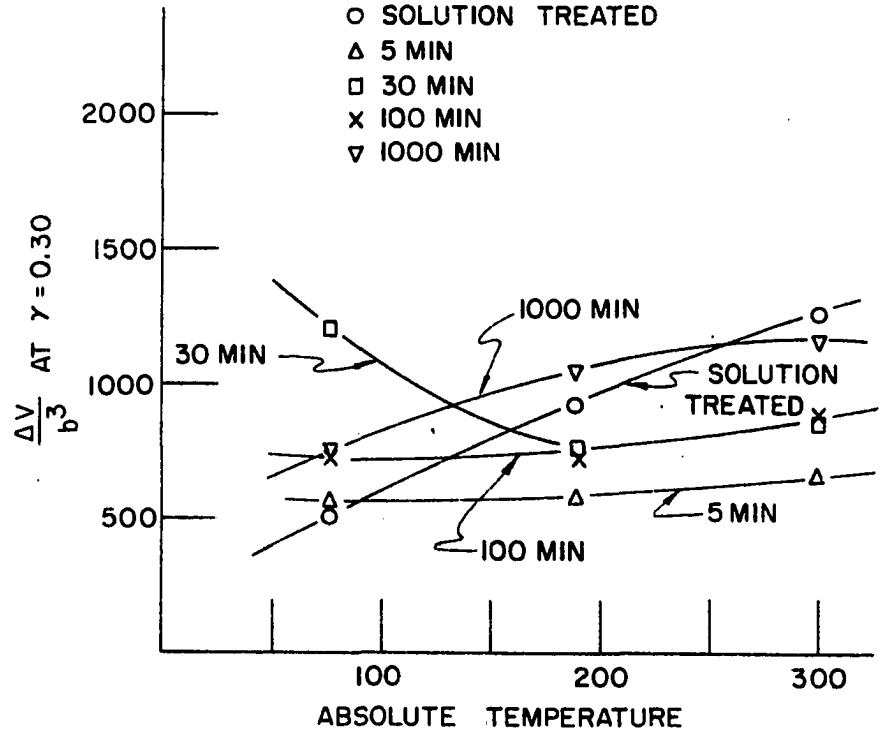

Figure 47. The temperature dependence of $\Delta V/b^3$ at 30% glide strain for Cu-1.9 wt % Co single crystals solution treated at 1298°K and aged for different times at 873°K

of the fact that the aged crystals glide almost entirely on one slip system until necking and fracture are initiated.

V. DISCUSSION OF RESULTS

A. Long Range Interactions

1. Particle size dependence of the flow stress

Flow stress theories of precipitation hardenable alloys must explain three things if the precipitate particles control deformation at a constant temperature.

1). The variation in flow stress with precipitate size.

2). The variation in flow stress with volume fraction of precipitate.

3). The actual magnitude of the flow stress.

It was mentioned in Section II that the flow stress varies as the square root of the particle size in alloys containing coherent, spherical precipitates with significant strain fields associated with them (16,18). To the author's knowledge, the only theories that predict this behavior are those due to Gerold and Haberkorn (18) and Gleiter (22,23). Both theories assume that the primary obstacles to deformation are the coherency strain fields surrounding coherent precipitates and predict the increase in yield stress due to the precipitates over that of the precipitate depleted matrix. Recall that Gleiter (22,23) predicted,

$$\Delta\tau = \left[\frac{27.4\ A^3E^3b}{\pi \cdot T(1+\nu)^3}\right]^{\frac{1}{2}} f^{5/6}R^{\frac{1}{2}} \qquad (2)$$

where

$$A = \frac{3K\epsilon}{3K + \frac{2E}{1+\nu}}$$

while Gerold and Haberkorn (18) predicted

$$\Delta\tau \simeq 3\mu\epsilon^{3/2}\left(\frac{fR}{b}\right)^{\frac{1}{2}} \qquad 2\text{Å} < R < 33\text{Å}$$

for $f \simeq 0.018$

and $b = 2.55$Å .

In both of the above expressions the symbols are defined as:

E = Young's modulus of the matrix

b = the Burgers vector of the matrix

T = the line tension of the dislocation which may be approximated by $\frac{1}{2}\ Gb^2$

ν = Poisson's ratio

f = the volume fraction of precipitate

R = the mean precipitate radius

μ = the shear modulus of the matrix

K = the bulk modulus of the matrix

ϵ = the absolute relative difference in lattice parameter between precipitate and matrix.

The yield stress increment in both cases is that due to

edge dislocations only. The increments computed for screw dislocations overcoming the particles are much smaller. In both theories the equations are valid for particle sizes which permit cutting to take place. At larger particle sizes where prismatic cross slip (92,93) or bowing out (18) may occur the formulas are not applicable. The limits of applicability of the Gerold-Haberkorn (GH) formula are defined next to the equation. It will be shown that these limits of particle size do not correspond to those observed.

The squares of the yield strengths of both single and polycrystals tested in this investigation are plotted as a function of particle radius in Figure 48. CRSS values were used for the single crystals and 0.2 percent offset values were used for the polycrystals. Tensile yield strengths of the polycrystals were converted into shear stresses by assuming a resolved shear stress factor of 0.32 (94). This type of plot is justified in verifying the above theories because it was shown that, throughout aging, the volume fractions of precipitate in both the polycrystals and single crystals remained essentially constant and equal. It is evident from the figure that the agreement of the observed yield strengths and $R^{\frac{1}{2}}$ is excellent. In addition the line passes through the

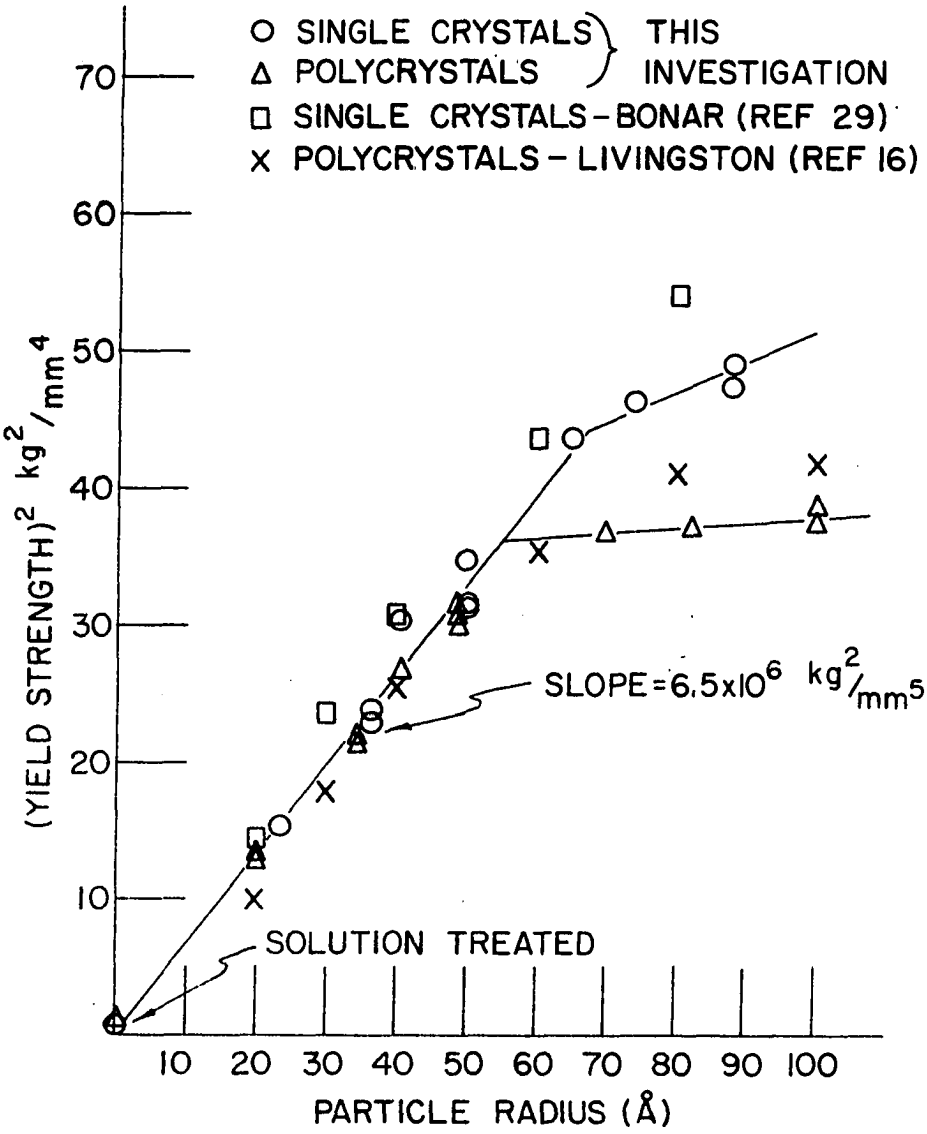

Figure 48. (Yield Strength)^2 vs. mean particle radius for Cu-1.9 wt % Co single crystals and polycrystals aged at 873°K and tested at ambient temperature. (CRSS values were used for single crystals and $\tau_{y.s.}$ values were used for polycrystals

origin as would be expected if the particles control the yield strength. Also included on the curve are data taken from Livingston's (16) tests on polycrystals of Cu-2% Co and Bonar's (29) tests on single crystals of Cu-2% Co. All data shown were from specimens aged at 600°C.

Since the $R^{\frac{1}{2}}$ dependence is verified it remains to determine which theory gives the closest correlation with the observed data. The volume fractions of precipitate in Livingston's specimens and those used in this investigation are almost identical as seen from the solubility limit of Co in Cu of 0.35 quoted in his paper (16) and 0.30 to 0.40 found in this study. Bonar (29) determined the volume fraction by transmission electron microscopy and, as mentioned earlier, probably underestimated it. The good agreement between Bonar's and the present data would seem to indicate that, since the particle sizes and yield strengths are similar, the volume fraction would be also. Since both the single and polycrystal data shown in Figure 48 fall on the same line, the indication that the particles are truly the deformation controlling obstacles is very strong.

Because the volume fractions at all data points in the figure may be considered essentially equal the slope of the

line may be compared with that predicted from Gleiter's equation and the GH equation. The experimental slope is 6.5×10^6 kg^2/mm^5. If isotropic elasticity is assumed with $\nu = 1/3$ then

$$E \simeq 8/3\mu$$

$$K \simeq E \ .$$

In addition, taking the following typical values

$$b = 2.55\text{Å}$$

$$\mu = 4100 \text{ kg/mm}^2 \quad (18)$$

$$\epsilon = 0.013 \quad (10)$$

$$f \simeq 0.018$$

the following results are obtained:

From Gleiter's theory,

$$\Delta\tau^2 = 41.4 \frac{\epsilon^3 \mu^2}{b} f^{5/3} R$$

$$= 7.4 \times 10^6 \text{ R kg}^2/\text{mm}^5$$

From the GH theory,

$$\Delta\tau^2 \simeq 9 \frac{\epsilon^3 \mu^2}{b} f R$$

$$\simeq 17 \times 10^6 \text{ R kg}^2/\text{mm}^5.$$

It is apparent that the agreement between Gleiter's theory and the experimental data is quite good and we conclude that his treatment adequately describes the strengthening due to

coherent precipitates in Cu-1.9 wt % Co at least up to a radius of about 55Å for the polycrystals and up to a radius of about 65Å for single crystals.

The breaks in the curves definitely indicate a change in deformation mechanism at larger particle sizes, the implications of which will be briefly discussed below. When the particle size and spacing become large enough to allow a dislocation to be bent to a radius of curvature on the order of one-half the interparticle spacing under the applied stress, a change in mechanism conceivably could occur. As mentioned, Gleiter (92,93) has shown that dislocation bowing-out results in the formation of prismatic loops around the particles as they are bypassed by dislocations. At this particle size the coherency stress fields of the particles become so large that the particles become impenetrable obstacles. Orowan (21) has considered the stress to bow dislocations between two obstacles and found

$$\tau = \frac{2\,T}{b\,l}$$

where T is the line tension

b is the Burgers vector

l is the interparticle spacing.

This, of course, is the familiar equation, defining the stress

to start a Frank-Read source. Ashby (95) has considered the "Orowan Stress" in detail and arrived at the following expression for the stress at which a dislocation loop pinned between two obstacles becomes unstable:

$$\tau_{critical} = \frac{\mu b}{2\pi \bar{l}} \ln \left(\frac{2R}{b} \right)$$

where μ = the shear modulus of the matrix

b = the Burgers vector of the matrix

$\bar{l}$ = the mean planar separation of the particles

R = the particle radius.

A number of calculations of $\bar{l}$ have appeared in the literature (2,96) each differing slightly from one another. Kocks (97) considered all the definitions of $\bar{l}$ known in the literature as well as some derived by himself and concluded that the definition of $\bar{l}$ using the simple planar approach (96) gives, at most, a 20% deviation from the others.

In the planar approach, randomly distributed spherical particles are hypothetically rearranged into slabs of thickness 2R and spacing 2R. The particles are then arranged into square arrays in the slabs. The volume fraction, f, of particles based on this model is:

$$f = \frac{4/3\ \pi R^3}{2\ \bar{l}^2 R} = \frac{2}{3} \frac{\pi R^2}{\bar{l}^2}$$

from which

$$\bar{l} = \left(\frac{2\pi}{3}\right)^{\frac{1}{2}} \frac{R}{f^{\frac{1}{2}}} .$$

In order to calculate the mean particle radius at which the particles are no longer cut by glide dislocations but are bypassed instead, the Orowan stress as given by Ashby (95), is simply equated to Gleiter's formula for the flow stress increase due to precipitates as follows:

$$\frac{\mu b}{2\pi\bar{l}} \ln\left(\frac{2R}{b}\right) = \left[\frac{27.4\ A^3E^3b}{\pi T(1+\nu)^3}\right]^{\frac{1}{2}} f^{5/6}R^{\frac{1}{2}}$$

where all symbols were defined above. In this case the line tension, T, of the dislocation is that corresponding to the dislocation when it is approximately a semi-circular arc. For this case Ashby (95) gave

$$T \simeq \frac{\mu b^2}{4\pi} \ln\left(\frac{\bar{l}}{b}\right) .$$

Inserting this expression for line tension into the above equation and solving graphically the critical radius corresponding to a change in deformation mechanism turns out to be 80Å. Examination of Figure 48 reveals that the yield strengths at constant volume fraction start to deviate from the $R^{\frac{1}{2}}$ dependence at about 55Å for the polycrystals and about 65Å for the single crystals. The agreement is good when one

considers that a distribution of particle sizes exists and that, when the mean radius is equal to the above values, some particles are already being bypassed. This effect would cause the observed premature change in deformation mechanism. As mentioned, Gleiter (92,93) has shown that when particles are no longer cut by dislocations, the bypassing process leaves prismatic loops around the particles instead of normal loops lying in the glide plane as predicted by Orowan (21) and Fisher, Hart, and Pry (98). Gleiter (92,93) has given quite detailed descriptions of this process so it will not be described here.

In light of the above discussion, one point deserves to be mentioned. Most theories of the flow stress in precipitation hardened metals and in pure metals as well, consider the athermal component of the flow stress to be made up of the sum of a number of contributions, e.g., those arising from elastic strain fields, solid solution effects, etc. Bonar (29) has suggested that the flow stress in aged Cu-Co alloys is made up of no less than four components. Gleiter (8,22, 23) has also stated that the stress given in his theory is that increment due to the presence of precipitates and must be added to the strength of the solid solution. When the

deformation of a metal is considered in terms of dislocations being pushed over obstacles by the action of an applied stress, the idea that the flow stress is the sum of many components, each representing a different type of obstacle, is justifiable only when the processes associated with the components are independent of one another. The flow stress is equal to that value of applied stress at which large scale plastic deformation occurs. In other words, when the applied stress equals the flow stress dislocations are moved large distances through the matrix. If a matrix contains many types of obstacles all characterized by a different height, it is hard to see how large scale dislocation motion may occur until the applied stress becomes equal to that value necessary to push glide dislocations over the strongest obstacles in the matrix. For this reason it is suggested here that the flow stress should be identified with the stress associated with the largest obstacle. In other words, the largest obstacles control the deformation of a material and the observed values of flow stress are, in reality, those associated with the interaction of dislocations and only the strongest barriers, unless the processes involved in overcoming the various barriers are independent of each other. In the present situation

the precipitate particles are probably the strongest barriers but dislocation movement through the solid solution may be an additional increment. However, the latter value may be virtually negligible by comparison with the increment due to the particles. According to the increment calculated from Gleiter's expression and the results shown in Figure 48 this possibility is true here.

2. Temperature dependence of the flow stress

Figures 8 to 15, 26, and 40 show quite clearly that the temperature dependence of the flow stress of Cu-1.9 wt % Co alloys aged to contain precipitates of up to 100Å mean radius is negative. Phillips' (28) work corroborates this observation and, as mentioned in Section II, he has attributed this to the decrease in coherency strain fields resulting from the differences in thermal expansion coefficients of the precipitate and matrix. Since it has been demonstrated that the athermal component of the flow stress in Cu-1.9 wt % Co is described satisfactorily by Gleiter's (22,23) formulation, (Equation 2 p. 173) the change in this component of flow stress should be predictable by considering the temperature dependence of the individual terms in the formula. It should be noted that, in most treatments of the temperature depend-

ence of the flow stress, the component associated with long range obstacles is generally considered to have the same temperature dependence as the shear modulus μ. Clearly this is not the case in aged Cu-Co alloys containing coherent particles of less than 100Å mean radius. Here the strong temperature dependence of the coherency strain fields must also be taken into account. From Gleiter's equation (Equation 2 p. 173)

$$\overline{\Delta\tau} \simeq 6.4\ f^{5/6}\mu(T)\epsilon[R(T)]^{3/2}\ \left(\frac{R(T)}{b}\right)^{\frac{1}{2}}$$

where $\epsilon[R(T)]$ is taken to imply that ϵ is an implicit function of T through the particle size R(T).

The thermal expansion coefficients of Cu and Co may be calculated from first principles of lattice thermodynamics[1] and the temperature dependence of μ is known (28). When these relations are inserted into the above equation it is found that $\overline{\Delta\tau}$ decreases with decreasing temperature (mainly due to the decrease of ϵ with temperature) down to about 150°K. Below this temperature the changes in thermal expansion between Cu and Co become negligible. It would be expected, then,

---

[1]Scott, T. E., private communication, Iowa State University of Science and Technology, Ames, Iowa (1967).

that the observed decrease in flow stress would level off in the vicinity of 150°K. It is apparent from the data that this is not the case and, in fact, the flow stress decrease appears to become more pronounced below 150°K at all particle sizes up to 100Å radius. At this time it is not obvious why this behavior is observed but it is certain that simple considerations of thermal expansion coefficients cannot explain it.

The "negative"[1] temperature dependence of the flow stress observed in solution treated single and polycrystals and overaged (15,000 min. at 600°C) polycrystals indicates that their "athermal" components of the flow stress have the temperature dependence of the shear modulus and that the increase observed is that due to the thermally activated component. The behavior of the solution treated material is in accord with that found in other solid solution alloys (99). The mechanisms leading to the thermally activated component of the flow stress in the solution treated solid solution will be considered later. The positive temperature dependence of the flow stress of the overaged polycrystals indicates that

---

[1] In this dissertation a "negative" temperature dependence of the flow stress means $\frac{d\sigma}{dT} > 0$.

the decrease in coherency strain fields (the majority of the particles are still coherent after 15,000 min. at 600°C (5)) does not affect the mechanism leading to the long range component of the flow stress. This is undoubtedly due to the fact that almost none of the particles are being cut and slight decreases in their size due to the decreasing temperature do not alter their role as impenetrable obstacles. Since the long range component of the flow stress is that necessary to bypass obstacles by bowing between them (the Orowan mechanism (21)) the temperature dependence of this stress is expected to be that of the shear modulus.

B. Short Range Interactions

1. The thermally activated component of the flow stress

In this section the thermally activated component of the flow stress and its relation to the state of aging (i.e., particle size, spacing, etc.) will be discussed. This component of the flow stress is directly related to the dislocation-obstacle interactions having activation energies small enough to allow the obstacles to be overcome by thermal activation and is both temperature and strain-rate dependent. It is not to be confused with the long range component of the flow stress. Writing the flow stress, τ, as:

$$\tau = \tau^* + \tau_\mu$$

where τ^* = the thermally activated component of the flow stress

τ_μ = the long range component of the flow stress,

it is clear that τ^* is temperature and strain rate dependent in all metals and alloys at low temperatures. τ_μ is generally only temperature dependent through the shear modulus μ. In Cu-1.9 wt % Co alloys aged to contain coherent precipitates, however, τ_μ depends on temperature both through μ and ε, the misfit parameter. In fact, the decrease in τ_μ with decreasing temperature due to the decrease in ε considerably overshadows the increase in τ^* in the same temperature interval and hence τ has an observed negative temperature dependence. It should be pointed out that τ^* is always positive and that the observed change in τ with decreased temperature contains contributions from τ_μ (decreasing) and τ^* (increasing). This point is quite evident when the strain-rate sensitivity of the flow stress is examined. The change in flow stress accompanying a positive incremental change in strain rate was shown always to be positive in this research. One concludes, therefore, that, although the decrease in τ_μ with decreasing temperature masks the effect of a positive τ^* increment, it is

still there and may be evaluated. τ^* may only be investigated, however, by differential strain-rate tests since differential temperature tests do not detect it. The only way τ^* may be separated from τ_μ in differential temperature tests and in the variation of τ with temperature is to determine directly the temperature variation of τ_μ.

It is implicit in the following discussion that the reversible change in flow stress accompanying a change in strain-rate be identified with the thermally activated component of the flow stress at that temperature and strain-rate ratio. This is valid if the structure, mainly the density of mobile dislocations, does not change during the strain-rate change. When this is true, as assumed here, the activation volume determined by these tests can be associated directly with the size of the activated event through the equation:

$$\Delta V = b\, d\, \bar{l}$$

where b = the Burgers vector

d = the activation distance

$\bar{l}$ = the spacing between obstacles.

The variation in activation volume at zero strain with temperature was shown in Figures 23 and 46. Values of ΔV at zero strain are quite meaningful because it is only at zero

strain that the state of the material can be fully characterized. Deformation distorts the particles and their change in morphology as a function of strain is not known. The change in $\Delta V/b^3$ of the aged material with temperature is quite unusual. $\Delta V/b^3$ should decrease continuously as the temperature is lowered because the available thermal energy is reduced; therefore, the glide dislocations must be pushed closer to the top of the force-distance "hill" before the activated event can take place. This behavior is evident in the curves of the solution treated single and polycrystals.

At present, the upward swing in the $\Delta V^*/b^3$ curves of the aged material in the vicinity of $77^{\circ}K$ is not clear and no explanation will be attempted.

The effect of deformation on the temperature dependence of $\Delta V/b^3$ is clearly indicated in Figure 24, which shows $\Delta V/b^3$ at 5% strain vs. T for the polycrystals. Deformation decreased the activation volume of the solution treated material but did not change its temperature dependence. Thus, it appears that the short range obstacles in solution treated material change in magnitude, not type, after deformation.

The striking similarity of the $\Delta V/b^3$ curves at 5% strain of the aged polycrystals to that of the solution treated

material indicates that, regardless of the rate controlling mechanism at zero strain, the mechanism at 5% strain is strongly matrix dependent. Conrad (3) has shown that the two most probable rate controlling dislocation mechanisms in f.c.c. metals are the intersection of dislocations and the conservative motion of jogs. Both models lead to activation volumes on the order of those shown in Figure 24. The two can be differentiated if the frequency factor $\dot{\epsilon}_o$ in the rate equation

$$\dot{\epsilon} = \dot{\epsilon}_o \, e^{-\frac{\Delta G}{RT}}$$

can be determined. Since the change in the thermally activated component of flow stress with temperature cannot be determined in aged Cu-1.9 wt % Co, $\dot{\epsilon}_o$ cannot be determined and the exact rate controlling mechanism in deformed samples cannot be predicted. The similarity of the curves in Figure 24 does strongly indicate, however, that in the polycrystals the matrix is responsible and not the precipitates themselves. The only argument against this is related to the dependence of $\Delta V_{.05}/b^3$ at any temperature on aging time (particle size). $\Delta V_{.05}/b^3$ increases with aging time which indicates that the particle size and spacing could be related to the activation distance d and obstacle spacing $\bar{l}$. If d and $\bar{l}$ increased with

aging time ΔV would also. Quantitative estimates cannot be made because of the undertainties in the particle morphologies after deformation.

2. Relation between activation volume at zero strain and particle size for polycrystals

A much clearer picture of the rate controlling dislocation mechanisms responsible for the thermally activated component of the flow stress at zero strain in aged Cu-1.9 wt % Co alloys is obtained by a consideration of the variation of $\Delta V^*/b^3$ with particle radius. These data, plotted in Figure 49 for the polycrystals, show a rather striking behavior. The curves at 77°K and 188°K have definite peaks at radii of about 35 and 72Å respectively. The curve at 133°K has a tendency to peak at a radius of about 60Å and is drawn as such because of its similarity in shape to the curves at 77°K and 188°K but it should be noted that a data point in the vicinity of the peak was not taken. For this reason the curve is dotted. Similar precautionary remarks should be put forward concerning the point at 70Å on the 188°K curve. The extrapolation of the $\Delta\sigma - \sigma$ curve to obtain $\Delta\sigma^*$ involved an uncertainty which resulted in a large variation of $\Delta V^*/b^3$ depending on how the curve was drawn. In any event, the

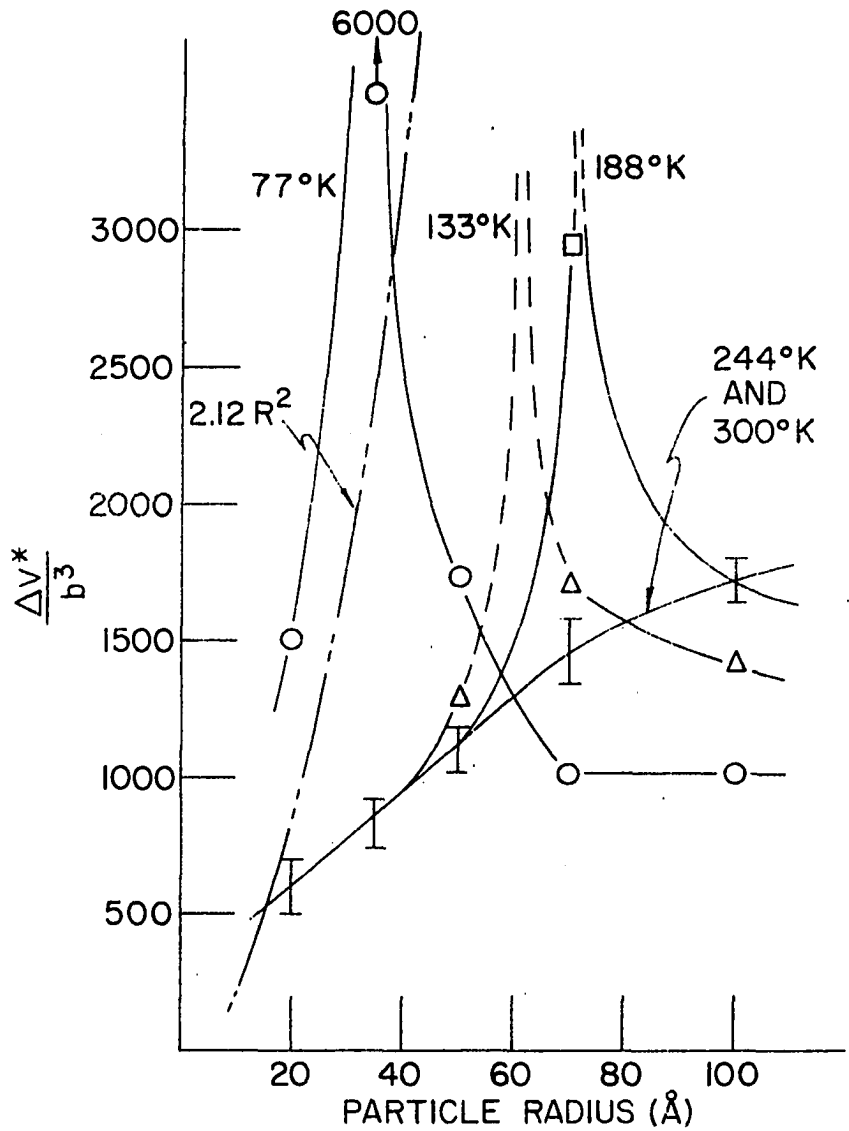

Figure 49. The dependence of $\Delta V^*/b^3$ on mean particle radius at different temperatures for Cu-1.9 wt % Co polycrystals solution treated at 1243°K and aged at 873°K

resulting $\Delta V^*/b^3$ at 70Å and 188°K was definitely higher than the other data points on that curve and the most probable value was drawn. This uncertainty did not arise in the 77°K curve peak because of sufficient data at low strains. All data not specified by symbols are contained within the error bracket symbols which show the maximum scatter of all data plotted as such.

The 244°K and 300°K $\Delta V^*/b^3$ vs R curves do not show peaks in the range of particle sizes investigated but do exhibit a change in slope near 90Å radius. It should be mentioned here that the particle sizes plotted are those measured at 300°K. It is not expected that the actual particle sizes will vary much with temperature and the differences in sizes due to cooling will be very close to those plotted. The coherency strain fields, on the other hand, might show large changes as noted in the discussion of the temperature variation of the flow stress.

From the data plotted in Figure 49 one may determine whether the particles themselves are in any was contributing to the rate controlling obstacles at small strains in the material. This may be done by assuming various models of the activation volume and comparing them with the observed data.

The high sensitivity of $\Delta V^*/b^3$ to particle radius indicates that this may be the case.

The simplest obstacles to consider are the particles themselves. If the activated event is the cutting of the particles by glide dislocations, the activation volume can be estimated. Recall,

$$\Delta V = b\ \bar{l}\ d$$

where b = the Burgers vector

$\bar{l}$ = the mean particle spacing

d = the activation distance.

Both d and $\bar{l}$ need to be estimated. The dislocations will be assumed to be relatively straight. $\bar{l}$ may be estimated from the planar approach (96,97) which gives:

$$\bar{l} = 2\ R \left[\frac{\pi}{6f}\right]^{\frac{1}{2}}$$

where f = the volume fraction and

R = the average particle radius.

In all cases $f \simeq 0.018$ so that

$$\bar{l} = 10.8\ R\ .$$

Since a dislocation generally will not intersect a particle at its diameter, the average length of a straight dislocation lying in a spherical precipitate is a better approximation to d than 2 R. The average length is given by Kelly and

Nicholson (2) as:

$$d = \frac{\pi}{\sqrt{6}} R = 1.28\ R\ .$$

Therefore:

$$\Delta V = b\ \bar{l}\ d = 13.8\ bR^2$$

or

$$\frac{\Delta V}{b^3} = 13.8\ \left(\frac{R}{b}\right)^2 = 2.12\ R^2$$

since $b = 2.55\text{Å}$.

The above predicted R^2 dependence of $\Delta V^*/b^3$ is shown in Figure 49 as the line marked $2.12R^2$. The similarity in shape between the predicted $\Delta V^*/b^3$ curve and the early parts of the 77°, 133°, and 188°K curves suggests that the particles themselves are intimately associated with the short range obstacles in the material, at least at the smaller particle sizes.

The situation is not as straightforward at the larger particle sizes shown in Figure 49. $\Delta V^*/b^3$ decreases with increasing particle size at 77°, 133°, and 188°K and the $\Delta V^*/b^3$ vs R curves at 244° and 300°K change in curvature at $R > 70\text{Å}$. This behavior indicates that one of two possible processes is at work during a differential change in strain rate. Either a change in short range mechanism occurs or the basic assumptions leading to the determination of ΔV do not

hold in this region of particle sizes. Recall that the $R^{\frac{1}{2}}$ dependence of the polycrystalline yield stress at 300°K shown in Figure 48 broke down at a particle size of about 55Å. This is precisely the range at which the curvature of the $\Delta V^*/b^3$ vs R curve at 300°K shown in Figure 49 changed. Thus the change in τ shown in Figure 48 at a particle radius of 55Å could be related to the change in short range obstacles shown in Figure 49, i.e., a change in mechanism might be taking place. On the other hand, the peaks might indicate that a basic assumption of the theory is not obeyed, namely the mobile dislocation density might change during a strain-rate change.

The stacking fault strengthening theory of Hirsch and Kelly (27) outlined in Section II predicted flow stresses much smaller than those observed. However, the magnitudes of the increments of flow stress attributed to the differences in stacking fault energy between the precipitates and matrix are of the same order of magnitude as the changes in flow stress that accompanied strain-rate changes on the Cu-1.9 wt % Co specimens tested in this investigation. Possibly, the $\Delta \tau_{SF}$ of the Hirsch-Kelly theory could account for the short range component of the flow stress in aged Cu-Co alloys.

In addition the theoretical $\Delta\tau_{SF}$ vs. particle radius curve contains a peak which could be related to the peak in the $\Delta V^*/b^3$ vs R curves[1]. When the values of $\Delta\tau_{SF}$ calculated from the theory were compared with the present data, however, it was found that the observed $\Delta\tau$ values were much smaller than those predicted. In addition the dependence of the experimental $\Delta\tau$ values on particle radius was not similar to the theoretical values. For these reasons, it was concluded that the Hirsch-Kelly theory of stacking fault strengthening was not responsible for the short range component of the flow stress in aged Cu-Co alloys. At present no other model can be put forward that adequately described the observed discontinuities in the $\Delta V^*/b^3$ vs R curves.

The other possible explanation of the peak in the $\Delta V^*/b^3$ vs R curves of Figure 49 is that at the particle sizes corresponding to the peaks the assumed constancy of mobile dislocation density breaks down and changes in mobile dislocation density accompany the strain-rate changes. This, of course, would lead to erroneous values of $\Delta\sigma^*$ and ΔV^*. A change in mobile dislocation density might be rationalized by admitting that a distribution of particle sizes exists and that at any

[1]See, for instance Figure 6 in their paper (27).

mean size some large impenetrable particles exist. In this situation, dislocations could be bowed-out between large impenetrable particles to near the critical radius of curvature. During a strain-rate change the accompanying flow stress increment could cause the bowed-out segments to become unstable and thereby mobilize them.

Since the volume fraction remains constant during aging, at small mean particle sizes the spacing between particles having radii greater than any arbitrary radius R^* will decrease with increased aging time since the density of these larger particles will increase. At large mean particle sizes, however, the reverse will occur and the interparticle spacing of particles with radii greater than R^* will increase as aging continues. At small mean particle sizes, then, the stress, τ, to activate critically bowed loops should increase with aging time because the spacings, ℓ^*, between the obstacles holding the loops, are decreasing and τ is inversely proportional to ℓ^* (21). This would lead to a decreasing change in the number of mobile dislocations as the mean particle size increased and would result in an observed $\Delta\sigma$ that would increase with particle size. The apparent activation volume would then decrease with increased particle size

as is observed in Figure 49. At this time, there is no way of verifying the above explanation. However, the changes in slope of the 244 and 300°K curves in Figure 49 at the same mean particle radius that Gleiter's (22,23) cutting theory breaks down seem to indicate that it may be reasonable.

3. Effect of strain on the short range component of flow stress of the polycrystals

The clearest evidence of the strong influence the matrix has on the short range component of the flow stress in the polycrystals is shown in the $\Delta\sigma$-σ plots in Figures 17 and 18. Since all aged samples obeyed a Cottrell-Stokes relation at all temperatures it can be assumed that the short range component of the flow stress is proportional to the long range components in all cases. As expected this was also true for the solution treated samples. The effect of deformation induced structure on activation parameters is also seen in Figure 24. It is evident that the temperature dependence of the activation volume at 5% strain of all the aged material closely resembles that of the solution treated specimens. On the other hand Figure 23 indicates that this is not the case at zero strain. The radius dependence of ΔV at finite strains cannot be discussed because the precipitates are

deformed with the matrix and cannot be characterized thereafter.

Apparently the thermally activated component of the flow stress in aged Cu-1.9 wt % Co polycrystals must be considered in two separate situations. At zero strain the particles themselves are closely associated with this component of the stress as shown by the strong dependence of $\Delta V^*/b^3$ on particle size. At finite strains the influence of the particles on the dislocation mechanisms leading to τ^* is less marked and the material behavior more closely resembles that of the solution treated samples. This strongly indicates that dislocation-dislocation interactions as well as dislocation-particle interactions contribute to the observed strain-rate dependence of the flow stress. The aging treatment still effects the rate controlling dislocation mechanisms leading to the thermally activated component of the flow stress because the $\Delta V/b^3$ vs T curves at 5% strain depend on aging time. Most probably, however, the state of aging effects the degree of deformation induced substructure and the dislocation-dislocation interactions. For these reasons it is suggested that the rate controlling dislocation mechanisms in aged and deformed Cu-1.9 wt % Co polycrystals are the same

but differ in magnitude according to the influence precipitates of different sizes have on the deformation induced substructure.

C. Rate Controlling Dislocation Mechanisms in Solution Treated Polycrystals

Since the temperature dependence of the flow stress of the solution treated material was seen to be positive the long range component of the flow stress τ_μ can be presumed to have the same temperature dependence as the shear modulus μ. In this case an "activation analysis" can be performed and the apparent activation energy ΔG of the rate controlling dislocation mechanisms associated with the thermally activated component of the flow stress τ^* can be determined. This has been done for solution treated polycrystals. A similar analysis has been performed on polycrystals aged 1000 min. and 15,000 min. at 600°C but the results are doubtful due to the unknown contribution of the coherency strain fields on the changes in flow stress accompanying temperature changes. For this reason only the activation energies obtained from solution treated samples will be presented.

Activation energies determined from differential strain-rate and temperature tests on solution treated polycrystals

are shown as a function of temperature in Figure 50. Data are plotted from results obtained at true strains of 0, 0.05, and 0.10. The $\epsilon = 0$ data were obtained by extrapolation. ΔG is a linear function of temperature and independent of strain up to about 200°K. At this temperature the data begin to reveal considerable scatter. A tentative second line corresponding to ΔG at 5 and 10% strain above 200°K has been dashed-in. Also included in the figure is the variation of the activation energy of pure copper with temperature taken from Conrad (3) who used a similar strain rate. The linearity of the low temperature ΔG vs T data indicates that a single rate controlling mechanism is operating. In addition, the similarity between the data taken on Cu and Cu-1.9 wt % Co suggests the rate controlling mechanism in the solution treated alloy is the same as that of Cu at least below 200°K. It was mentioned in Section II that values of $\dot{\epsilon}_o$ in the range of 10 to 10^4 indicate that the rate controlling mechanism probably is the motion of jogged dislocations. Conrad (3) pointed out, however, that the uncertainty in the mobile dislocation density assumed in making the above prediction makes definite statements difficult. The problem of picking the exact mechanism is still unsolved and, at best, it can be said

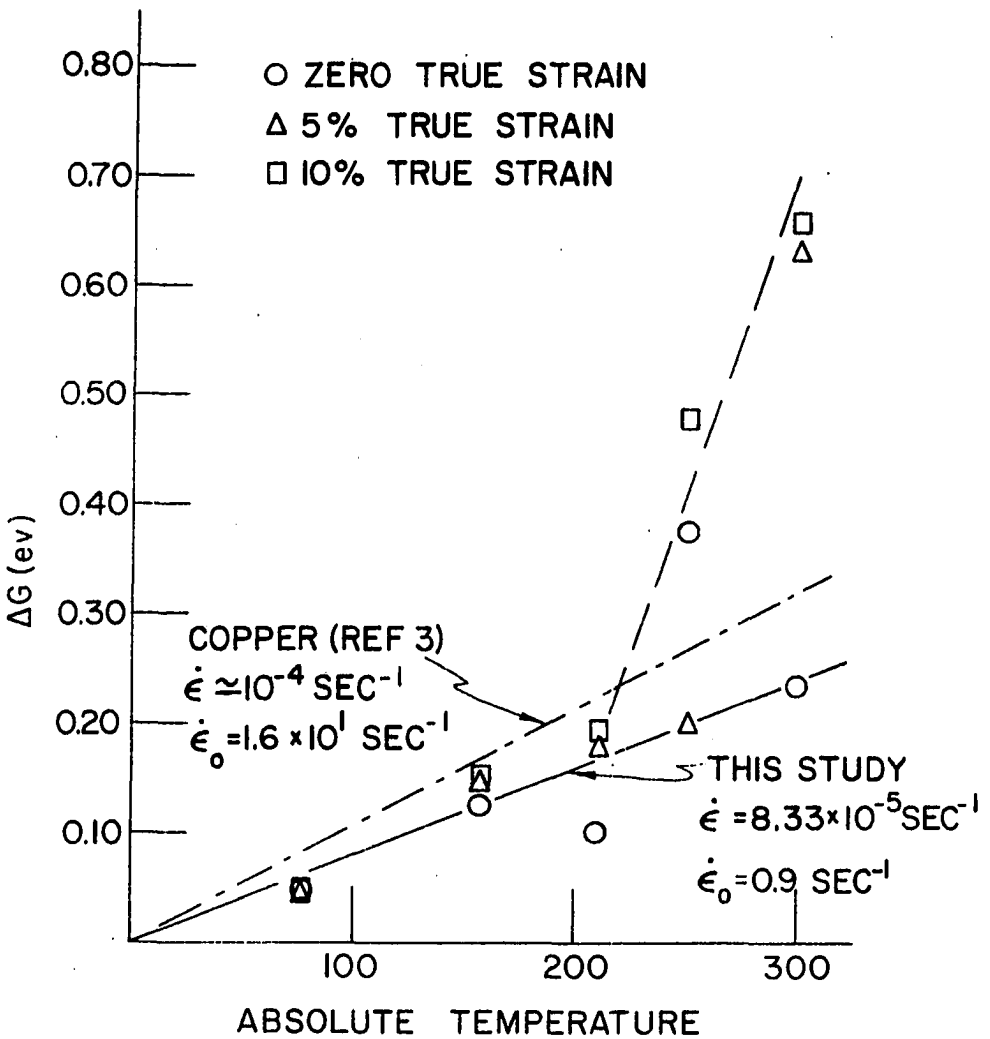

Figure 50. The temperature dependence of the activation energy for Cu-1.9 wt % Co polycrystals solution treated at 1243°K. Also included are data for Cu polycrystals taken from Conrad (3)

that the above data indicate that the rate controlling mechanism in solution treated Cu-1.9 wt % Co is either the intersection of dislocations or the motion of jogged dislocations. In any case the activation energies are quite close to those of pure f.c.c. metals.

The scatter at 200°K and the appearance of a second branch of the ΔG-T curve at the higher strains indicate a change in short range mechanism. The change in mechanism undoubtedly is associated with the appearance of deformation induced precipitation. The large difference at 300°K between the values of activation energy at zero strain and those at 5 and 10% strain also support this. Since the structure changes no definite comments can be made because the basic assumptions of the theory of thermally activated deformation are violated.

D. Plastic Behavior of Single Crystals

1. General comments

The tests conducted on single crystals revealed the following characteristics of the deformation behavior of the solution treated and of the aged Cu-1.9 wt % Co crystals oriented for easy glide.

i) Solution treated crystals showed three distinct staged of work hardening and had a positive temperature

dependence of the CRSS.

ii) Aged crystals yielded discontinuously by a Luders mechanism and had a CRSS that decreased when the temperature was lowered.

iii) The work hardening rate of aged crystals was low and depended slightly on aging time.

iv) All crystals slipped predominantly on the primary system and overshot the symmetry boundary by typically 10^{o}.

v) Crystals aged up to 100 min. at 600^{o}C showed an anomalous increase in work hardening rate just prior to necking.

vi) Necking coincided with the onset of conjugate slip and occurred at approximately a constant resolved shear stress on the conjugate slip system for all aged crystals tested.

vii) The radius dependence of $\Delta V^{*}/b^{3}$ in the single crystals was similar to that found for the polycrystals.

The occurrence of yielding by the propagation of a Luders front of coarse slip bands has been observed in other alloy crystals containing coherent precipitates (20). Luders yielding is not, however, a phenomenon peculiar only to this case. It was mentioned in Section IV that alpha brass crystals (82, 84) have been observed to yield by a Luders mechanism. Other

copper base alloy solid solutions also exhibit Luders yielding (100). In addition, the behavior has also been observed in irradiated copper single crystals (101). To the author's knowledge, no detailed mechanism of Luders yielding has been advanced. Although detailed reasons for its occurrence are unknown, Luders yielding does seem to appear only when the crystal matrix has been strengthened by secondary means. (i.e.: precipitation, irradiation, solute addition, etc.). It is possible that both the appearance of a yield point and suppression of conjugate slip, as suggested by Brindly et al. (100) strongly affect the tendency to deform by a Luders mechanism.

The low work hardening rate and large overshoot of the symmetry boundary in aged crystals indicate that the amount of latent hardening on secondary systems is quite high. This is especially evident by the observation that necking commences by the initiation of conjugate slip and is accompanied by a load drop. In addition, any conjugate activity during deformation of the aged crystals should lead to a work hardening rate larger than that of the solution treated crystals. This was not observed. Any detailed comments concerning the deformation behavior of aged Cu-1.9 wt % Co crystals would

require knowledge of the changes in particle morphology with strain. Because this knowledge does not exist the above comments have been brief.

2. Fracture behavior of aged crystals

The fracture characteristics of the crystals investigated in this dissertation are of interest because plastic instability was always observed to occur by the formation of secondary (presumed conjugate) slip bands. The initiation of conjugate slip can then be investigated by examining the "necking" stress.

As pointed out in the presentation of results, the resolved shear stresses on the conjugate system at the onset of necking were surprisingly similar for all the aged crystals tested. The increased work hardening rate just prior to necking in the 30, 50, and 100 min. crystals is unexplained at present but is possibly related to minor conjugate slip occurring over short distances relative to the crystal dimensions at large strains[1]. The onset of the region of increased work hardening rate is not related to the tensile axis crossing the symmetry boundary during deformation as shown in

---

[1]Basinski, Z. S., private communication, National Research Council, Ottawa, Ontario, Canada (1967).

Figures 32, 33, and 34. In these figures the glide strain where the tensile axis crossed the symmetry boundary has been marked by an inverted arrow. In any case, the crystals do not neck until the resolved shear stress on the conjugate slip system is about 11-13 kg/mm^2. This stress appears to be only slightly affected by temperature and particle size and its constancy strongly points to the breakdown of some specific matrix barrier as the mechanism for the onset of necking. This has also been suggested by Price and Kelly (87) to explain similar behavior in Al-Cu, Al-Ag, and Al-Zn crystals. They suggested that the breakdown of Lomer-Cottrell sessile dislocations might initiate necking. Stroh (102) has shown, however, that the stress to do this is quite temperature dependent which was not the case in this investigation. When appropriate values are used, a calculation of this stress using Friedel's (103) approximation yields ≈ 9 kg/mm^2 which is close to the values obtained. As mentioned above, however, the appeal of this mechanism is dampened by the lack of variation of the observed necking stress with temperature. The incependence of the stress on particle size variations suggests it is a matrix phenomenon. The fact that it is athermal shows that it is related to long range stresses. The exact

nature of these long range barriers however remains unknown.

3. Relation between activation volume and particle size for single crystals

Figures 51 and 52 show the variation in activation volume at zero and 30% glide strain with particle radius. The striking similarity of the activation volume-radius curves of the single crystals to those of the polycrystals indicates the strong radius dependence of ΔV to be real. The short range stresses are then likely related closely to cutting of the particles themselves at the smaller particle sizes. At the larger particle sizes the data become uncertain due to the possibility of a change in mechanism with particle size occurring. It should suffice to say here that the similarity between the $\Delta V^*/b^3$ vs R curves taken from single crystals and those from polycrystals indicates that the short range barriers in both are the same. In addition the curves in Figure 51 support the hypothesis that a change in the mechanism occurs near 40Å radius. The similarity between the curves in Figures 51 and 52 show that the strong particle size dependence of ΔV persists in the single crystals to strains of 30% or more. This was not observed in the polycrystals where the disappearance of the strong particle size dependence with

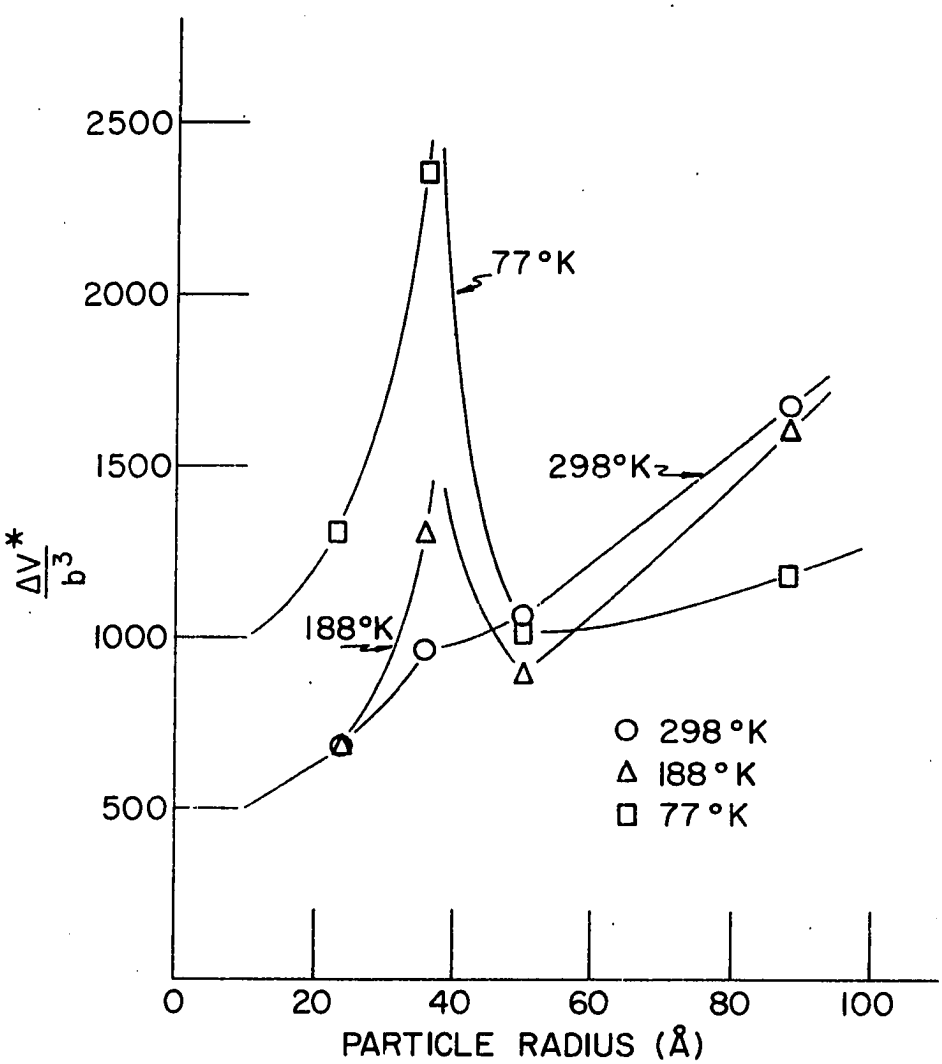

Figure 51. The dependence of $\Delta V^*/b^3$ on mean particle radius at different temperatures for Cu-1.9 wt % Co single crystals solution treated at 1298°K and aged at 873°K

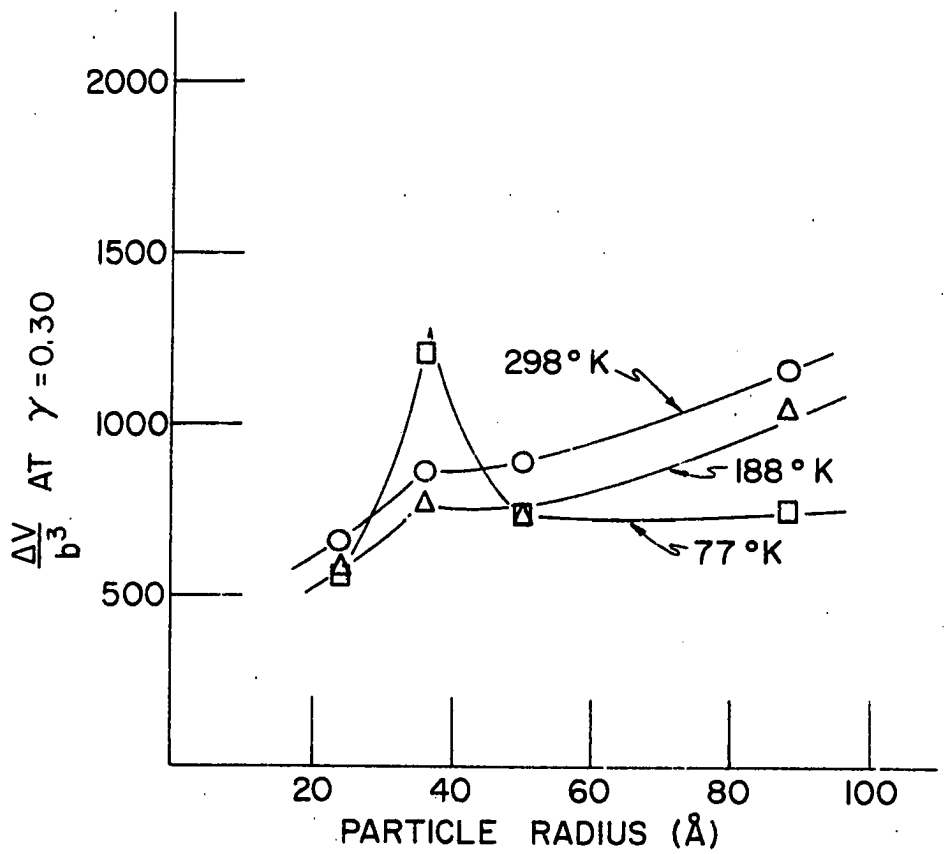

Figure 52. $\Delta V/b^3$ at 30% glide strain vs. mean particle radius at different temperatures of Cu-1.9 wt % Co single crystals solution treated at 1298°K and aged at 873°K

strain was undoubtedly due to the turbulent nature of slip in polycrystals as opposed to the single glide in the single crystals.

VI. SUMMARY OF RESULTS AND CONCLUSIONS

A major portion of this research was directed toward an understanding of the effects of coherent, dispersed particles on the rate dependent component of the flow stress, τ^*, in an aged Cu-1.9 wt % Co alloy and these results will be emphasized. It was shown in Section II that the temperature sensitivity, $d\tau/dT$, of the flow stress, τ, was needed to obtain the activation energy ΔG of the rate controlling dislocation mechanism responsible for τ^*. In addition, it was pointed out that, in its present form, the derivation of ΔG relied on the assumption that the long range stress τ_μ had the same temperature dependence as the shear modulus μ. The negative temperature dependence of the flow stress demonstrated by polycrystals aged to peak hardness indicated that the temperature dependence of τ_μ is unknown in Cu-1.9 wt % Co. ΔG could then only be determined with certainty for solution treated samples. For this reason most emphasis was placed on the effects of test temperature and particle size on the strain rate dependent component of the flow stress. These results were presented in terms of the particle size and temperature dependence of the activation volume, ΔV. Since ΔV is related to the "size" of the rate controlling, acti-

vated event, information about the relation between coherent particles and short range obstacles could be obtained.

The major results obtained during this research are listed below.

1. The particle size dependence of the yield stresses of both single crystals and polycrystals of aged Cu-1.9 wt % Co is described quite well by Gleiter's (22,23) equation:

$$\Delta\tau = \left[\frac{27.4A^3E^3b}{\pi T(1+\nu)^3}\right]^{\frac{1}{2}} f^{5/6}R^{\frac{1}{2}}$$

where $A = \dfrac{3K\varepsilon}{3K + \dfrac{2E}{1+\nu}}$

E = Young's modulus of the matrix

b = Burgers vector of the matrix

T = the line tension of the dislocation which may be approximated by $\frac{1}{2}\mu b^2$

ν = Poisson's ratio

f = the volume fraction of precipitate

R = the mean precipitate radius

μ = the shear modulus of the matrix

K = the bulk modulus of the matrix

ε = the absolute relative difference in lattice parameter between precipitate and matrix.

The above relation was derived by considering the major source of strengthening to be the interaction of dislocations and the stress fields associated with spherical, coherent precipitates. The good agreement between experiment and theory strongly indicates that the long range obstacles in aged Cu-1.9 wt % Co are the coherency stress fields of the precipitates.

2. The temperature dependence of the yield stress and flow stress up to at least 10% true strain of aged polycrystals has been found to be negative. The same type of behavior was demonstrated by the CRSS of aged single crystals. This behavior has been found by others (28) and has been attributed to the differences in thermal expansion of the Co-rich precipitates and Cu-rich matrix.

3. Single crystals and polycrystals in all stages of aging exhibited Cottrell-Stokes behavior without exception. In all cases the $\Delta\tau$-τ curves could be described by the following relation:

$$\Delta\tau = D + E\tau$$

where D and E are constants.

4. The activation volume of solution treated polycrystals was found to be a monotonically increasing function of

temperature at all strains. This is typical of f.c.c. solid solutions.

5. The temperature dependence of the activation volume at zero strain of aged polycrystals did not at all resemble the solution treated series. The curves tended to swing up at both 77 and 300°K and a small peak appeared to develop with increased aging time in the vicinity of 188°K. After small amounts of deformation the temperature dependence of aged polycrystals tended to approach that of the solution treated material.

6. The activation volume at zero strain ΔV^*, of aged polycrystals was a strong function of particle size. In fact, ΔV^* vs. particle size curves at 77, 133, and 188°K tended to peak at particle sizes in the vicinity of 30-50Å radius. The lower particle size portions of these curves closely resembled a curve derived on the basis of a cutting model in which the short range barriers were assumed to be the particles themselves.

7. Deformation was found to significantly reduce the effect of particle size on the activation volume of aged polycrystals. The particle size dependence of ΔV was found to be quite similar to the solution treated series after 5 per cent

true strain.

8. The activation volume at zero strain vs. particle size curves for aged single crystals exhibited peaks similar to those found for the polycrystals. The only difference between the two was that deformation did not completely remove the discontinuities in the single crystals and peaks were still present after 30% shear strain.

9. The Gibbs free energy of activation, ΔG, of the rate controlling dislocation mechanism in solution treated Cu-1.9 wt % Co polycrystals has been found to be a linear function of temperature between 77 and 300^{o}K. Its magnitude suggests the mechanism is either cutting of forest dislocations or dragging of jogs.

10. Some unusual effects were observed during the deformation of aged single crystals oriented for easy glide. These are:

a. The crystals yielded by the formation of coarse slip bands which propagated by a Luders-type mechanism.

b. In all cases glide occurred on the primary system until necking commenced. Overshoot of the symmetry boundary was typically 10^{o}.

c. Crystals which necked at resolved shear stresses

less than about 10 kg/mm^2 exhibited an anomalous increase in work hardening rate just prior to necking. In these cases necking occurred by the formation of coarse slip bands on the conjugate system. The bands propagated by a Luders-type mechanism similar to that observed during yielding. The strains associated with this type of necking were quite high.

d. Crystals which necked at resolved shear stresses greater than about 10 kg/mm^2 did so abruptly by conjugate slip and fractured shortly thereafter. No anomalous increase in work hardening rate occurred.

VII. REFERENCES

1. Cottrell, A. H., Dislocations and Plastic Flow in Crystals, Oxford University Press, London (1953).

2. Kelly, A. and Nicholson, R. B., Prog. Mat. Sci., 10, No. 3, 149 (1963).

3. Conrad, H., in Zackay, V. F. ed., High Strength Materials, p. 436, Wiley and Sons, New York, New York (1965).

4. Mitchell, J. B., Mitra, S. K., and Dorn, J. E., Trans. Quart. Amer. Soc. Met., 56, 236 (1963).

5. Phillips, V. A., Trans. Amer. Inst. Min. Met. Eng., 230, 967 (1964).

6. Mott, N. F. and Nabarro, F. R. N., in Rep. Conf. Strength of Solids, p. 1, Physical Society, London (1948).

7. Seeger, A., Handbuch der Physik 7, p. 1, Springer-Verlag (1958).

8. Gleiter, H. and Hornbogen, E., Mater. Sci. Eng., 2, 285 (1968).

9. Merz, W. and Gerold, V., as cited by Gerold, V. and Haberkorn, H., Phys. Stat. Sol. 16, 675 (1966).

10. Ashby, M. F. and Brown, L. M., Phil. Mag. 8, 1083 (1963).

11. Mott, N. F. and Nabarro, F. R. N., Proc. Phys. Soc., 52, 86 (1940).

12. Mott, N. F., Journ. Inst. Met., 72, 367 (1946).

13. Nabarro, F. R. N., Proc. Phys. Soc., 58, 669 (1946).

14. Haberkorn, H. and Gerold, V., Phys. Stat. Sol., 15, 167 (1966).

15. Dash, J. and Fine, M. E., Acta Met., 9, 149 (1961).

16. Livingston, J. D., Trans. Amer. Inst. Min. Met. Eng., 215, 566 (1959).

17. Price, R. J. and Kelly, A., Acta Met., 10, 980 (1962).

18. Gerold, V. and Haberkorn, H., Phys. Stat. Sol., 16, 675 (1966).

19. Fleischer, R. L., in Peckner, D., ed., The Strengthening of Metals, p. 94 , Reinhold, New York, New York (1964).

20. Haberkorn, H., Phys. Stat. Sol., 15, 153 (1966).

21. Orowan, E., Symp. on Internal Stresses in Metals and Alloys, Institute of Metals, 451 (1948).

22. Gleiter, H., Z. Angew, Physik, 23, 108 (1967).

23. Gleiter, H., Z. Metallk., 58, 99 (1967).

24. Peach, M. and Koehler, J. S., Phys. Rev., 80, 436 (1950).

25. Fleischer, R. L., Acta Met., 8, 598 (1960).

26. Williams, R. O., Acta Met., 5, 385 (1957).

27. Hirsch, P. B. and Kelly, A., Phil. Mag., 12, 881 (1965).

28. Phillips, V. A., Phil. Mag., 11, 775 (1965).

29. Bonar, L. G., Precipitation Hardening, Unpublished Ph.D. thesis, Cambridge University, England (1962).

30. Fleischer, R. L., G. E. Report No. 61-RL-2676M-April 1961.

31. Kelly, A. and Fine, M. E., Acta Met., 5, 365 (1957).

32. Kelly, A., Phil. Mag., 3, 1472 (1958).

33. Weertman, J. and Weertman, J., Elementary Dislocation Theory, Macmillan, New York, New York (1964).

34. Koda, S., Matsura, K., and Takahashi, N., in Kelly, A. and Nicholson, R. B., Prog. Mat. Sci., 10, No. 3, 320

(1963).

35. Gleiter, H., unpublished results cited by Gleiter, H. and Hornbogen, E., Mater. Sci. Eng., 2, (1968).

36. Conrad, H., Acta Met., 6, 339 (1958).

37. Conrad, H., Journ. of Met., 16, 582 (1964).

38. Dorn, J. E., Mitchell, J., and Hauser, F., Exper. Mech. 5, 1 (1965).

39. Gibbs, G. B., Phys. Stat. Sol., 5, 693 (1964).

40. Gibbs, G. B., C.E.G.B. Report RD/B/N.416, [Central Electricity Generating Board, Leatherhead, Surrey, England] c.1965.

41. Gibbs, G. B., Phys. Stat. Sol., 10, 507 (1965).

42. Schoeck, G., Phys. Stat. Sol., 8, 499 (1965).

43. Basinski, Z. S., Phil. Mag., 4, 393 (1959).

44. Mitra, S. K., Osborne, P. W. and Dorn, J. E., Trans. Amer. Inst. Min. Met. Eng., 221, 1206 (1961).

45. Ono, K., Journ. Appl. Phys., 39, 1803 (1968).

46. Byrne, J. G., Fine, M. E. and Kelly, A., Phil. Mag., 6, 1119 (1961).

47. Mott, N. F., Phil. Mag., 48, 568 (1956).

48. Seeger, A., Second International Conference on the Peaceful Uses of Atomic Energy, A/COMF/15/P/989, (1958).

49. Metals Handbook, ASM, 1191 (1948).

50. Corsen, M. G., U.S. Patent 1,723,922 (1929).

51. Gordon, R. B. and Cohen, M., in Age Hardening of Metals, p. 161, ASM, Cleveland, Ohio (1940).

52. Tamman, G. and Oelsen, W., Z. für Anorg. Allge. Chemie, 186, 257 (1930).

53. Becker, J. J., Trans. Amer. Inst. Min. Met. Eng., 209, 59 (1957).

54. Cahn, J. W., Trans. Amer. Inst. Min. Met. Eng., 209, 1309 (1957).

55. Becker, J. J., Trans. Amer. Inst. Min. Met. Eng., 212, 138 (1958).

56. Bean, C. P., Livingston, J. D. and Rodbell, D. S., Acta Met., 5, 682 (1957).

57. Livingston, J. D. and Becker, J. J., Trans. Amer. Inst. Min. Met. Eng., 212, 316 (1958).

58. Rodbell, D. S., Journ. Appl. Phys., 29, 311 (1958).

59. Greenwood, G. W., Acta Met., 4, 243 (1956).

60. Ashby, M. F. and Brown, L. M., Proc. Fifth Int. Cong. for Electron Microscopy, Vol. 1, K5, Academic Press, New York, New York (1962).

61. Phillips, V. A. and Livingston, J. D., Phil. Mag. 7, 969 (1962).

62. Phillips, V. A., Guard, R. W. and Livingston, J. D., Aeronautical Research Laboratories Report No. ARL-62-357, [Wright-Patterson Air Force Base, Ohio] May, 1962.

63. Tanner, L. E. and Servi, I. S., Acta Met., 14, 231 (1966).

64. Servi, I. S. and Turnbull, D., Acta Met., 14, 161 (1966).

65. Cottrell, A. H. and Stokes, R. J., Proc. Roy. Soc., A 233, 17 (1955).

66. Gerstein, B. C., USAEC Rept. IS-331, [Iowa State University of Science and Technology, Ames, Iowa], (1960).

67. Miller, A., A study of some nonstoichiometric rare-earth oxides. Unpublished Ph.D. thesis. Library, Iowa State University of Science and Technology, Ames, Iowa (1964).

68. Schmid, E. and Boas, W., Plasticity of Crystals, Hughes, London, (1950).

69. Krop, H., Mizia, J. and Korbel, A., Acta Met., 15, 463 (1967).

70. Ardell, A. J. and Nicholson, R. B., Journ. Phys. Chem. Solids, 27, 1793 (1966).

71. Lifshitz, I. M. and Slyozov, V. V., Journ. Phys. Chem. Solids, 19, 35 (1961).

72. Wagner, C., Z. Elektrochem, 65, 581 (1961).

73. Livingston, J. D., in Kelly, A. and Nicholson, R. B., Prog. Mat. Sci., 10, No. 3, 299 (1963).

74. Thornton, P. R., Mitchell, T. E. and Hirsch, P. B., Phil. Mag., 7, 337 (1962).

75. Orava, R. N., Stone, G. and Conrad, H., Trans. Quart. Amer. Soc. Met., 59, 171 (1966).

76. Zerwekh, R. P. and Scott, T. E. unpublished data, Iowa State University of Science and Technology, Ames, Iowa (1966).

77. Koepke, B. G., Gibson, E. D. and Scott, T. E., Trans. Quart. Amer. Soc. Met., 60, 409 (1967).

78. Clarebrough, L. M. and Hargraves, M. E., Prog. Met. Phys. 8, 1 (1960).

79. Nabarro, F. R. N., Basinski, Z. S., and Holt, D. B., Advances in Physics, 13, 193 (1964).

80. Thornton, P. R., Mitchell, T. E. and Hirsch, P. B., Phil. Mag., 7, 1349 (1962).

81. Haasen, P. and King, A., Z. Metallk., 51, 722 (1960).

82. Mitchell, T. E. and Thornton, P. R., Phil. Mag., 8, 1127 (1963).

83. Mitchell, T. E. and Thornton, P. R., Phil. Mag., 10, 315 (1964).

84. Piercy, G. R., Cahn, R. W. and Cottrell, A. H., Acta Met., 3, 331 (1955).

85. Kelly, A. and Nicholson, R. B., Prog. Mat. Sci., 10, No. 2, 310 (1963).

86. Beevers, C. J. and Honeycombe, R. W. K., in Averbach, B. L., Felbeck, D. K., Hahn, G. T., and Thomas, D. A. eds., Fracture, p. 474, Wiley, New York, New York (1959).

87. Price, R. J. and Kelly, A., Acta Met., 12, 979 (1964).

88. Price, R. J. and Kelly, A., Acta Met., 11, 915 (1963).

89. Kelly, A., Lassila, A. and Sato, S., Phil. Mag., 4, 1260 (1959).

90. Dew-Hughes, D. and Robertson, W. D., Acta Met., 8, 156 (1960).

91. Jackson, P. J. and Basinski, Z. S., Can. Journ. Phys., 45, 707 (1967).

92. Gleiter, H., Acta Met., 15, 1213 (1967).

93. Gleiter, H., Acta Met., 15, 1223 (1967).

94. Kocks, U. F., Acta Met., 6, 85 (1958).

95. Ashby, M. F., Acta Met., 14, 679 (1966).

96. Westmacott, K. H., Fountain, C. W. and Stirton, R. J., Acta Met., 14, 1629 (1966).

97. Kocks, U. F., Acta Met., 14, 1629 (1966).

98. Fisher, J. C., Hart, E. W. and Pry, R. H., Acta Met., 1, 336 (1953).

99. Honeycombe, R. W. K., Prog. Mat. Sci., 9, No. 2, 93 (1961).

100. Brindley, B. J., Corderoy, D. J. H., and Honeycombe, R. W. K., Acta Met., 10, 1043 (1962).

101. Rukweid, A., Z. Metallk., 55, 146 (1964).

102. Stroh, A. H., Phil. Mag., 1, 489 (1956).

103. Friedel, J., Dislocations, p. 168, Pergamon Press, London (1964).

VIII. ACKNOWLEDGEMENTS

I want to thank my advisor, Dr. T. E. Scott, for his helpful advise and continued interest during this investigation. I am especially grateful to him for the many stimulating discussions concerning this and other research.

The able experimental assistance of Messrs. L. K. Reed, G. L. Ahrens, R. L. Roehrkasse and H. H. Baker is gratefully acknowledged.

In addition I want to thank Metallurgy Group XIII in general for making my stay in the laboratory a pleasant and rewarding experience.

My thanks to my wife for typing the rough draft and to Miss Verna Thompson for typing the final manuscript.